Phosphorus removal and recovery from sludge centrate by membrane and steel-making slag

by Truong Minh Vu

Thesis submitted in fulfilment of the requirements for the degree of

Doctor of Philosophy

under the supervision of

Professor Duc Long Nghiem
Distinguished Professor Huu Hao Ngo

University of Technology Sydney
Faculty of Engineering and Information Technology

September 2022

CERTIFICATE OF ORIGINAL AUTHORSHIP

I, Truong Minh Vu, hereby declare that this thesis is submitted in fulfilment of the requirements for the award of Doctor of Philosophy, in the School of Civil and Environmental Engineering, Faculty of Engineering and Information Technology at the University of Technology Sydney.

This thesis is wholly my own work unless otherwise referenced or acknowledged. In addition, I certify that all information sources and literature used are indicated in the thesis.

This document has not been submitted for qualifications at any other academic institution.

Signature:

Production Note:
Signature removed prior to publication.

Date: 30/09/2022

ACKNOWLEDGMENTS

and Environmental Engineering, especially Ms. Van Le. With their continuous support, my study at UTS has become much smoother and easier.

In addition, I would like to thank our group members, including Dr. Lei Zheng, Ms. Chelsey Vu, Ms. Allie Nguyen, and Ms. Lisa Aditya. Their kind help and support have made my study and life in Australia a wonderful time. During my PhD training at UTS, I was fortunate to meet great friends, including Dr. Thanh Nguyen, Dr. Phong Vo, Dr. Thuc Nguyen, Dr. Huy Tran, Dr. Niren Pathak, Dr. Hang Do, Dr. An Le, Dr. Loan Nguyen, Ms. Lan Wu, and Mr. Quyet Truong. I would like to thank them for a cherished time spent together in the lab and in social settings.

Last but not least, no words would be enough to express my gratitude to my parents and relatives for their love and encouragement throughout my life. Sincerely, I wish them health and happiness. In particular, I would like to take this opportunity to spend the most profound appreciation and special thanks to my beloved wife, Ngoc (Emily) Hoang for her unconditional love, continuous sacrifice, encouragement, and care for me. Due to my study, she had to leave her job as a professional medical doctor in a public hospital in Vietnam and moved to Australia where we have together built up everything from "zero". In Australia, she has been still working full-time six days per week; however, every single day, no matter what happened, she still always woke up with me, prepared every single meal for me, and took care of all housework so that I could totally focus on my research work and the development of my career. I really feel extremely lucky and proud when I have her as an understanding and extremely considerate life-friend with whom I could share all joy and sorrow in my work and life. Without her, I would have never made this thesis happen. All things that I have achieved so far are dedicated to her. Emily, thank you so much for coming into my life!

TABLE OF CONTENTS

LIST OF FIGURES

LIST OF TABLES

LIST OF ABBREVIATIONS

Symbol	Description
AD	Anaerobic Digestion
AcoD	Anaerobic Codigestion
BET	Brunauer-Emmett-Teller
BOF	Basic Oxygen Furnace
CA	Contact Angle
COD	Chemical Oxygen Demand
CP	Concentration Polarisation
CSIRO	Commonwealth Scientific and Industrial Research Organisation
DI	Deionised
DM	Dry Matter
DNA	Deoxyribonucleic Acid
DS	Draw Solution
EAF	Electric Arc Furnace
ED	Electrodialysis
EDS	Energy Dispersive X-ray Spectroscopy
FO	Forward Osmosis
FS	Feed Solution
FTIR	Fourier Transform Infrared
HAP	Hydroxyapatite
HRT	Hydraulic Retention Time
IAP	Ion Activity Product
IC	Inorganic Carbon or Ion Chromatography
ICP-MS	Inductively Coupled Plasma Mass Spectrometry
IP	Intra-particle Diffusion
IWA	International Water Association
LMH	$L/m^2.h$

MD	Membrane Distillation
MF	Microfiltration
MPR	Membrane Photo-bioreactor
N	Nitrogen
NF	Nanofiltration
NSW	New South Wales
P	Phosphorus
PA	Polyamide
PRO	Pressure Retarded Osmosis
PZC	Point of Zero Charge
RNA	Ribonucleic Acid
RO	Reverse Osmosis
SEM	Scanning Electron Microscopy
SI	Saturation Index
TAS	Tasmania
TFC	Thin Film Composite
TN	Total Nitrogen
TP	Total Phosphorus
TS	Total Solids
TSS	Total Suspended Solids
UF	Ultrafiltration
US-EPA	United States Environmental Protection Agency
UV	Ultraviolet
WWTP	Wastewater Treatment Plant
XRD	X-ray Powder Diffraction

LIST OF PUBLICATIONS

1. Peer-reviewed journal publications and book chapters related to this thesis work

1. **M.T. Vu,** H.C. Duong, Q. Wang, Z. Cai, N.B. Hoang, N.T.T. Viet, L.D. Nghiem, A low-cost method using steel-making slag to quench the residual phosphorus from wastewater effluent, Environmental Technology & Innovation (2023) 103181 **(Q1)**.

2. **M.T. Vu,** H.C. Duong, Q. Wang, A. Ansari, Z. Cai, N.B. Hoang, L.D. Nghiem, Recent technological developments and challenges for phosphorus removal and recovery toward a circular economy, Environmental Technology & Innovation 30 (2023) 103114 **(Q1).**

3. **M.T. Vu**, L.N. Nguyen, I. Ibrahim, M. Abu Hasan Johir, N. Bich Hoang, X. Zhang, L.D. Nghiem, Nutrient recovery from digested sludge centrate using alkali metals from steel-making slag, Chemical Engineering Journal, 450 (2022) 138186 **(Q1)**.

4. **M.T. Vu**, L.N. Nguyen, M. Mofijur, M.A.H. Johir, H.H. Ngo, T.M.I. Mahlia, L.D. Nghiem, Simultaneous nutrient recovery and algal biomass production from anaerobically digested sludge centrate using a membrane photobioreactor, Bioresource Technology, 343 (2022) 126069 **(Q1)**.

5. **M.T. Vu**, L.N. Nguyen, M.A. Hasan Johir, X. Zhang, L.D. Nghiem, M. Elimelech, Biogas sparging to control fouling and enhance resource recovery from anaerobically digested sludge centrate by forward osmosis, Journal of Membrane Science, (2021) 119176 **(Q1)**.

6. **M.T. Vu**, L.N. Nguyen, M.A. Hasan Johir, H.H. Ngo, C. Skidmore, A. Fontana, B. Galway, H. Bustamante, L.D. Nghiem, Phosphorus removal from aqueous solution by steel making slag – Mechanisms and performance optimisation, Journal of Cleaner Production, 284 (2021) 124753 **(Q1)**.

7. **M.T. Vu**, L.N. Nguyen, J.A.H. Mohammed, J. Zdarta, M. Mofijur, N. Pathak, L.D. Nghiem, Nutrient recovery from anaerobic digestate, in: Anaerobic Digestate Management, IWA Publishing, 2022, pp. 131-150.

8. **M.T. Vu**, L.N. Nguyen, J. Zdarta, J.A.H. Mohammed, N. Pathak, L.D. Nghiem, Chapter 1 - Wastewater to R3 – resource recovery, recycling, and reuse efficiency in urban wastewater treatment plants, in: A. An, V. Tyagi, M. Kumar, Z. Cetecioglu (Eds.) Clean Energy and Resource Recovery, Elsevier, 2022, pp. 3-16.

2. Other peer-reviewed journal publications and book chapters

9. L.N. Nguyen, **M.T. Vu**, H.P. Vu, M.A.H. Johir, L. Labeeuw, P.J. Ralph, T.M.I. Mahlia, A. Pandey, R. Sirohi, L.D. Nghiem, Microalgae-based carbon capture and utilization: A critical review on current system developments and biomass utilization, Critical Reviews in Environmental Science and Technology, 53 (2023) 216-238 **(Q1)**.

10. **M.T. Vu**, K. Bachosz, L.D. Nghiem, J. Zdarta, L.N. Nguyen, T. Jesionowski, Enzyme-based control of membrane biofouling for water and wastewater purification: A comprehensive review, Environmental Technology & Innovation, 25 (2022) 102106 **(Q1)**.

11. L.N. Nguyen, **M.T. Vu**, M. Abu Hasan Johir, M. Pernice, H.H. Ngo, J. Zdarta, T. Jesionowski, L.D. Nghiem, Promotion of direct interspecies electron transfer and potential impact of conductive materials in anaerobic digestion and its downstream processing - a critical review, Bioresource Technology, 341 (2021) 125847 **(Q1)**.

12. H.C. Duong, L.T.T. Tran, **M.T. Vu**, D. Nguyen, N.T.V. Tran, L.D. Nghiem, A new perspective on small-scale treatment systems for arsenic affected groundwater, Environmental Technology & Innovation, 23 (2021) 101780 **(Q1)**.

13. J.A. Khan, **M.T. Vu**, L.D. Nghiem, A preliminary assessment of forward osmosis to extract water from rumen fluid for artificial saliva, Case Studies in Chemical and Environmental Engineering, 3 (2021) 100095.

14. **M.T. Vu**, L.N. Nguyen, K. Li, Q. Fu, M.A.H. Johir, A. Fontana, L.D. Nghiem, Biomethane production from anaerobic co-digestion and steel-making slag: A new waste-to-resource pathway, Science of the Total Environment, (2020) 139764 **(Q1)**.

15. **M.T. Vu**, H.P. Vu, L.N. Nguyen, G.U. Semblante, M.A.H. Johir, L.D. Nghiem, A hybrid anaerobic and microalgal membrane reactor for energy and microalgal biomass production from wastewater, Environmental Technology & Innovation, 19 (2020) 100834 **(Q1)**.

16. L.N. Nguyen, **M.T. Vu**, A.Q. Nguyen, M.A.H. Johir, A.S. Commault, P.J. Ralph, G.U. Semblante, L.D. Nghiem, A sequential membrane bioreactor followed by a membrane microalgal reactor for nutrient removal and algal biomass production, Environmental Science: Water Research & Technology, 6(2020) 189-196 **(Q1)**.

17. L.N. Nguyen, J. Kumar, **M.T. Vu**, J.A.H. Mohammed, N. Pathak, A.S. Commault, D. Sutherland, J. Zdarta, V.K. Tyagi, L.D. Nghiem, Biomethane production from anaerobic co-digestion at wastewater treatment plants: A critical review on development and innovations in biogas upgrading techniques, Science of the Total Environment, 765 (2021) 142753 **(Q1)**.

18. H.P. Vu, L.N. Nguyen, **M.T. Vu**, M.A.H. Johir, R. McLaughlan, L.D. Nghiem, A comprehensive review on the framework to valorise lignocellulosic biomass as biorefinery feedstocks, Science of the Total Environment, 743 (2020) 140630 **(Q1)**.

19. H.P. Vu, L.N. Nguyen, **M.T. Vu**, L. Labeeuw, B. Emmerton, A.S. Commault, P.J. Ralph, T.M.I. Mahlia, L.D. Nghiem, Harvesting Porphyridium purpureum using

polyacrylamide polymers and alkaline bases and their impact on biomass quality, Science of the Total Environment, 755 (2021) 142412 **(Q1)**.

20. L.N. Nguyen, **M.T. Vu**, M.A. Johir, N. Pathak, J. Zdarta, T. Jesionowski, G.U. Semblante, F.I. Hai, H. Khanh Dieu Nguyen, L.D. Nghiem, A novel approach in crude enzyme laccase production and application in emerging contaminant bioremediation, Processes, 8 (2020) **(Q2)**.

21. **M.T. Vu**, W.E. Price, T. He, X. Zhang, L.D. Nghiem, Seawater-driven forward osmosis for pre-concentrating nutrients in digested sludge centrate, Journal of Environmental Management, 247 (2019) 135-139 **(Q1)**.

22. L.N. Nguyen, **M.T. Vu**, H.P. Vu, J. Zdarta, J.A.H. Mohammed, N. Pathak, P.J. Ralph, L.D. Nghiem, Chapter 4 - Seaweed carrageenans: Productions and applications, in: H. Ngo, W. Guo, A. Pandey, J.-S. Chang, D.-J. Lee (Eds.) Biomass, Biofuels, and Biochemicals, Elsevier, 2022, pp. 67-80.

23. M.B. Asif, Z. Zhang, **M.T. Vu**, J.A.H. Mohammed, N. Pathak, L.D. Nghiem, L.N. Nguyen, Membrane bioreactor for wastewater treatment: Current status, novel configurations and cost analysis, in, Springer Berlin Heidelberg, 2022, pp. 1-21.

ABSTRACT

Phosphorus is an essential element for all lives on earth. It is also a finite resource, derived primarily from phosphorus rock. Given the imminent depletion of minable phosphate rock, phosphorus recovery from nutrient-rich streams is essential for future generations.

Sludge centrate as a by-product from anaerobic digestion of sewage sludge is a phosphorus-rich stream that can be considered as an alternative for renewable phosphorus supply. This study initiated a systematic approach to develop an innovative integrated framework using steel-making slag and membrane-based processes to maximise phosphorus removal and recovery from sludge centrate. The proposed complete framework involved pre-treatment process (i.e. biogas sparging and sand filtration), enrichment process by forward osmosis followed by recovery process using steel-making slag and post treatment of the recovery process effluent by steel-making slag and a membrane photo-bioreactor.

The obtained results demonstrated the proof-of-concept of biogas sparging to control membrane fouling and enhance nutrient enrichment during sludge centrate pre-concentration by forward osmosis. Biogas sparging also resulted in a significant improvement in the enrichment of phosphate ions to close to the theoretical value based on mass balance calculation. In other words, phosphate ions were retained in the concentrated sludge centrate for subsequent recovery.

Results in this study highlighted for the first time the potential of nutrient recovery from sludge centrate using calcium and other alkali metals from steel-making slag. Up to 96% phosphate and 71% ammonia could be recovered from sludge centrate at the optimal conditions. The results also showed that pre-treatment by sand filtration and forward osmosis enrichment was essential to achieve high nutrient recovery. Sand filtration pre-

treatment decreased the total suspended solid of sludge centrate by eightfold, leading to mitigated membrane fouling and reduced nutrient loss during forward osmosis pre-concentration.

In addition, the study demonstrated the feasibility of using steel-making slag to polish the aqueous solution followed by the application of steel-making slag in quenching residual P from the recovery process effluent. At the optimal conditions (i.e. pH 8.5 and steel-making slag dosage of 5 g/L), approximately 98% phosphorus removal could be achieved with the output level of less than 0.1 mg/L.

Furthermore, the study successfully demonstrated the feasibility of using a novel sequencing batch membrane photobioreactor for simultaneous nutrient removal and algal biomass production from sludge centrate. In comparison to the batch mode reactor, the membrane photobioreactor allowed for continuous cultivation of microalgae with 40% higher biomass content.

Keywords: Phosphorus recovery; sludge centrate; membrane filtration; steel-making slag; biogas sparging; microalgae cultivation.

Chapter 1. Introduction

1.1. Introduction

The existing exploitation model of water resources has been linear and unsustainable [1]. In this model, water is extracted from sources, treated and used, and the impaired water (i.e. wastewater) is then treated and discharged (Figure 1). This fact not only puts a strain on the environment but also causes a high cost of treatment and disposal as well as such remarkable loss of natural resources (e.g. water, energy, and nutrients) via wastewater discharge. It is reported that 50 – 100% of lost resources are contained in wastewater [2].
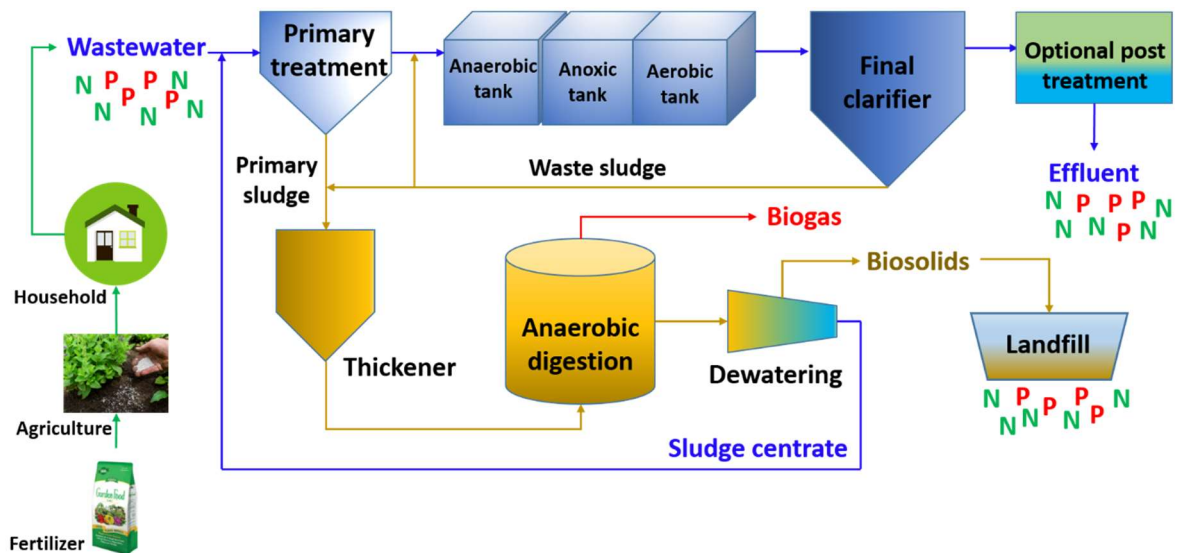
Figure 1: Current typical wastewater treatment system with loss of the essential nutrients.

Given the depletion of natural resources (i.e. fossil fuels and natural minerals) [3], the concept of circular economy has been conceived. In this concept, the amount of waste release is expected to be minimized and their reuse is expected to be maximized, thus promoting sustainable management of materials and energy [2]. In a circular economy perspective, wastewater is no longer a problem but a solution and a resource from which other valuable resources (e.g. clean water, energy, and nutrients) can be recovered and

recycled. Wastewater treatment plants (WWTPs) are therefore becoming an important part of circular economy (Figure 2).
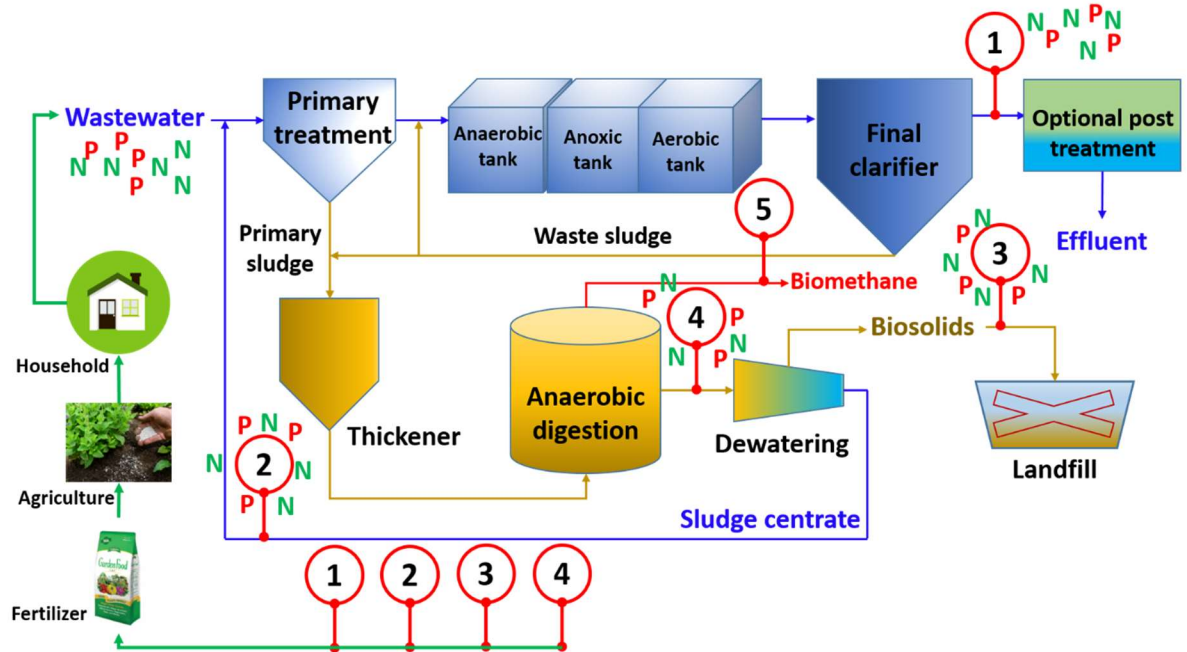
Figure 2: Schematic circular model of future wastewater treatment coupled with energy and nutrient recovery.

In WWTPs, most of the organic input from wastewater is anaerobically digested to produce biogas (a source of clean energy) and digestate (a mixture of solid and liquid residue from anaerobic digestion) [4]. The liquid fraction called sludge centrate is obtained from dewatering anaerobic digestate. This stream is rich in nutrients (i.e. nitrogen (N) and phosphorus (P)). The ammonia and phosphate contents in sludge centrate can reach up to 1 and 0.5 g/L, respectively [5-8]. Sludge centrate offers an excellent opportunity for nutrient recovery given the high content of N and P and small volume compared to the initial volume of wastewater input to the treatment plant.

Under the circular economy perspective, recycling and recovery of valuable resources (e.g. P and N) from sludge centrate are a win-win solution for nutrient management in WWTPs. Up to 30% of nutrients present in sewage end up in sludge centrate. The current

practice of circulating this stream to the head of work for further treatment can cause a number of negative impacts on WWTPs [9]. Examples include accumulation of nutrients in the entire system, nutrient organic carbon imbalance, struvite blockage, and failure to meet stringent effluent discharge standards [10, 11]. Thus, nutrient recovery from sludge centrate can simultaneously improve compliance with effluent discharge standards while also lowering maintenance costs due to the significant reduction in struvite blockage. At the same time, valuable fertilizers can be made from the recovered nutrients.

In addition to advantages to WWTPs, nutrient removal and recovery from sludge centrate can also bring numerous benefits to the environment and society. P and N are essential ingredients for all living organisms on our planet [12-14]. Moreover, phosphorous and nitrogenous compounds are feedstock for many key industrial processes [15, 16]. The fact is that the shortage of P reservation due to the over-exploitation of minable phosphate rocks for agricultural production [13, 17] has threatened food security and the operation of other industries. Hence, the recycling and recovery of P from sludge centrate to produce fertilizers can compensate for this depletion as well as ensure the conservation of natural ores for sustainable development. Furthermore, the excess of nutrients in the aquatic environment can cause eutrophication and bloom algae [13, 18] as well as detrimental health impacts, such as the blue baby syndrome in infants caused by consumption of water rich in nitrate [19]. The recycling and recovery of P and N from nutrient-rich sources (e,g. sludge centrate) can be promising approaches to handle these environment- and health-related issues.

Given the finite and non-renewable source of P, P removal and recovery from sludge centrate is a more pressing need compared to N. Nitrogenous fertiliser can be synthesised from N_2 gas in the air. Thus, the primary purpose of this study is to focus on the

advancement of technologies for P removal and recovery processes from sludge centrate. N removal and recovery are considered an accompanying process.

1.2. Problem statement

Sludge centrate is a highly complex waste stream with a high content of total suspended solids, nutrients, and organic matter. To maximise the removal and recovery of nutrients from this stream, the combination of different technical solutions is needed. To date, there has been a wide range of technologies developed and applied for nutrient removal and recovery in recent years. They include adsorption [20, 21], chemical precipitation [22, 23], membrane-based processes [11, 24-26] and biological treatment [17, 27, 28]. Each of them has its own pros and cons in extracting nutrients from wastewater. Thus, the development of an innovative approach using these technologies properly is essential for the effective management of nutrients in sludge centrate.

1.3. Research objectives

The ultimate goal of the thesis is to generate new knowledge for an integrated system (Figure 3) to remove and recover nutrients, especially P from sludge centrate effectively using membrane and steel-making slag. This goal will be achieved by implementing the following objectives:

- Assess the effectiveness of using cost-effective methods to pretreat sludge centrate and tackle the existing bottleneck of a forward osmosis system applied to enrich nutrients in sludge centrate for subsequent recovery;

- Evaluate the efficiency of sludge centrate preconcentraiton by forward osmosis and subsequent P recovery using steel-making slag;

- Evaluate the performance of steel-making slag as adsorbent to remove residual P from the process effluent;

4

- Evaluate nutrient removal and microalgal biomass production rate from sludge centrate using a novel membrane photobioreactor.

Sludge centrate

Pre-treatment process	(i.e. Biogas sparging/ sand filtration)
Enrichment process	(i.e. Forward osmosis pre-concentration)
Recovery process	(i.e. Precipitation using steel-making slag)
Post-treatment of the recovery process effluent	(i.e. Steel-making slag adsorption/ membrane photobioreactor)
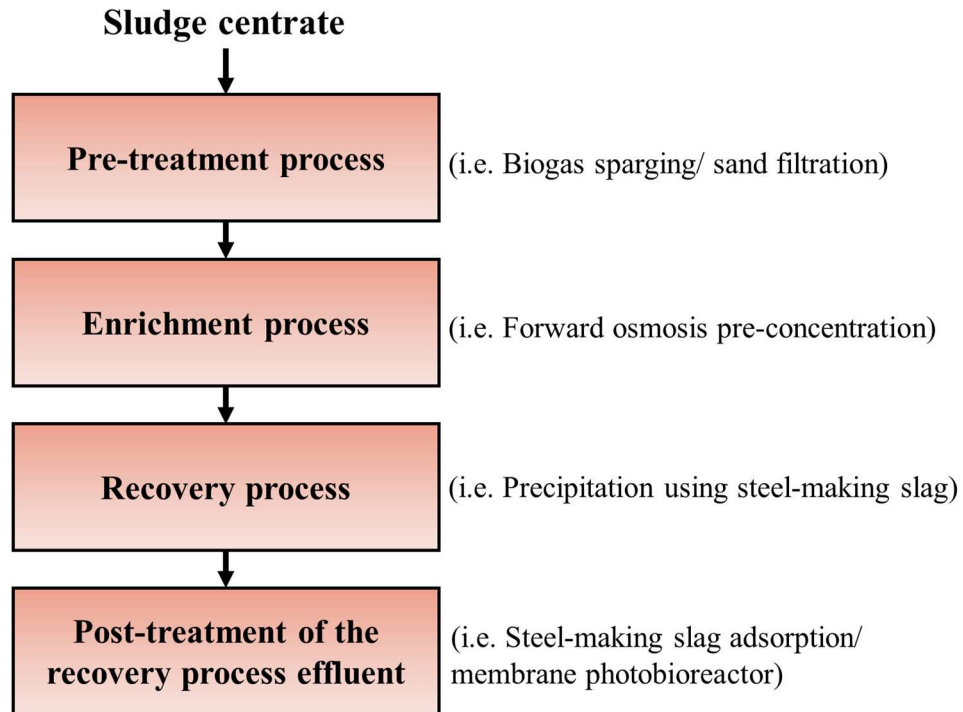
Figure 3: The proposed integrated system to remove and recover P from sludge centrate using membrane and steel-making slag.

1.4. Thesis organisation

The thesis structure is schematically described in Figure 4. This thesis involves seven chapters. Chapter 1 briefly describes the background information about the paradigm shift from a linear economy to the modern circular economy under which the need for P removal and recovery from wastewater is emphasised. The problem statement and research objectives are presented afterward. Chapter 2 provides an overview of the key information related to P removal and recovery from sludge centrate. The chapter highlights the vital role of P in the economy, sources of P supply, alarming depletion of global P reserves, and an urgent need to find out an alternative for renewable P supply. Subsequently, the chapter presents the origin and compositional characteristics of sludge

centrate to emphasise its potential for P recovery. In this chapter, a strategic roadmap combining the state-of-the-art technologies properly to remove and recover P is introduced herewith. Chapter 3 initiates the proof-of-concept system using biogas sparging to control membrane fouling and enhance P enrichment during forward osmosis pre-concentration of sludge centrate for subsequent recovery. Chapter 4 investigates the efficiency of P recovery from forward osmosis pre-concentrated sludge centrate using steel-making slag. Chapter 5 demonstrates the feasibility of using steel-making slag for quenching residual P from the recovery process effluent prior to effluent discharge. Chapter 6 investigates the potential of using a novel sequencing batch membrane photobioreactor to simultaneously remove P and produce algal biomass from sludge centrate. Chapter 7 involves the summaries of the obtained results and findings of this thesis study and the recommendations for further research work.
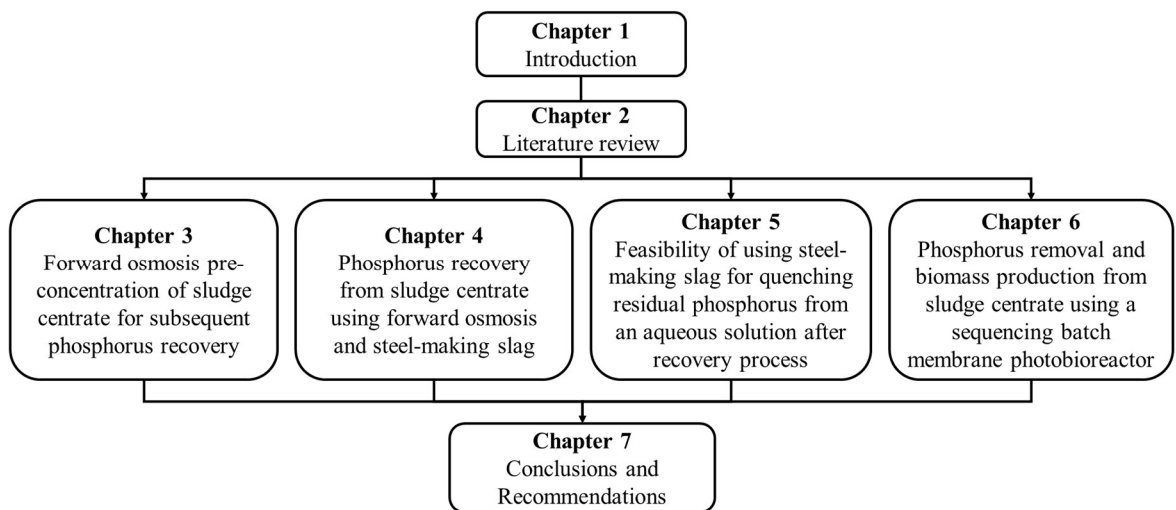
Figure 4: The thesis outline.

Chapter 2. Literature review

2.1. Phosphorus in the economy

2.1.1. Phosphorus flow

P is essential to life in many aspects [13]. P is a key element in the molecular structure of nucleotides in DNA and RNA, primary energy carrier in cells (e.g. adenosine triphosphate), bones and teeth [29, 30]. In the economy, P is a key ingredient of fertilisers for agricultural production [19]. Elementary P is also essential for many high-tech industries such as pharmaceutical, fine chemical, food, and electronic manufacturing [30, 31]. A sustainable supply of P is essential to future generations.

Most of the current global P consumption is in the form of fertilizers for agricultural production. Yet, there are several major leakage points, through which P is lost and pollute the aquatic environment. Using annual fertiliser consumption data in the world and the mass flow of P fertiliser through agricultural production in a well define region [32, 33], the magnitude of these leakages at the global scale is illustrated in Figure 5. These leakage points also present major opportunities for P recovery for circularity to ensure future availability of this essential mineral.

Approximately 70% of total P fertiliser is lost to the aquatic environment through agriculture run-off. P loss in agriculture run-off from farmland occurs via three processes including the attachment to the sediment eroding from the field, its dissolution in the surface water runoff, and the dissolution in leachate followed by transportation through the soil profile [34, 35]. On tilled land, most of P loss is through erosion, whereas on

untilled land, P loss is mostly through the dissolution in surface water runoff or leachate [35]. P loss through agriculture run-off can be minimised by a range of modern cultivation techniques such as soil conservation (to reduce erosion and run-off), on-demand irrigation and water reuse, and controlled release fertiliser [36].

The remaining 30% of P loss is via waste and wastewater discharge (Figure 1). Although this is smaller than P loss from agriculture run-off, the opportunity for P recovery is much more significant. Urine and faeces from human and livestock are rich in P. Each year, through urine and faeces, livestock animals and humans release about 10 Mt of P to the environment [37]. If recovered, P from urine and faeces can offset 25% of the global P demand for fertilizer [37]. In practice, only about 10% of P from these sources is currently recovered and reused [37]. Most of this is in biosolids from wastewater treatment and is used for land application.
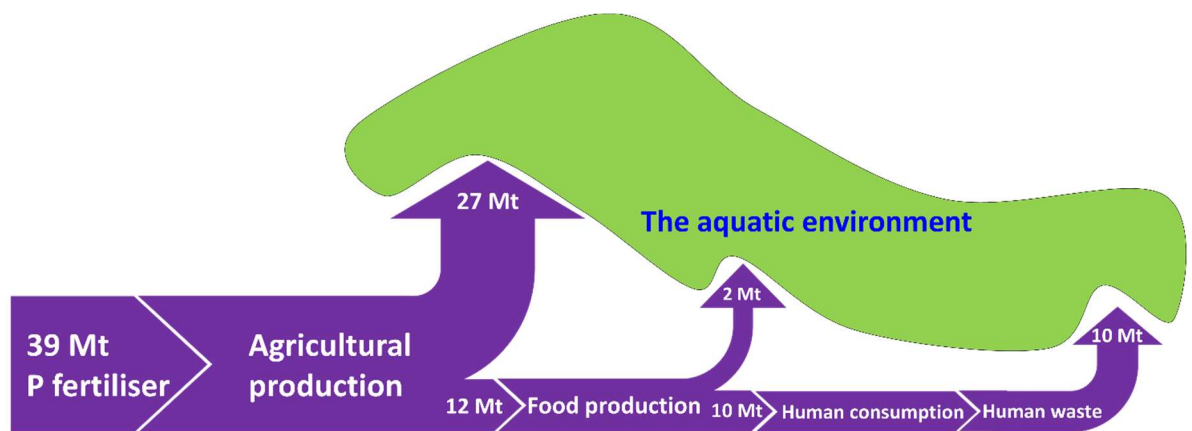
Figure 5: Mass flow of P through agricultural production.

2.1.2. Elementary phosphorus for high-tech industries

Elementary (white) P is a key feedstock for producing high-purity P compounds for the high-tech industries. Examples of these industrial P compounds include phosphoric acid, P trichloride, P sulphide and sodium hypophosphite. Pure phosphoric acid is indispensable for some food processing and semi-conductor manufacture [30, 31]. P trichloride is important in producing chlorinating agents, additives for the plastics,

lubrication oils, insecticides and flame retardants [38-40]. P sulphide is used to produce insecticides and lubrication oils [38, 41]. Sodium hypophosphite is used for nickel plating to produce hard disc drives for computers [42].

2.1.3. Peak phosphorus and a need for recovery

Without urgent P recovery, supply shortage (or peak P) is widely expected within the next decade and complete depletion of P is expected by the middle of the next century [43] (Figure 6). The prediction of peak P is based on the proven global P reserve, current P demand, and business as usual in terms of P recovery. Phosphate rock, which is a finite resource, is currently the main source of P supply [44]. The global distribution of phosphate rock is rather uneven. Three quarters of minable phosphate rock are in Morocco and Western Sahara [42]. The remaining is scattered over several countries including China, the USA, and Russia, which also have a significant demand for P for domestic consumption [42]. This geographically uneven distribution of such an essential resource is further exacerbated by geopolitical tension to create price volatility and unstable supply, heightening the risk of global food shortage. The price of P has dramatically increased in recent years, especially since the tension and armed conflict between Russia and Ukraine. At the current mining rate, complete depletion of the current reserve of phosphate rock is expected within the next 100 years [44]. Figure 6 also shows that if 60% of the current P consumption can offset through recovery or loss prevention, peak P can be delayed by at least two decades and complete P depletion can potentially be avoided.

In addition to the forecast of P exhaustion from the peak model, the environmental and socio-economical issues associated with the mining activities of phosphate rock and inefficient use of P have encouraged an increasing need for P removal and recovery from other renewable sources (e.g. wastewater). The exhaustion of global P reserves affects

food security negatively due to the reliance of agricultural production on P supply from phosphate rock. The over-exploitation of phosphate rock and the abundance of P in the aquatic environment due to discharge of wastewater and agricultural run-off into water bodies are major causes of ecological disasters (e.g. irreversible eutrophication, algae bloom, and toxic heavy metal contamination in mining areas) [13, 18, 44].
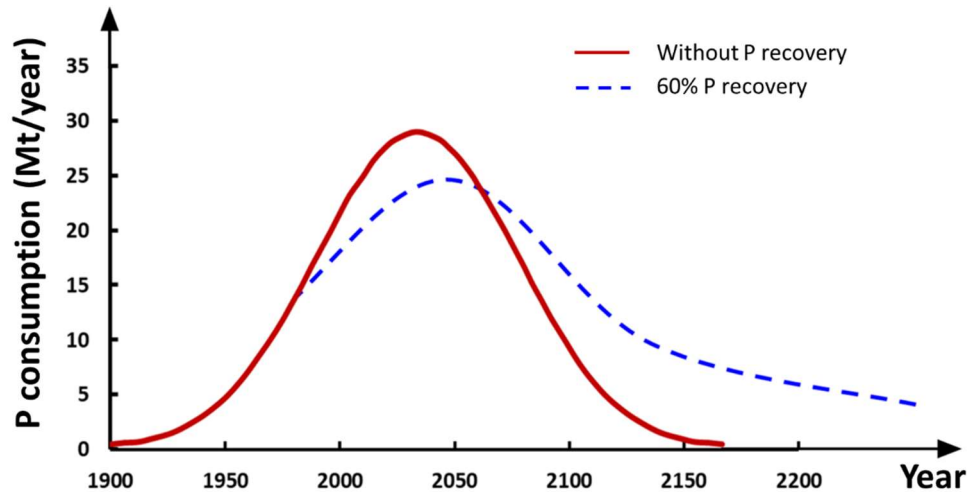
Figure 6: Peak P curve indicating a peak in consumption by 2033. Historical data are from [43]. Blue dash line is constructed by modelling 60% P recovery.

2.2. Sludge centrate as an alternative for renewable phosphate supply

2.2.1. Characteristics of anaerobic digestate

Sludge centrate is a liquid phase of anaerobic digestate, so the compositional characterisation of anaerobic digestate is of importance. The composition of digestate is governed by the types of feedstock used for digestion and operating conditions (e.g. anaerobic digestion configurations, temperature, retention time, and pressure). The pH range of digestate varies from neutral to alkaline. A typical digestate includes digested organic matter, nutrients (e.g. N, P, potassium, calcium, magnesium, and heavy metals) (Table 1). Although digestate can be produced from various types of feedstock (e.g. pig slurry, cattle and chicken manure, agricultural waste, food waste, and sewage sludge), the

10

composition of the final digestion products is similar [45]. Due to only transformation among nutrient forms of feedstock during anaerobic digestion, digestate has normally the same content of nutrients as feedstock [46-48].

Nitrogen in digestate is derived from the N-bounded proteins and its composition is highly dependent on the type of the feedstock. The concentration of total N could account for up to 24% dry biomass [46]. Digestate using protein-rich sources (e.g. food waste) as feedstock has 40% total N content higher than that from manure [49, 50]. During hydrolysis and fermentation of organic matter in anaerobic digestion, organically bound N is released as ammonical N (i.e. ammonium (NH_4^+) and free ammonia (NH_3)) [51]. Total ammonical N accounts for 35-81% total N [47, 51, 52]. The concentration of ammonium N (NH_4^+-N) in digestate is ranged from 0.8 to 5 g/L [53-55].

The total input P content in digestate is governed by the feedstock composition [45, 56] and is independent of the anaerobic digestion process. Due to microorganisms' metabolism under anaerobic conditions, organically bound P present in the feedstock is transformed to soluble orthophosphate [57]. P content can reach 1.2 g/L in digestate [58]. The anaerobic conditions are favourable for the precipitation of orthophosphate in digestate under the forms of calcium phosphate ($Ca_3(PO_4)_2$) and magnesium phosphate ($Mg_3(PO_4)_2$) [51]. It is estimated that approximately 90% of total P in digestate is within these precipitates, while the dissolved fraction only accounts for around 10% [51].

Table 1. Nutrient characteristics of unprocessed digestate from various feedstock.

Parameters	Food waste	Sewage sludge	Agricultural feedstock	Cattle manure and slurry	Co-digestion organic matter (i.e. sewage sludge and vegetable waste or manure and industrial waste)
pH	7.9 – 8.3	7.5	7.5 – 8.4	7.3 – 8.89	5.6 – 8.3
Dry matter (DM) (%)	1.4 – 7.88	1.9 – 2.97	6.41 – 24	22 – 9.2	1.83 – 34.2
Organic matter (% DM)	38 – 73	48.4 – 73.6	69 – 77	23.9 – 81.5	23.9 – 81
Total carbon (% DM)	0.44 – 45.2	4.38	1.92 – 40	0.59 – 5.07	0.41 – 11.6
Total N (% DM)	0.06 – 15.7	0.005 – 0.378	0.14 – 8.8	0.05 – 0.62	0.12 – 5.04
Ammonical N (% DM)	0.05 – 10.8	-	0.04 – 4.5	0.16 – 2.358	0.0476 – 0.1987
Total P (% DM)	0.008 – 1.6	0.04	0.058 – 6.6	0.034 – 0.616	0.01 – 1.001
Total potassium (% DM)	0.03 – 8.1	0.00019	0.324 – 10	0.03 – 1.273	0.03 – 2.52
Total magnesium (% DM)	0.079 – 5.2	-	0.041 – 3.1	0.013 – 0.166	0.006 – 0.26
Total calcium (% DM)	0.014 – 1	-	0.077 – 3.1	0.044 – 0.846	0.01 – 1.56
Total sulphur (% DM)	0.01 – 1	-	0.01 – 0.041	0.008 – 0.048	0.004 – 0.096
References	[47, 56, 59]	[46, 48, 57]	[46, 47, 50, 60, 61]	[56, 62, 63]	[60, 62, 64, 65]

2.2.2. Solid-liquid separation of digestate to release sludge centrate

Anaerobic digestate can be valorised through direct use for land application and a solid-liquid mechanical separation process. The direct use of digestate for land application is a simple and economical method to recover nutrients. However, given the environmental and social concern (e.g. odour, pathogenic contamination, and eutrophication), the use of digestate for direct land application is limited and strictly regulated in most nations [45]. The separation of digestate into two phases (i.e. solid and liquid) is to facilitate the subsequent resource recovery process (Figure 7).

The solid fraction called biosolids contains 60-80% of the digestate dry matter, only 20-25% of the initial N, and almost all P of the digestate (40-90%) [46, 53, 66]. However, most nutrients are present in organically bound compounds [45]. Thus, the possibility to recover nutrients from the solid fraction is limited. This biosolids fraction can be directly applied as an organic fertilizer in the field or can be used as a precursor for a variety of valuable materials (e.g. fuel, pyrochar, carbon-based materials, and nanocellulose) [56, 67, 68]. The nutrient recovery from the solid fraction can be performed through composting, thermal treatment, drying, and biodrying.
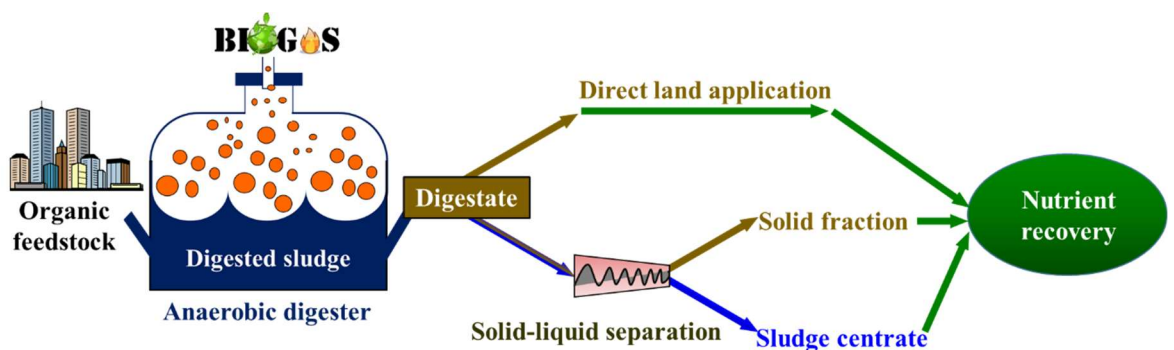
Figure 7: Overview of a current digestate processing approach.

In contrast, the liquid fraction known as sludge centrate is represented by lower dry matter (3.3-6.6% of the digestate dry matter), P, and organic carbon but is rich in

ammonium N (40-80% of the initial N) [45, 60, 69]. Sludge centrate with very high concentrations of soluble nutrients (i.e. 1,100 mg/L NH_3-N and 500 mg/L PO_4^{3-}) is favourable for subsequent recovery (Table 2) [11, 70]. The possible technologies for nutrient recovery from sludge centrate include ammonia stripping, chemical precipitation, adsorption and ion exchange, phycoremediation, and membrane-based processes (Figure 8) [45, 46, 56, 66].

Mechanical separation using a screw press, and centrifuge is extensively applied in full-scale applications [46]. Screw presses are usually selected for dewatering fibrous substrate-derived digestate while the centrifuge is adopted for non-fibrous feedstock. In general, a screw press is cheaper than a centrifuge due to less energy consumption [46, 71]. In practice, flocculants/coagulants such as $Al_2(SO_4)_3$, $FeCl_3$, $Fe_2(SO_4)_3$, $Ca(OH)_2$, and cationic polymers are mixed with digestate prior to the mechanical separation to improve separation efficiency for further improvement in subsequent nutrient recovery [72]. Adding precipitating additives, such as $FeCl_3$ and $CaCO_3$ could improve the dewatering efficiency from 46% to 75% [72]. Chen et al. used a template copolymer of acryloxy trimethylammonium chloride and acrylamide for dewatering sludge from a WWTP and achieved a filter biosolids cake moisture content of 74.7% at the polymer dosage of 40 mg/L [73].
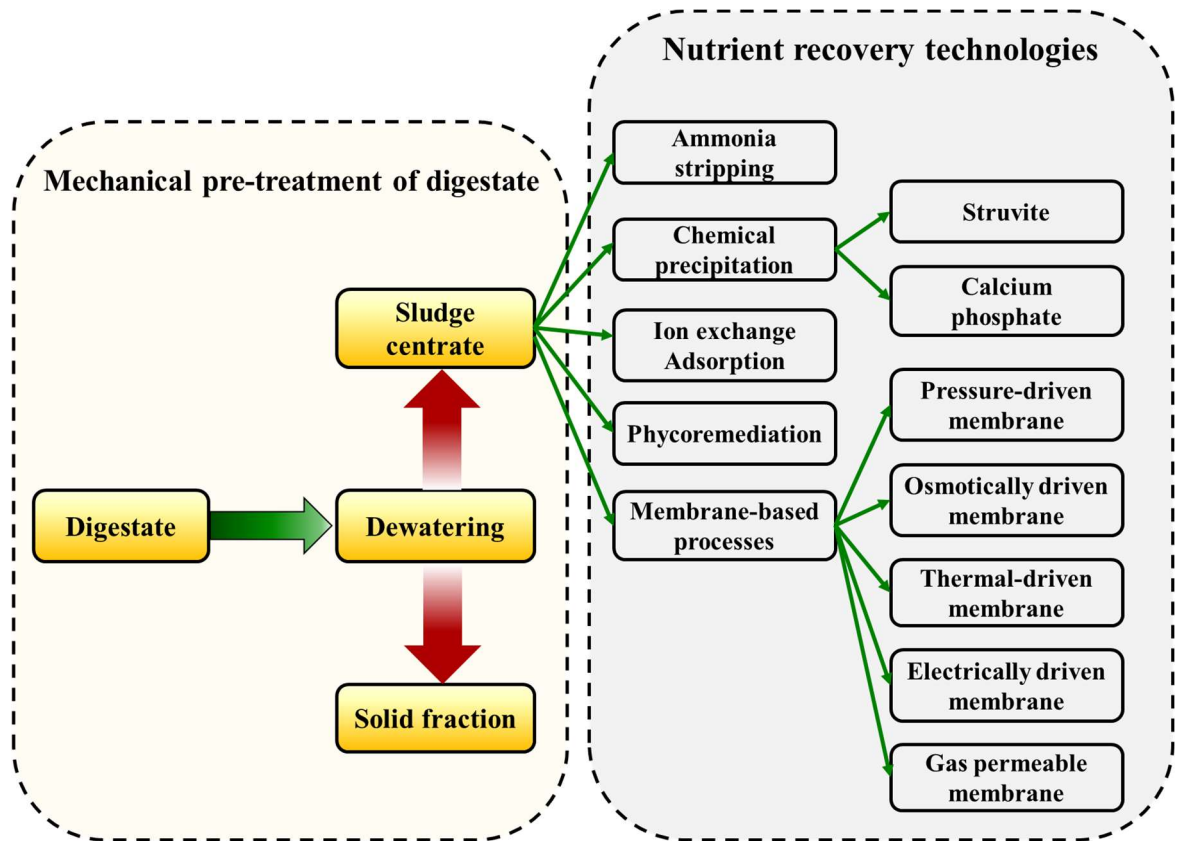
Figure 8: Overview of the latest technologies available for nutrient recovery from digestate.

Table 2. Typical compositional characteristics of sludge centrate from WWTPs [10, 11, 70, 74].

Parameter	pH (-)	Total solids (g/L)	NH_3-N (mg/L)	PO_4^{3-} (mg/L)	Ca (mg/L)	Mg (mg/L)
Value	7.6 – 7.8	1.2 - 1.7	486 - 1141	284 - 421	49 - 65	5.8 - 20

2.3. Technologies for phosphorus removal and recovery from sludge centrate

2.3.1. Hierarchy for phosphorus preservation

There are a variety of technologies for P management from immobilisation to recovery for slow release P fertilisers (e.g. struvite). In general, the cost of treatment and recovery increases as the P content in the waste stream decrease (Figure 9). The PO_4-P content of 50 mg/L has been suggested in the literature as the threshold for considering P recovery [43]. P concentration in wastewater determines the treatment method. In practice, economic viability of P recovery depends on many factors and will increase significantly as the PO_4-P content increase beyond 50 mg/L. At the PO_4-P content below 50 mg/L, indirect P recovery may still be possible using wetland and microalgae cultivation for P uptake and subsequent utilisation. These indirect P recovery processes are primarily to polish and remove P from environmental water to avoid eutrophication.

P recovery results in both financial and environmental benefits. Revenue from recovered P products (e.g. struvite and calcium phosphate as fertilisers and elementary P for the high-tech industries) can compensate for recovery cost. It has been established that the demand (therefore cost) for chemical (e.g. calcium and magnesium) addition per unit of recovered P is inversely proportional to P content in the waste stream. At a low level of P, the application of wetland, microalgae cultivation, and adsorption technologies is less cost-effective given the large footprint and water requirements and low value of products obtained after treatment [18]. In these cases, environmental benefits can justify for P recovery and removal. For example, water quality benefits from P removal is estimated at 9,000 $AUD/kg by the Department of Environment and Conservation NSW [75].

Given the aforementioned discussions, increasing the P level in sludge centrate through an enrichment process is necessary to reduce the cost for recovery process. The P recovery as struvite or calcium phosphate usually requires the addition of external chemicals due to low levels of calcium and magnesium in sludge centrate. Thus, higher level of P in sludge centrate can result in the reduction of chemical amounts added to the solution for the recovery process, thus further decreasing the chemical cost.
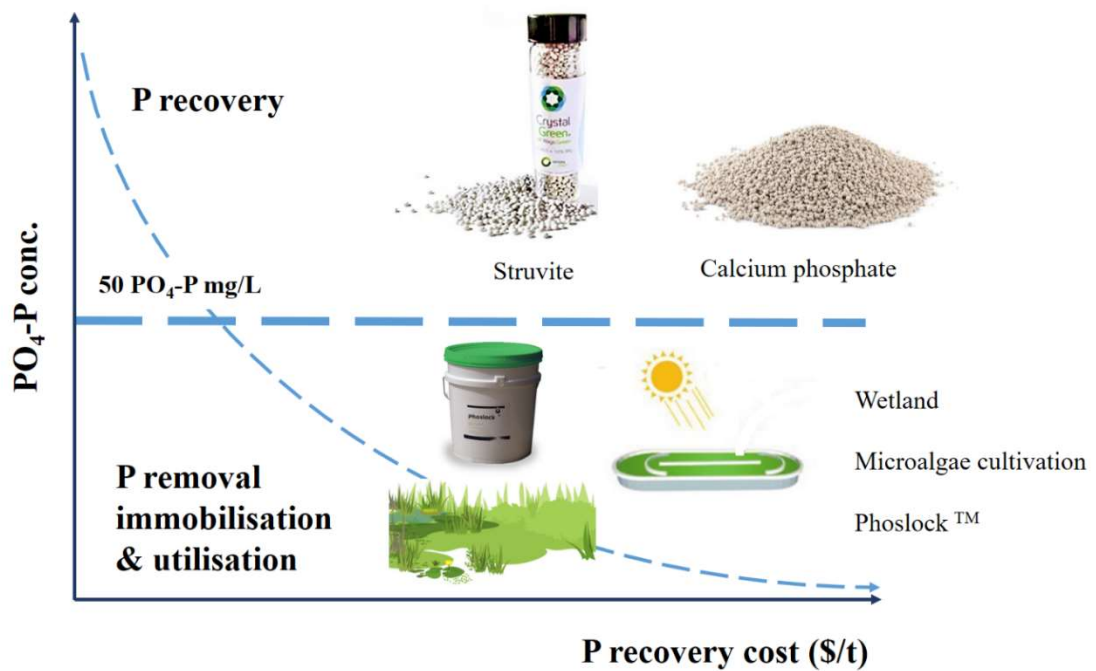
Figure 9: A proposed schematic diagram for P management with respect to different ranges of P input concentrations in the liquid phase [18, 43, 76].

2.3.2. Phosphorus removal and recovery from sludge centrate

2.3.2.1. Major processes for phosphorus recovery

Sludge centrate is a highly complex waste stream, whereby the development of a complete integrated system is crucial to maximise the efficiency of the recovery process and minimise its impacts on the environment. P recovery from sludge centrate can be accomplished in four sequential steps, namely pre-treatment, enrichment, recovery (i.e. extraction), and post-treatment (Figure 10). The pre-treatment of sludge centrate aims at

facilitating the subsequent enrichment and recovery process via the removal of suspended solids and the simple modification of sludge centrate chemistry. Sand filtration, microfiltration (MF), and ultrafiltration (UF) could be applied as the pre-treatment techniques. Enrichment is an optional step to increase the P level in sludge centrate and reduce the demand (thus costs) of chemical addition for subsequent recovery by precipitation. High rejection membrane processes such as reverse osmosis (RO), nanofiltration (NF), forward osmosis (FO), membrane distillation (MD), and electrodialysis (ED), hydrophobic gas-permeable membrane could be considered for pre-concentrating P prior to recovery. After the enrichment process, P is recovered using phosphate precipitation in the form of struvite or calcium phosphate. Finally, post treatment is applied to the recovery process effluent to remove the residual P prior to effluent discharge. As discussed in section 2.3.1, the use of adsorption and biological processes (i.e. wetlands and microalgae cultivation) to immobilise P for beneficial utilisation is preferred at a low level of P. The post treatment as a polishing step is needed to remove the residual P from the recovery process effluent.
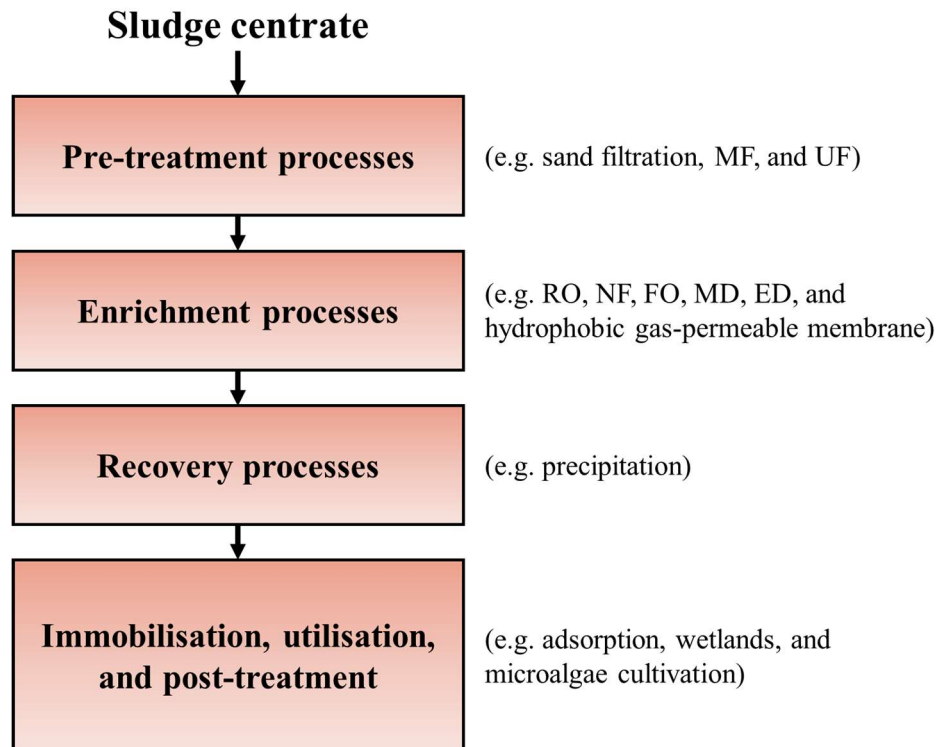
Figure 10: Schematic diagram showing major steps in P removal and recovery from sludge centrate.

2.3.2.2. Pre-treatment

Pre-treatment by CO_2 stripping could make the chemistry of the sludge centrate (i.e. pH) favourable for subsequent P recovery. CO_2 stripping has been applied as a pre-treatment step in full-scale nutrient recovery plants [77]. In this process, sludge centrate is aerated to strip dissolved CO_2 out of the solution, thereby increasing the solution pH and facilitating the subsequent nutrient recovery via precipitation.

Sand filtration and membrane-based processes could be used to avoid interference with P precipitation and prevent membrane fouling during the enrichment process. These pre-treatment techniques rely on their capability of removing suspended solids from sludge centrate. The total suspended solid (TSS) content in sludge centrate varies in the range of 100-250 mg/L [74, 78]. The TSS level is strongly related to fouling severity when the nonporous membranes (e.g. RO and FO) are used to enrich P in sludge centrate. It is

19

reported that membrane fouling could cause increased filtration time, high-energy consumption, and reduced enrichment efficiency. Hence, removing TSS can alleviate these issues. Sand filtration is a simple and cost-effective technique using a sand bed as a roughing filter to remove large-sized impurities. The porous membrane-based processes (e.g. MF and UF) have been widely used to separate solids from the solution these days. It is demonstrated that complete TSS removal could be achieved using MF and UF due to the size exclusion effect [70]. Once membrane fouling is still an inherent issue of these processes, sand filtration followed by MF or UF filtration could be a feasible configuration for an effective solid removal. The pre-treated sludge centrate with very low TSS content can enhance the efficiency of the enrichment process.

2.3.2.3. Phosphorus enrichment

High rejection membrane processes (e.g. RO and NF) can be applied to enrich P in wastewater before the recovery process. NF can achieve 5 - 23% NH_4^+ and 90 – 98% PO_4^{3-} rejections [46, 79]. In RO, the separation efficiency of these ions can achieve 99 – 100% [46]. Nutrients can be recovered from these ammonium and phosphate concentrated streams by using ammonia stripping or precipitation. However, using a pressure-driven membrane process for nutrient recovery from highly complex wastewater (e.g. anaerobic digestate and sludge centrate) has not yet been applied at a commercial scale due to membrane fouling and significant energy requirements [80]. These membrane processes often suffer from irreversible fouling and have a short membrane lifetime [81, 82]. Thus, recent research has also explored the use of FO, which is an osmotically driven membrane process to enrich P in sludge centrate [11, 78, 83]. In addition, the use of MD and ED for nutrient enrichment and recovery from sludge centrate has been recently demonstrated [84-86].

The potential of FO for pre-concentrating wastewater and sludge centrate for subsequent resource recovery has been demonstrated in several recent studies [10, 11, 78, 87]. In the FO process, only water is transported through a semipermeable membrane from a feed solution (e.g. sludge centrate) to a draw solution (i.e. a high salinity solution) due to the difference in osmotic pressure of these two solutions, which leads to increased nutrient contents in sludge centrate (Figure 11). Unlike the pressure-driven membrane technologies, the fouling layer on the FO membrane surface is not compacted, thus, is readily reversible by hydraulic flushing or osmotic backwashing [11, 88]. Several studies demonstrated the feasibility of using FO to concentrate sludge centrate with high enrichment factors [74, 78, 89]. Xie et al. demonstrated five times pre-concentration of sludge centrate using FO driven by $MgCl_2$ draw solution [89].
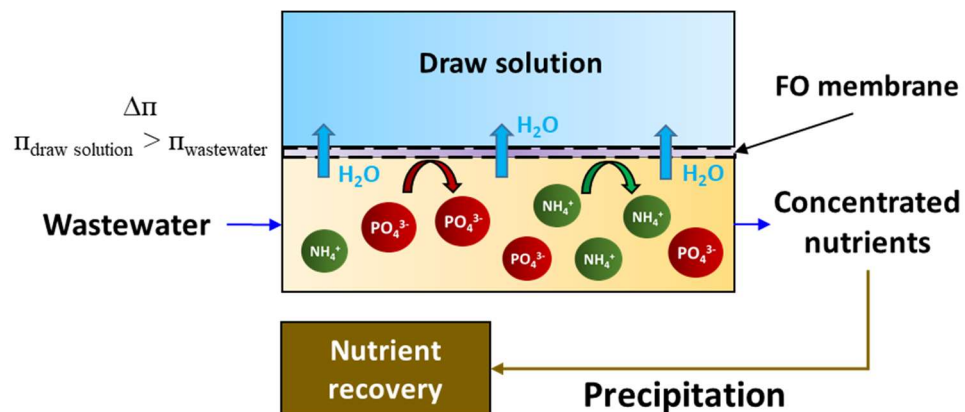
Figure 11: The schematic diagram of the FO-based system for nutrient recovery.

Unlike FO, the enrichment of nutrients (ammonium and phosphate) for subsequent recovery using ED is an electrically driven membrane process (Figure 12) [86, 90]. In this process, the transportation of nutrients in the bulk feed is oriented by an electrical field produced by a cathode and an anode. Under the direct current, cations (i.e. NH_4^+-N) move towards the cathode, while anions (PO_4^{3-}) move to the anode [46]. PO_4^{3-} ions are enriched at the anode chamber, while NH_4^+ ions are driven to the cathode chamber for

their enrichment. The ED process is equipped with ion exchange membranes including cation-selective exchange membranes, anion-selective exchange membranes, and bipolar membranes [86, 90]. It is reported that NH_4^+-N content in sludge centrate could be concentrated to $16 - 21$ g/L using ED [46, 58]. This figure is even much higher than that obtained from RO. The combination of ED process and chemical precipitation can recover over 80% of phosphate under the form of calcium phosphate precipitates [91]. It is also indicated that struvite precipitation using the P-rich effluent from the ED process can achieve high P recovery efficiency (93%) [91]. ED has been applied to recover nutrients from the digestate and sludge centrate in the lab- and pilot-scale [46, 86]. To date, there have been two ED pilot scale systems in Netherland and Australia that reported recovery of ammonium and potassium carbonates from digestate and sludge centrate [46, 86].
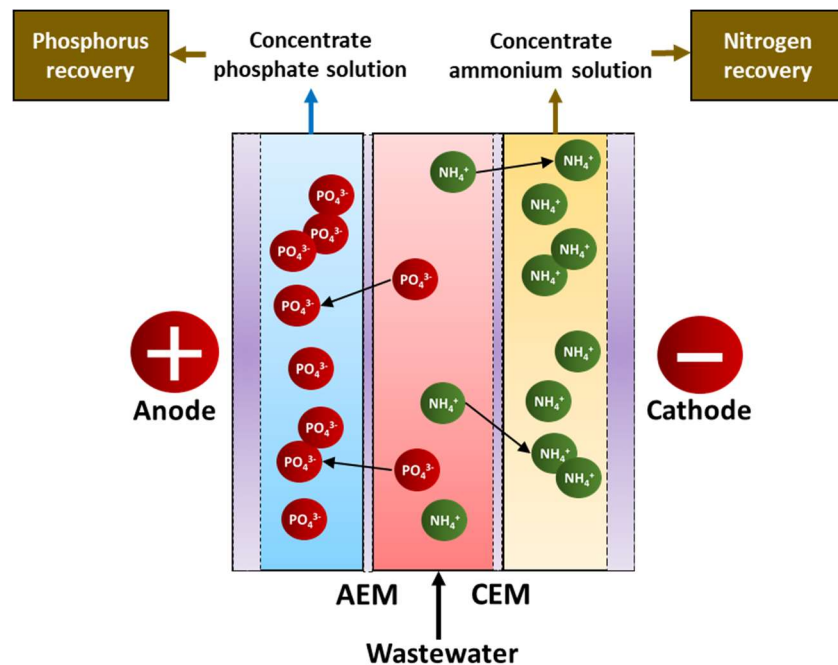
Figure 12: The schematic diagram of the ED-based system for nutrient recovery.

MD can be an option to pre-concentration of sludge centrate for subsequent recovery [46, 58]. The separation and enrichment of nutrients using MD is a thermally driven

process. In MD, the volatile components (i.e. NH_3 and water) in sludge centrate are converted to their gaseous phases before penetrating through the MD membrane to the permeate side, whereas non-volatile components (e.g. PO_4^{3-}) are retained in the feed side of the membrane (Figure 13). The concentrated phosphate stream in the feed side is recovered using precipitation or adsorption. On the permeate side, acidic solutions (e.g. HCl or H_2SO_4) are applied to absorb NH_3 gas for direct fertiliser production. At pH > 9.68 and temperature of 45 °C, ammonium in sludge centrate could be enriched in the permeate up to 18.3 g/L [58]. Ershad et al. reported > 98% P and nearly 100% total ammmonia N removals from sludge centrate using an air gap MD [85].
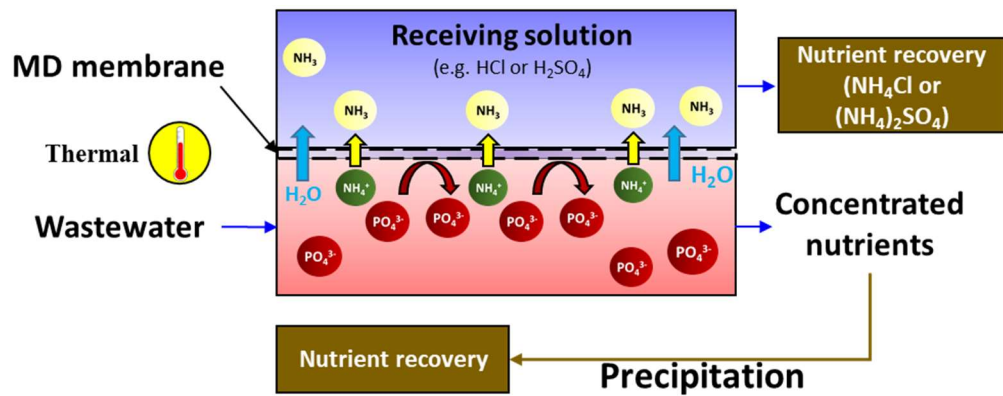
Figure 13: The schematic diagram of the MD-based system for nutrient recovery.

Hydrophobic gas-permeable membrane technology is intended for ammonia recovery but can be used for P recovery as a secondary purpose [92, 93]. In this system, the ammonium-ammonia balance shifts towards ammonia gas under an alkaline environment (Figure 14). Ammonia gas is transported through the membrane due to the difference in NH_3 concentration between the two sides of the membrane, and phosphate ions are retained on one side of the membrane [93]. This gradient remains constant due to the continuous reaction of NH_3 gas with sulphuric acid to form ammonium sulfate on the other side of the membrane. Hasanoglu et al. successfully demonstrated the feasibility of

using a macroporous hydrophobic membrane for ammonia recovery as $(NH_4)_2SO_4$ [92]. The concentrated phosphate stream on one side of the membrane can be used as feedstock for the recovery process via precipitation or adsorption.
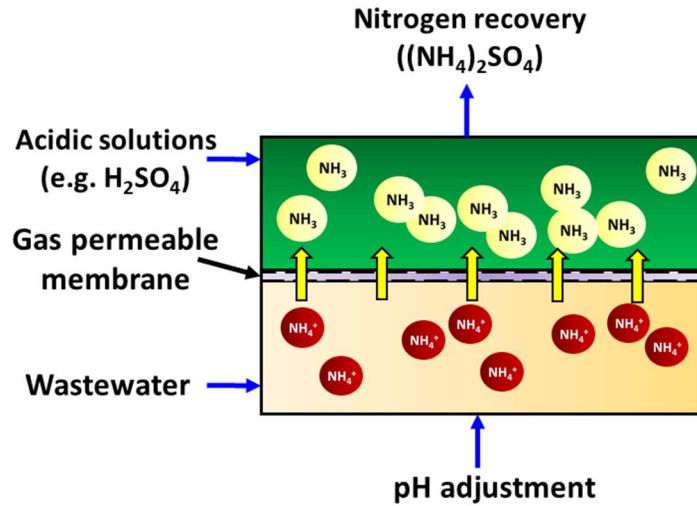
Figure 14: Gas-permeable membrane principle for nutrient recovery.

2.3.2.4. Phosphorus recovery

Chemical precipitation is a core component of P recovery technology. Indeed, chemical precipitation is used in most commercially available technologies for P recovery from anaerobic digestate and sludge centrate (Table 3). P can be precipitated for separation from the aqueous phase in the form of calcium phosphate or struvite. In commercially available technologies, P precipitation is achieved in either a continuously mixed tank (e.g. NuReSys® process) [94] or a fluidised bed reactor (e.g. Pearl™ process) [95]. The precipitated P can be readily settled for separation from the remaining liquid. These precipitates can be used directly as fertilisers or further purified for other industrial applications. The formation of P precipitates can be expressed in the following reactions:

$$10Ca^{2+} + 6PO_4^{3-} + 2OH^- \rightarrow Ca_{10}(PO_4)_6(OH)_2\downarrow$$

$$Mg^{2+} + NH^{4+} + H_nPO_4^{3-n} + 6H_2O \rightarrow MgNH_4PO_4.6H_2O\downarrow + nH^+, \text{ where } n - 0, 1 \text{ or } 2$$

To facilitate struvite precipitation, the addition of magnesium and caustic soda into digestate or sludge centrate is required for the occurrence of the reaction. The optimum pH for struvite precipitation is in the range of 8.5-9.5 [22, 58, 96]. Due to the continuous release of protons during the struvite formation, the continuous supply of alkali is needed to maintain the pH in a suitable range for struvite precipitation. In addition to pH, the molar ratio of magnesium to ammonium to phosphate significantly affects the struvite formation efficiency and its purity. At the optimum magnesium to ammonium to phosphate ratio of 1.6:0.6:1.0, between 85-97% of P can be recovered via struvite precipitation [97]. In sludge centrate, ammonium and phosphate are abundant while magnesium content is insufficient to ensure an effective reaction [98]. For this reason, a magnesium source in the form of $MgCl_2$, $MgSO_4$, MgO, or $Mg(OH)_2$ is added into anaerobic digestate [99, 100]. As a high cost commodity, magnesium addition can account for 75% of total costs of struvite production from waste and wastewater [46]. Several studies have explored the use of low-grade thus cheaper magnesium sources such as seawater and bittern to reduce the cost of P recovery via struvite precipitation [98, 99].

P recovery in the form of calcium phosphate is an alternative to struvite [46, 101-103]. Instead of adding magnesium to form struvite, calcium (which is a much cheaper chemical) is added to induce calcium phosphate formation. The amount of $Ca(OH)_2$ required will regulate the operational costs of this precipitation process. The pH range of 8-11 is most favourable for the calcium phosphate precipitation [103]. CO_2-stripping could be carried out prior to precipitation to prevent the competing formation of calcium carbonate. P recovery efficiency of 50-90% can be achieved via calcium phosphate [45].

Table 3. Current commercial full-scale technologies for P recovery from digestate and sludge centrate.

Input materials	Process	Developer/ location	Recovery principles	Product
Sludge centrate	Ostara Pearl	Ostara, Canada	Precipitation/ crystallisation	Struvite
Sludge centrate	MagPrex^{TM}	Centrisys/CNP, USA	Precipitation/ crystallisation	Struvite
Sludge centrate	Crystalactor^{TM}	Royal HaskoningDHV, Netherland	Precipitation/ crystallisation	CaP
Sludge centrate	Phosnix	Unitikia Ltd., Japan	Precipitation/ crystallisation	Struvite
Sludge centrate	Seaborne Gifhorn	Seaborne Environmental Research Laboratory, Germany	Precipitation/ crystallisation	Struvite
Sludge centrate	Struvia	Veolia Water	Precipitation/ crystallisation	Struvite
Sludge centrate / digestate	ANPHOS$^{®}$	Colsen, Netherland	Precipitation/ crystallisation	Struvite
Sludge centrate / digestate	PHOSPAQ^{TM}	Paques, Netherland	Precipitation/ crystallisation	Struvite
Sludge centrate / digestate	NuReSys	Nutrient Recovery Systems, Belgium	Precipitation/ crystallisation	Struvite

2.3.2.5. Immobilisation, utilisation, and post treatment

After the recovery process, the post treatment is required to quench the residual P (i.e. below 50 mg/L) from the exhausted solution before effluent discharge. Under the circular economy perspective, P recovery could be conducted via recycling and utilisation of P-contained products after the post treatment. At a low level of P in the recovery process effluent, the treatment technologies using adsorption and biological processes (e.g. wetlands and microalgae cultivation) are preferred in consideration with the economic viability.

2.3.2.5.1. Immobilisation, utilisation, and post treatment via adsorption

Adsorption has been widely used to capture P from wastewater at the low level [18, 46]. This method relies on the ion selective retention ability of active sites of sorbents (e.g. biochars [104, 105], steel-making slag [106], red mud [107], and activated carbon [108]). After the adsorption, these sorbents can be either used directly as fertilisers or reused for other applications, thus P recovery. Biochars produced by thermal treatment of organic waste materials (e.g. coconut shell, rice straw, bamboo wood, corn stalk, and iron-rich sludge) could be used to capture P in an aqueous solution [96, 104, 105]. The P capturing capacity of biochars results from the presence of Mg, Ca, and Fe in their composition [96, 104]. The P-captured biochars could be composted and then used as fertilisers, thus P recovery.

Recently, the use of secondary or by-products from industry (e.g. fly ash, coal cinder, and blast furnace slag) as absorbents for nutrient removal and recovery have been attracting more attention due to the cost reduction and provision of a new application for what often considered as wastes. A typical example of using an industrial by-product as an absorbent is slag from steel-making industry. There are two types of steel-making slag including basic oxygen furnace (BOF) slag and electric arc furnace (EAF) slag. BOF-slag

is produced from the iron refining process in BOF, while EAF-slag is generated from the melting process of recycled scrap in an EAF [109]. Steel-making slag primarily involves heterogeneous metal oxides (e.g. CaO, Fe_2O_3, Al_2O_3, and SiO_2) [110]. The presence of these metal oxides makes steel-making slag an ideal adsorbent for P immobilisation via adsorption [106, 111]. Indeed, steel-making slag has demonstrated its effectiveness in removing P from an aqueous solution [106, 112, 113]. The weathered and stabilised steel-making slag after P removal could be used as an aggregate for asphalt roads [113].

The P removal and recovery efficiency by adsorption is governed by sorbent properties, physicochemical characteristics of sludge centrate, and operating conditions [45, 114]. Sorbents with high surface area, high porosity, and more reactive sites are beneficial for the treatment process. In addition, the key characteristics of sludge centrate, such as initial suspended solid and nutrient concentrations, temperature, pH, and presence of other competitive ions need to be taken into consideration when applying this technology. Fouling of the sorbent bed due to the high suspended solid in sludge centrate and the competition of other ions (e.g. Mg^{2+}, Ca^{2+}, Cl^-, SO_4^{2-}, and CO_3^{2-}) in this stream are challenges of this approach. To date, the application of adsorption in P recovery has been mostly implemented in lab-scale [45, 106]. Further investigation into the process efficiency at pilot-scale is necessary. The costs of this technology are subject to the sorbent materials used, pre-treatment of the influent, and methods and frequency of regeneration.

2.3.2.5.2. Immobilisation, utilisation, and post treatment via microalgae cultivation and biomass production

The use of microalgae to uptake P for biomass production could be a cost-effective and environmentally friendly approach for P recovery from wastewater at a low level [18, 45, 55, 56]. Microalgae are photoautotrophic microorganisms that can be capable of using

inorganic carbon (i.e. CO_2), light energy, and nutrients (e.g. N and P) to produce biomass via its metabolism. P is taken up as orthophosphate and stored as polyphosphate granules (Figure 15) [18]. These phosphorous compounds are utilised for the growth process when there is a P shortage in the environment [18]. Where inorganic orthophosphate is unavailable, the enzyme phosphatase of microalgae can be able to convert organic P in the aquatic environment to orthophosphate at the cell surface [115]. Microalgae biomass is then harvested, whereby P is extracted from an aqueous solution. Microalgae biomass can be directly applied to the field or used as feedstock for other processes (e.g. biochemical and biofuel productions) [56]. The abundance of nutrients in sludge centrate is beneficial for microalgae cultivation. Once the nutrient usage alone accounts for 50% total cost of microalgae cultivation, using sludge centrate as an alternative for nutrient supply is expected to reduce significantly the cost of cultivation [56]. The feasibility of using microalgae to remove P and produce algal biomass from wastewater has been demonstrated in lab- and pilot-scale studies [70, 116, 117]. For example, it is reported that approximately 90% of P could be removed and recovered via algal biomass production when multi-culture of *Chlorellaceae*, *Scenedesmaceae*, *Chlamydomonadaceae* is used to treat piggery farm wastewater in a pilot-scale high rate algal pond.
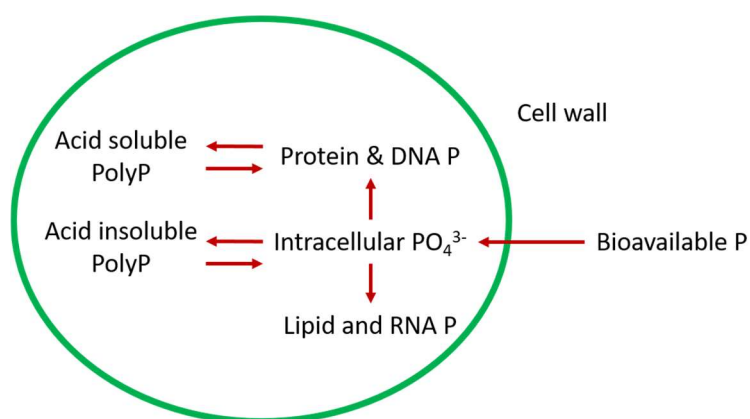
Figure 15: P transport and storage associated with microalgal cells [18].

Microalgae can be cultivated photoautotrophically, heterotrophically, and mixotrophically, which is dependent of the carbon source for their growth [56, 70]. In autotrophic metabolism, microalgae use inorganic carbon (e.g. CO_2) as a carbon source and sunlight as an energy source to produce the essential organic compounds. In heterotrophic cultivation, microalgae use organic carbon for their metabolism under dark conditions. In the presence of both organic and inorganic carbon, microalgae can be capable of using these carbon sources for their growth under the mixotrophic mechanism. Thus, sludge centrate with plenty of organic and inorganic carbon can promote the mixotrophic growth of microalgae.

The nutrient uptake capacity of microalgae hinges on the extent of microalgae growth. The growing rate of microalgae is affected by abiotic and biotic factors (Table 4) [25, 115, 118]. The growth of *Chlorella sp.* has been reported to decrease as the concentrations of N and P reduced to 31.5 and 10.5 mg/L, respectively [119]. The optimal temperature for most microalgae is in the range of 20 – 30ºC [120]. pH ranges from 6 to 8.76 is favourable for the growth of microalgae [120].

Table 4. Factors that influence the growth of microalgae [121-123].

Abiotic factors	Biotic factors	Operating conditions
Light (wavelength and intensity)	Pathogens (bacteria, protozoan, fungi, viruses)	Mixing (type and intensity) and light: dark cycle
CO_2 loading, temperature, pH, salinity, and toxic chemicals	Predation in zooplankton	Cultivation configurations and operation modes (i.e. batch, semi-continuous, and continuous)
Carbon sources; macro-nutrients and micro-nutrients	Competition between species	Harvesting frequency

Several studies have been conducted using microalgae-based treatments in photobioreactors for simultaneous nutrient recovery and biomass production from sludge centrate. Many types of microalgae, such as freshwater microalgae (e.g. *Chlorella pyrenoidosa*, and *Chlorella sorokiniana*) and marine microalgae (e.g. *Nannochloropsis salina* and *Phaeodactylum tricornutum*) can grow well in sludge centrate [56]. Sayedin et al. demonstrated that *Chlorella sorokiniana* could grow well and remove 95% and 78% of N and P, respectively from anaerobic digestate [124]. However, microalgae-based technology normally requires high hydraulic retention time, thus a high footprint due to the slow kinetics of microalgae growth. Consequently, it has been rarely commercially applied for removing nutrients from wastewater [55]. The aforementioned challenge can be addressed by integrating the microalgae system with a membrane separation (e.g. UF) to form a membrane photobioreactor. In the membrane photobioreactor, a high microalgal

biomass concentration resulting from the excellent retention of the membrane can reduce the hydraulic retention time for the assimilation process, thereby decreasing the footprint required.

2.3.2.5.3. Immobilisation, utilisation, and post treatment via constructed wetlands

Constructed wetland can also immobilise P through a combination of physical, chemical, and biological processes [125-127]. These processes involve sedimentation, photolysis, hydrolysis, microbial degradation, adsorption, and plant uptake. It is difficult to separate the P removal efficiency of the individual process as constructed wetland is a complex ecology. The presence of different types of substrates (e.g. biochar, fly ash, steel-making slag, and alum sludge) in constructed wetlands allows for P removal mostly via adsorption [128]. P is biologically removed from wastewater in wetlands through the plant and microorganism uptake and metabolism processes [129]. The effectiveness of using constructed wetlands in P removal has been demonstrated at all treatment scales [18, 130-132]. A full-scale constructed wetland treating wastewater in Indonesia has shown 90% phosphate removal [131].

The P removal efficiency of constructed wetlands depends on the type of substrates, plants, construction sites, and operating design parameters (e.g. water depth, hydraulic load, retention time, and inlet distribution regime) [127-129]. The most widely used substrates in constructed wetlands for nutrient removal include gravel, zeolite, and slag (i.e. steel slag and coal slag) [129]. Adding additives such as Ca, Mg, Al, and Fe could enhance the nutrient removal efficiency [128, 129]. Of these additives, calcium has been demonstrated to have a maximum enhancement of nutrient removal [129]. Plants used in constructed wetlands can be classified into three groups (i.e. emergent plants, submerged plants, and free-floating plants with over 150 different species [129]. However, local plants should be prioritised to avoid invasion of alien species. Factors, such as

32

topography, geography, soils, hydrography, and rainfall should be taken into consideration when a site is selected to construct wetlands. In addition, water depth is a critical parameter affecting the water load and oxygen permeability. Constructed wetlands at depth of 0.27 m illustrate better performance compared to those of 0.5 m [133].

2.4. Summary

This chapter provides an overview of the key information related to P removal and recovery from sludge centrate. At first, the chapter highlights the vital role of P in economy, sources of P supply, alarming depletion of global P reserves, and urgent need to find out an alternative for renewable P supply followed by removal and recovery process to compensate for the P deficit. Subsequently, the chapter presents the origin and compositional characteristics of sludge centrate to emphasise the potential for P recovery. The chapter also provides a summary of the state of the art technologies for P removal and recovery. These technologies are systematically discussed and analysed with respect to a threshold PO_4-P content of 50 mg/L in order to develop a roadmap towards sustainable and economically viable P management. P recovery is usually accomplished in four sequential steps, namely pre-treatment, enrichment, recovery (i.e. extraction), and post-treatment. Chemical precipitation is a core component of P recovery technology and is the most commonly applied method in the commercial recovery systems. Further research converging on the innovations for pre-treatment, enrichment, and post-treatment is necessary to complement chemical precipitation for enhancing the efficiency of P recovery.

Chapter 3. Forward osmosis pre-concentration of sludge centrate for subsequent phosphorus recovery

This chapter has been published as: *M.T. Vu, L.N. Nguyen, M.A. Hasan Johir, X. Zhang, L.D. Nghiem, M. Elimelech, Biogas sparging to control fouling and enhance resource recovery from anaerobically digested sludge centrate by forward osmosis, Journal of Membrane Science (2021) 119176.*

3.1. Introduction

Anaerobic digestion is extensively applied to treat organic wastes such as sewage sludge, food waste, and crop residue and produce energy in the form of biogas [134, 135]. In addition to biogas, anaerobic digestion also generate a liquid stream known as sludge centrate and a solid product commonly called biosolids [136]. The sludge centrate is rich in nutrients (i.e. ammonia and phosphate), thus, must be returned to the head of work for treatment or treated separately [88].

Sludge centrate from anaerobic digestion is both a problem and an opportunity. Returning sludge centrate to the head of work results in the accumulation of nutrients, possible nutrient overloading and potential struvite blockage [11]. Uncontrolled nutrient release to the aquatic environment can cause eutrophication and even harmful algae blooms [137]. On the other hand, the high ammonia and phosphate content in sludge centrate makes it an ideal target for nutrient recovery for fertilizer production and other industrial applications [104, 138, 139].

P can be directly extracted from sludge centrate as struvite, calcium phosphate, or vivianite by chemical precipitation using commercially available processes such as Phosnix, Ostara, and P-RoC. The efficiency of these commercial processes depends on initial P level. Low level of P requires more chemical addition and longer crystal retention

time, thus higher operational costs. To increase the economics of nutrient recovery, sludge centrate is pre-concentrated prior to chemical precipitation [140]. FO has been identified as an ideal platform for enriching N and P in sludge centrate [5, 140, 141]. Low fouling propensity, high fouling reversibility, and low energy consumption especially when seawater can be used as the draw solution have made FO an ideal technology for pre-concentrating complex and challenging feed solutions without any pre-treatment [5, 142-147]. Numerous FO studies have been recently reported to explore the enrichment of nutrients in sludge centrate for subsequent recovery [10, 11, 87-89].

Previous studies have demonstrated the feasibility of using a seawater-driven FO system to pre-concentrate nutrients and organic matter in sludge centrate for subsequent resource recovery [11, 87]. Seawater is freely available in coastal areas and the spent draw solution can be returned directly to the ocean without further treatment. These studies also highlighted the challenge to control fouling due to the deposition of the phosphate precipitates directly on the membrane surface during the enrichment process. Vu et al. (2019) proposed to buffer the seawater draw solution using acetate to control the increase of sludge centrate pH during the filtration, thus hindering nutrient precipitation [11]. Although they have successfully demonstrated this technique with experimental data, the addition of external chemical (i.e. acetate) into seawater to prevent the increase in the solution pH is unlikely to be economically practical. Thus, it is essential to discover a cost-saving measure to improve the maturity of this technology in resource recovery from sludge centrate.

CO_2 from biogas can provide acidity to the sludge centrate to maintain low pH for fouling mitigation. It is hypothesized that phosphate precipitation and ammonia volatilisation can be prevented by the addition of CO_2 to the sludge centrate prior to the

FO process. In other words, the equilibrium of CO_2 in biogas in aqueous solution can act as a buffer system to maintain low pH of sludge centrate, thereby preventing the formation of phosphate precipitates and ammonia volatilisation. The use of biogas which is plentiful in WWTPs to buffer sludge centrate during the enrichment process brings multiple benefits. The need of external chemical addition is eliminated, thus saving operating costs. The sparged biogas after the buffering process can be upgraded further to produce biomethane. It is envisaged that flue gas or any readily available and low cost CO_2 can also be used to buffer the sludge centrate.

In this work, the effectiveness of using biogas pH buffering in terms of fouling mitigation, organic matter and nutrient enrichment is examined. Major mechanisms governing the biogas buffering of sludge centrate are elucidated and discussed. Results from this study contribute to the current effort to recover nutrients from wastewater and organic waste.

3.2. Materials and methods

3.2.1. Materials

Flat-sheet commercial thin film composite polyamide (TFC PA) membrane was obtained from Porifera, Inc. (Hayward, California, USA). Membrane samples were soaked into deionized (DI) water over night for complete hydration before use. The physiochemical properties of the membrane (i.e. water permeability (A), solute permeability (B), structural parameter (S), NaCl and Ca rejections) were characterized using nanofiltration and FO protocols reported elsewhere [148] and presented in Table 5.

Table 5. Physiochemical properties of the FO membrane.

Parameters	Values
Pure water permeability (L/m^{2}h-bar)	3.1 ± 0.6
Salt (NaCl) permeability (L/m^{2}h)	0.3 ± 0.1
Membrane structural parameter (mm)	0.4 ± 0.1
Observed NaCl rejection (%)	90.1 ± 4.2
Observed Ca rejection (%)	98.2 ± 1.6
Contact angle of active layer (°)	43 ± 1
Contact angle of supporting layer (°)	69 ± 2
Zeta potential at pH 7 (mV)	-18

Seawater collected from Bondi Beach, Sydney, NSW, Australia was used as a draw solution (DS). The obtained seawater was pretreated using 0.45 μm filter paper before use. The filtered seawater has pH of 8.06 ± 0.03 and total dissolved salt of 30 g/L. The concentrations of Ca^{2+} and Mg^{2+} in this seawater were 440 and 1270 mg/L, respectively.

Digested sludge centrate denoted as sludge centrate was obtained from a high speed centrifuge of a WWTP in Sydney and used as a feed solution (FS). Key properties of this sludge centrate are summarized in (Table 6).

Table 6. Characteristics of sludge centrate (values indicated average ± standard deviation of at least three samples).

Parameters	Unit	Sludge centrate
pH	-	7.75 ± 0.04
Electrical conductivity	mS/cm	12.74 ± 0.68
Total solids	g/L	1.2 ± 0.2
COD	mg/L	440 ± 14
Phosphate (PO_4^{3-})	mg/L	421 ± 17
Ammonia (NH_3-N)	mg/L	1141 ± 21
Total N (TN)	mg/L	1368 ± 11
Calcium (Ca^{2+})	mg/L	49.0 ± 3.1
Magnesium (Mg^{2+})	mg/L	5.8 ± 0.3

3.2.2. Anaerobic co-digestion and forward osmosis system

3.2.2.1. Forward osmosis with biogas sparging

The FO system (Figure 16) consisted of an acrylic glass cross-flow membrane cell, two variable speed gear pumps (Micropump, Vancouver, Washington, USA), conductivity meters, and a digital balance to measure the flux. The feed and draw solutions were circulated through the two symmetric rectangular semi-cells of the FO membrane module at the same cross-flow velocity of 12 cm/s in a counter-current mode. The internal dimensions of each semi-cell were 10 cm in length, 2 cm in width and 0.2 cm in height. In other words, the effective membrane area was 20 cm^2. The FO membranes were orientated either in active layer facing the FS (FO mode), or active layer facing the DS (PRO mode).
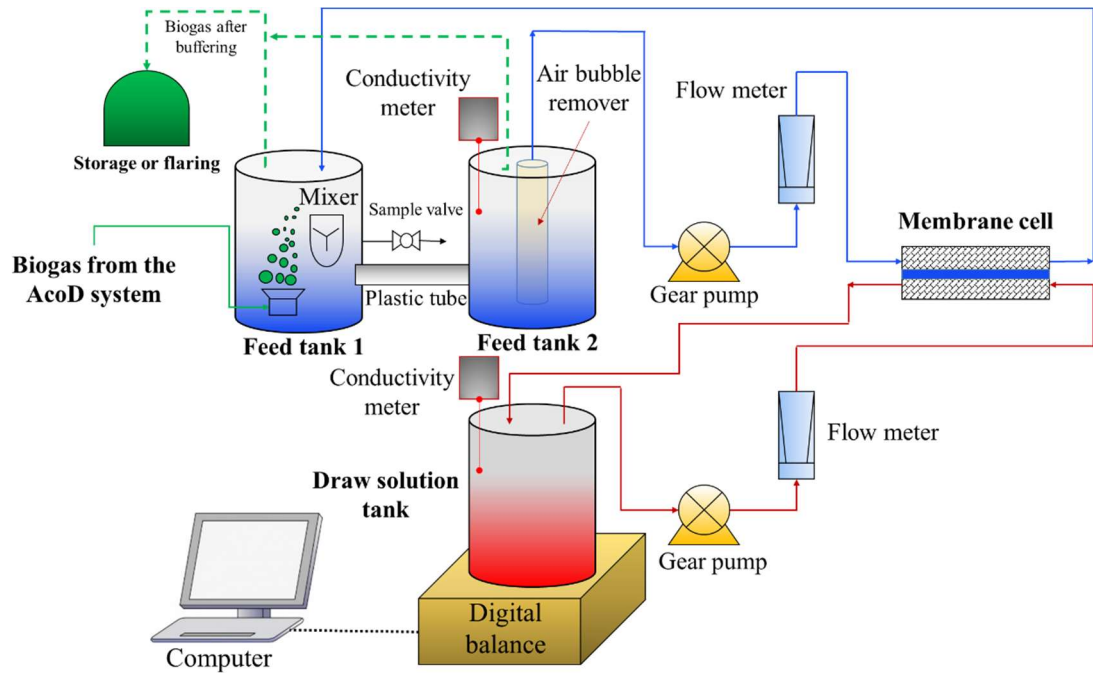
Figure 16: Schematic diagram of an anaerobic co-digestion and forward osmosis system for organic carbon and nutrient enrichment for subsequent resource recovery.

Two cylindrical plastic containers connected via a plastic tube were used to provide FS to the FO membrane cell (Figure 16). In the first feed container (i.e. feed tank 1), agitation and biogas sparging were carried out. The FS was then transferred to the second container where precipitate settling took place to minimize the impacts of agitation on membrane fouling as reported in a previous study [11]. Moreover, this design also reduced the transfer of biogas bubbles to FO membrane cell unit. Biogas from anaerobic co-digestion system was introduced via an air-stone diffuser at the bottom of the feed tank 1. Methane is sparingly soluble in water at about 23 mg/L at 20 ⁰C. In the anaerobic digestion process, the sludge is already saturated with methane gas. Thus, methane loss due to sparging is expected to be insignificant and the remaining biogas can be utilised for beneficial use. In this study, after the buffering process, the remaining biogas is stored in a plastic gas bag for disposal by flaring. The retentate from the membrane cell was returned to the feed tank 1. In the second feed container (i.e. feed tank 2), an air-bubble

39

remover was inserted inside to minimize the interference of air bubbles to the FO system (Figure 16). This bubble remover is a composite mesh with small pores (i.e. pore diameter of approximately 150 μm) in tubular configuration, which allows the passage of liquid, but not air bubbles. The feed solution moving into the membrane cell was withdrawn from the inside of this bubble remover.

3.2.2.2. Biogas production

Biogas was obtained from a small-scale anaerobic digestion (AD) system (Figure 17). The system included a 28 L stainless steel conical reactor, two peristaltic hose pumps (DULCO® Flex from Prominent Fluid Controls, Australia) and a biogas counter (RITTER, MilliGascounter, Germany). A water bath (Thermo Fisher Scientific, Australia) was utilized to maintain the temperature of the anaerobic reactor at 35 ± 0.5 °C by pumping hot water from the water bath through a rubber tube firmly surrounded the reactor. Polystyrene foam and aluminium foil were employed to insulate the reactor.
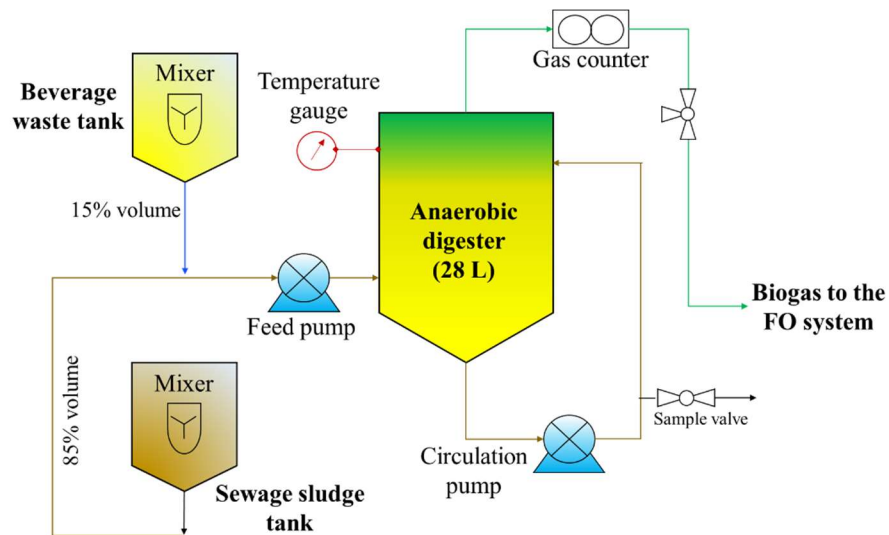
Figure 17: The lab-scale anaerobic co-digestion system.

Raw sewage sludge for anaerobic co-digestion operation was collected from a WWTP in Sydney, Australia. The digested sludge centrate used for seeding the anaerobic digester

was also taken from the same WWTP. After arrival, sewage sludge and beverage waste were preserved at - 4 °C in the dark and used within 2 weeks. Beverage waste was collected from a commercial waste container and used as a co-substrate to ensure a continuous supply of biogas to the FO experiment. This beverage waste is a mixture of soft drinks unsuitable for consumption (e.g. out of date, contamination and damaged packaging). Key properties of the beverage waste and sewage sludge are presented in Table 7.

Table 7. Sewage sludge and beverage waste characteristics (values indicated average ± standard deviation of at least three samples).

Feed stock	COD (g/L)	pH	Total solid (%)	Volatile solid (%)
Sewage sludge	31.7 ± 2.5	5.46 ± 0.29	1.95 ± 0.20	1.76 ± 0.17
Beverage waste	125.8 ± 1.3	4.84 ± 1.12	0.04 ± 0.00	0.04 ± 0.00

The anaerobic digester was inoculated with 15 L of digested sludge from a WWTP in Sydney. Every day, 750 mL of digestate was withdrawn and replaced with the same volume of feed to maintain sludge retention time of 20 days. The anaerobic digester was mixed by sludge recirculation at 30 L/h (i.e. 36 turnover volumes per day) using a hose pump.

In this study, sewage sludge was co-digested with beverage waste to ensure adequate biogas for the FO experiment. After acclimatisation, the reactor was first operated using only the sewage sludge as the substrate (referred to as mono-AD) for 30 days. The organic loading rate during this period was 1.59 (kg COD/m^3.day). From day 31, the system was transitioned to the stage 1 of anaerobic co-digestion (denoted as AcoD-1), in which the digester was operated with a mixture of sewage sludge and beverage waste (95:5 %, v/v)

to obtain an organic loading rate of 1.82 (kg COD/m^3.day) for 30 days. From day 61, ratio between sewage sludge and beverage waste was changed to 85:15% (v/v) to achieve approximately 50% increase in organic loading rate (2.30 kg COD/m^3.day) in the stage 2 of anaerobic co-digestion (denoted as AcoD-2).

3.2.2.3. Forward osmosis experimental design

All FO experiments were performed in four steps at room temperature. In the first step, the membrane pure water flux was determined for 1 hour using DI water as the FS and seawater as the DS. Then, sludge centrate was used as the FS, and the FO experiments were conducted until 60% water recovery to evaluate carbon and nutrient enrichment. Throughout this second step, biogas was continuously sparged into sludge centrate. At specific time intervals, a 5 mL sample was collected from the FS for analyses. In the third step, hydraulic flushing of fouled membrane was conducted through replacing the feed and draw solutions by DI water and increasing the cross-flow velocity to 24 cm/s for 10 min. In the final step, pure water was determined again to evaluate flux recovery. DI water was used as the FS under the same experimental conditions as in the first step. In all FO experiments, initial volumes of feed and draw solutions were 1 and 3 L, respectively. The used high ratio of DS to FS volume aimed at minimizing the dilution effect of the DS during FO operation. The temperature, pH and conductivity of the FS were regularly monitored.

3.2.2.4. Membrane performance

Water flux (J_w) was calculated based on the change in weight of the DS, and expressed as in Eq. (1)

$$J_w = \frac{\Delta m_i}{\Delta t_i \times \rho \times A_m}$$
(1)

In which:

Δm_i: the change in weight of DS over a time interval (g); Δt_i: a time interval (hours); ρ: water density (g/cm^3); A_m: effective membrane area (m^2).

Water recovery was determined based on the ratio of the cumulative permeate volume and the initial volume of the FS, and presented as in Eq. (2).

$$\text{Water recovery (\%)} = \frac{\int_0^t J_w \times A_m \times dt}{V_{initial}} \times 100\% \qquad (2)$$

In which:

J_w: the observed water flux at time t (LMH); $V_{initial}$: initial volume of the FS (L).

Solute rejection by the FO membrane was determined based on the mass balance, and presented as in Eq. (3).

$$\text{Rejection (\%)} = \left(1 - \frac{C_{DS(f)} \times V_{DS(f)} - C_{DS(i)} \times V_{DS(i)}}{C_{FS(i)} \times V_{FS(i)}}\right) \times 100\% \qquad (3)$$

In which:

$C_{DS(i)}$ and $C_{DS(f)}$: the initial and final solute concentrations in the DS, respectively (mg/L); $V_{DS(i)}$ and $V_{DS(f)}$: the initial and final volumes of the DS, respectively (L); $C_{FS(i)}$: the initial solute concentration in the FS solution (mg/L); $V_{FS(i)}$: the initial volume of the FS (L).

3.2.3. Analytical methods

pH, electrical conductivity and temperature were analysed using an Orion 4 – Star pH/conductivity meter (Thermo Scientific, Waltham, MA). COD was measured using a HACH DRB200 COD reactor and HACH DR3900 spectrophotometer following the US-EPA Standard Method 5220. Ammonia (NH$_3$-N) and total nitrogen (TN) were determined using the US-EPA Standard Method 10205 and 10208, respectively and a HACH DR3900 spectrophotometer. Orthophosphate (PO$_4^{3-}$) was measured using ion chromatography (IC) (Thermo Fisher, Australia). The system was prepared with a Dionex

AS-AP autosampler and a Dionex AS19 IC column (7.5 μm pore size, 4 mm diameter and 250 mm length). The sample injection volume was 10 μL. The sample was delivered in an isocratic mode with the hydroxide gradient (time [min]: concentration [mM]) (0-10: 10 10-25: 45; 25-27: 45; 27-30: 10; 31 stop run). The levels of Ca, Mg and other metal ions in sludge centrate were analysed using an Inductively Coupled Plasma-Mass Spectrometry (Agilent 7900 ICP-MS).

The surface characteristics of the FO membranes were characterized using a scanning electron microscopy (SEM) and energy-disperse X-ray spectroscopy (EDS) system (i.e. a Zeiss Supra 55VP SEM and Oxford EDS system). A Bruker V70 Fourier transform infrared spectrometer was employed to test the Fourier transform infrared spectroscopy (FTIR) of fouled membrane samples and the wavenumber range was from 4000 to 600 cm^{-1}. Hydrophilicity of the membrane before and after fouled was characterized by measuring the contact angle using the sessile drop method at different locations. Zeta potential of the membrane was measured using the Malvern zeta analyser.

Biogas production was continuously monitored via the gas counter. The composition of biogas was daily measured using a portable GA5000 gas analyser (Geotechnical Instruments, UK) [149]. Alkalinity, total solid, and volatile solid were determined following the standard method 2320B and 5560C, respectively. Digestate pH was recorded every second day following the aforementioned method.

3.3. Results and discussions

3.3.1. Biogas production

The increase in organic loading rate as a result of co-digestion led to an increase in daily biogas production without any discernible impacts on biogas composition (Figure 18). The high soluble and biodegradable COD content (Table 7) in beverage waste during co-digestion was favourable for biogas transformation. In details, the co-digestion with

45% increase in organic loading rate resulted in almost threefold increase in biogas yield (Figure 18). This observation could be explained by the synergistic effects reported in some previous studies [134, 149].
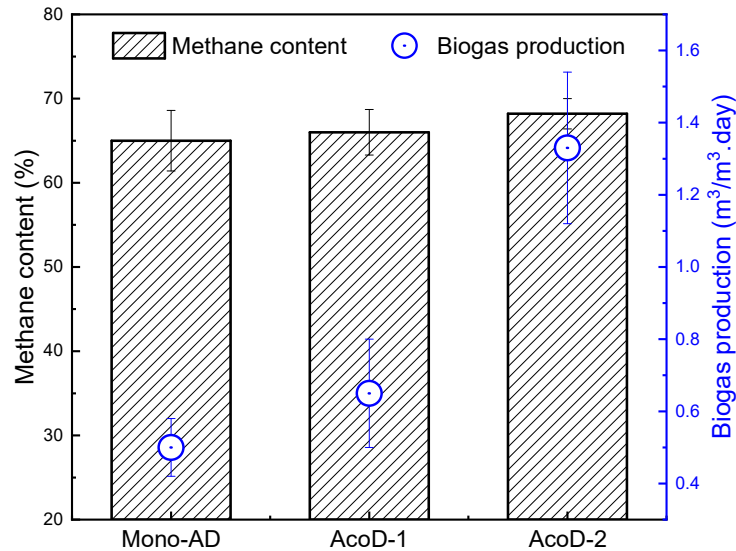
Figure 18: Performance of anaerobic co-digestion system in terms of biogas composition and production. Values and error bars are the mean and standard deviation of at least 20 samples.

Negligible impacts of AcoD on biogas composition are evidenced by a slight increase in methane content compared to mono-AD with only sewage sludge (Figure 18). The increase in methane content appeared to be concurrent with minor improvements in COD and TS removal efficiency (Figure 19). These phenomena could be due to the highly biodegradable organic content in beverage waste as discussed above. These results were consistent with the observations from previous studies that have reported a slightly improved performance of AcoD system in terms of methane content, COD and TS removal [149, 150]. It is noted biogas composition was stable throughout all anaerobic digestion stage. The CO_2 content in biogas was about 35% (Figure 20).
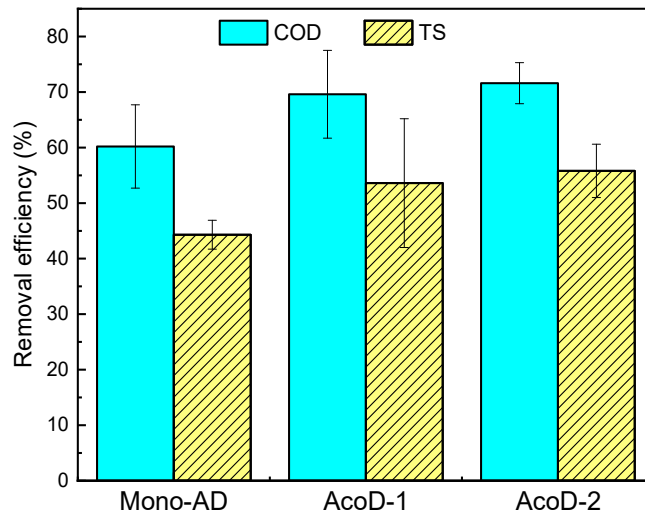
Figure 19: Performance of the anaerobic co-digestion system in terms of COD and TS removal efficiency. Values and error bars are the mean and standard deviation of at least 20 samples.
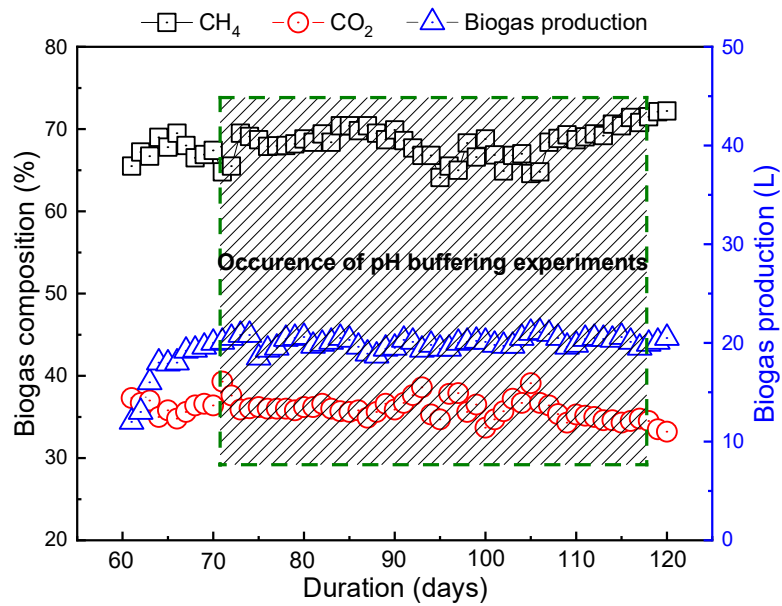
Figure 20: Performance of the anaerobic co-digestion system in the phase AcoD-2 during which the pH buffering experiments took place.

3.3.2. The performance of seawater-driven FO system

3.3.2.1. Water flux and recovery

In all experiments, water flux decline was significant during the enrichment process (Figure 21A). This flux decline was due mostly to the formation of cake layer (i.e. organic matter, inorganic substances and precipitates) on the membrane surface, and the dilution effect of DS caused by the water transportation from the FS to the DS. The results also indicated more severe fouling in PRO mode, compared to FO mode. This consequence resulted from the much higher pure water flux (i.e. 33 LMH), more severe concentration polarization (CP), higher surface roughness of the supporting layer, and more potential occurrence of pore blocking in PRO mode compared with FO mode [87]. FO mode was selected for biogas sparging experiments because this mode showed less membrane fouling than PRO mode.
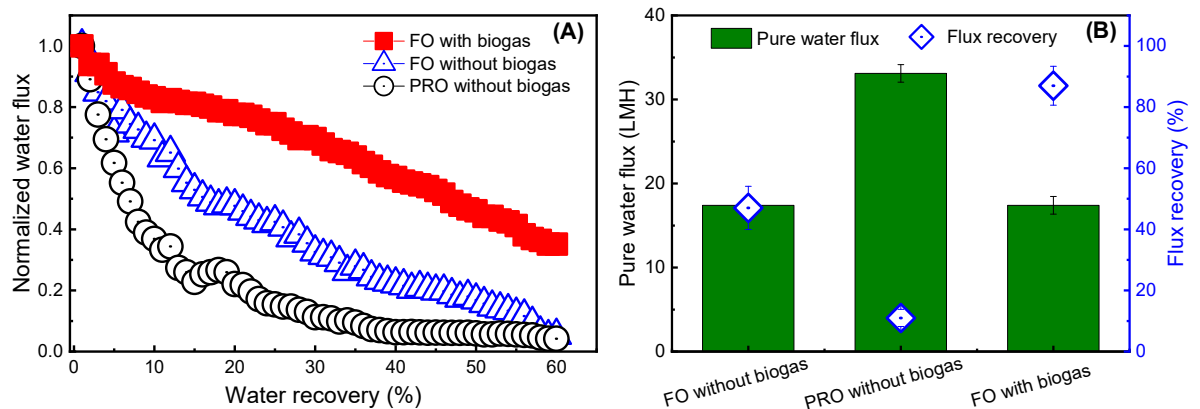
Figure 21: Effects of membrane orientation and biogas purging on (A) water flux and (B) fouling reversibility during seawater-driven FO pre-concentration of sludge centrate. Values and error bars are the mean and standard deviation of two replicate experiments.

Compared to without biogas sparging, the system operated in FO mode with biogas sparging showed significant decrease in membrane fouling (Figure 21A). Without biogas

sparging, water flux declined by over 95% towards both membrane orientations, while this value was only approximately 60% in FO mode with biogas sparging at water recovery of 60%. The decreased membrane fouling in FO mode with biogas sparging could be ascribed to the synergistic effects of smoothness of active layer in FO mode and changes in FS chemistry (i.e. pH and alkalinity). The impacts of FS chemistry modifications on fouling behaviour are discussed further in section 3.3.2.2. Less fouling in FO mode with biogas sparging could be supported by FTIR spectra of the pristine and fouled membrane surface in different experimental conditions (Figure 22).
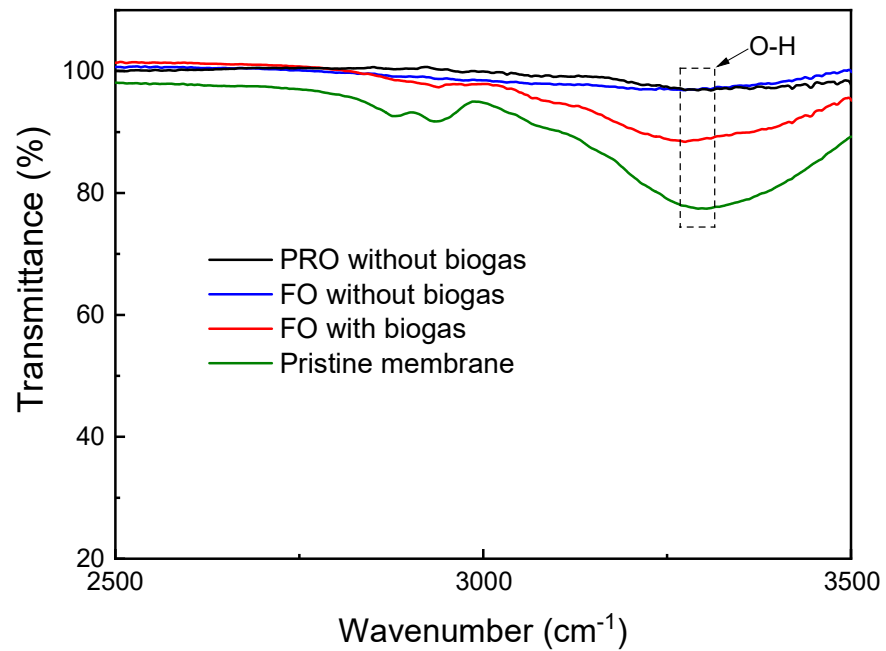
Figure 22: Differences in FTIR spectra of fouled membranes between with and without biogas sparging in different membrane orientations.

The highest flux recovery (92%) by physical flushing using DI water was observed in FO mode with biogas sparging (Figure 21B). The high flux reversibility in this case could be a result of less formation of compact cake layer on the membrane surface as discussed above. Moreover, once the fouled membrane surface was more hydrophilic in FO mode with biogas sparging, compared to the others (Figure 23), the affinity of fouling layer in

this regard upon water was stronger. Thus, increased shear force produced by increasing cross-flow velocity could detach the foulants from the membrane surface, thereby restoring water flux more efficiently.
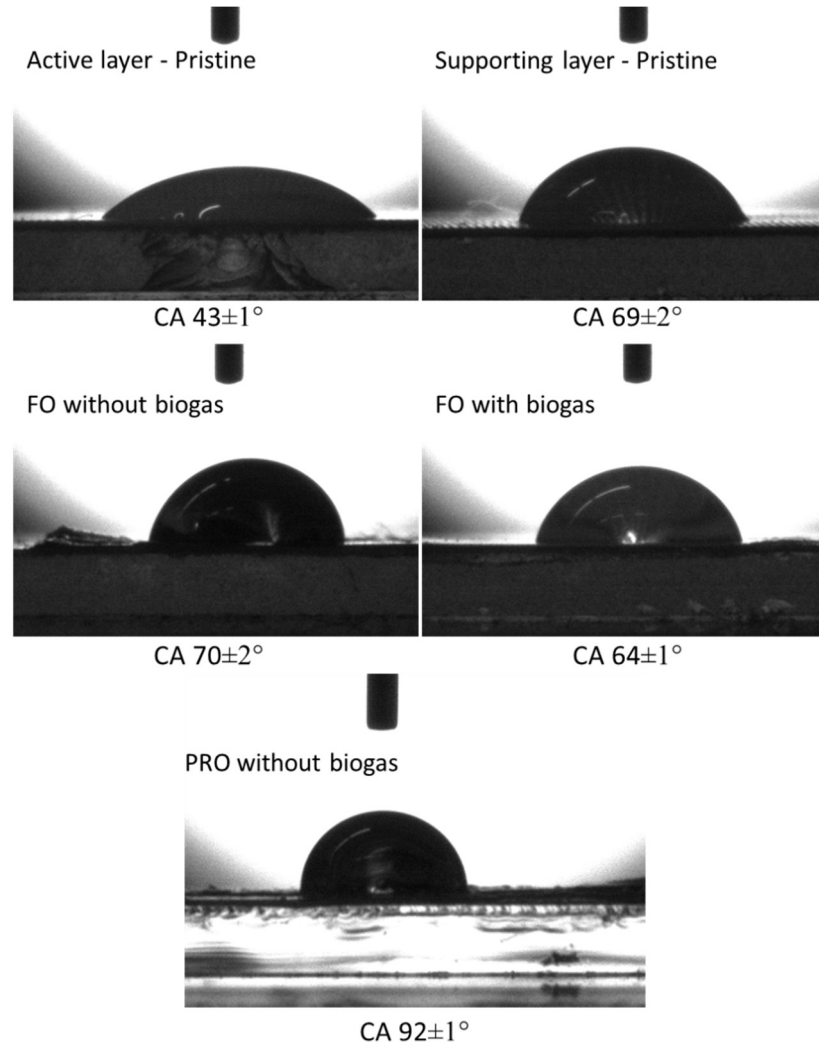
Figure 23: Differences in wettability between pristine and fouled membrane surface at different experimental conditions.

Physical flushing was inefficient to remove fouling layer in FO and PRO modes without biogas sparging with less than 20% pure water flux recovery. This result is predominantly due to the enhanced aggregation and compaction of fouling layer caused by greater pure water flux [151], and the high roughness of supporting layer in PRO mode [152]. More compact fouling layer is more challenging to be detached from the membrane

surface. Greater roughness of supporting layer led to weakening shear force created by physical flushing, thus reducing the number of foulants swept away from the membrane surface.

3.3.2.2. Improvement of organic carbon and nutrient enrichment

Overall, FO pre-concentration of sludge centrate led to a proportional increase in organic carbon content with water recovery, but FO mode with biogas sparging showed the best enrichment performance (Figure 24A). In all cases, the experimental COD values were lower than the maximum theoretical values that assumed complete COD retention by FO membrane. Indeed, the COD rejection of the FO membrane is almost 100% (Figure 25). The observed difference in COD enrichment between theoretical calculations and experimental results is ascribed to the deposition of organic matter on the membrane surface. In fact, the efficiency of COD enrichment was closely associated with the magnitude of fouling observed in section 3.3.2.1. The best performance of COD enrichment in FO mode with biogas sparging could be attributed to the significant reduction in membrane fouling in this scenario. This result is well supported by the observed magnitude of hydrophobicity of fouled membrane (i.e. PRO mode with biogas > FO mode without biogas > FO mode with biogas) which may represent the level of hydrophobic organic matter deposition on the membrane surface (Figure 23).
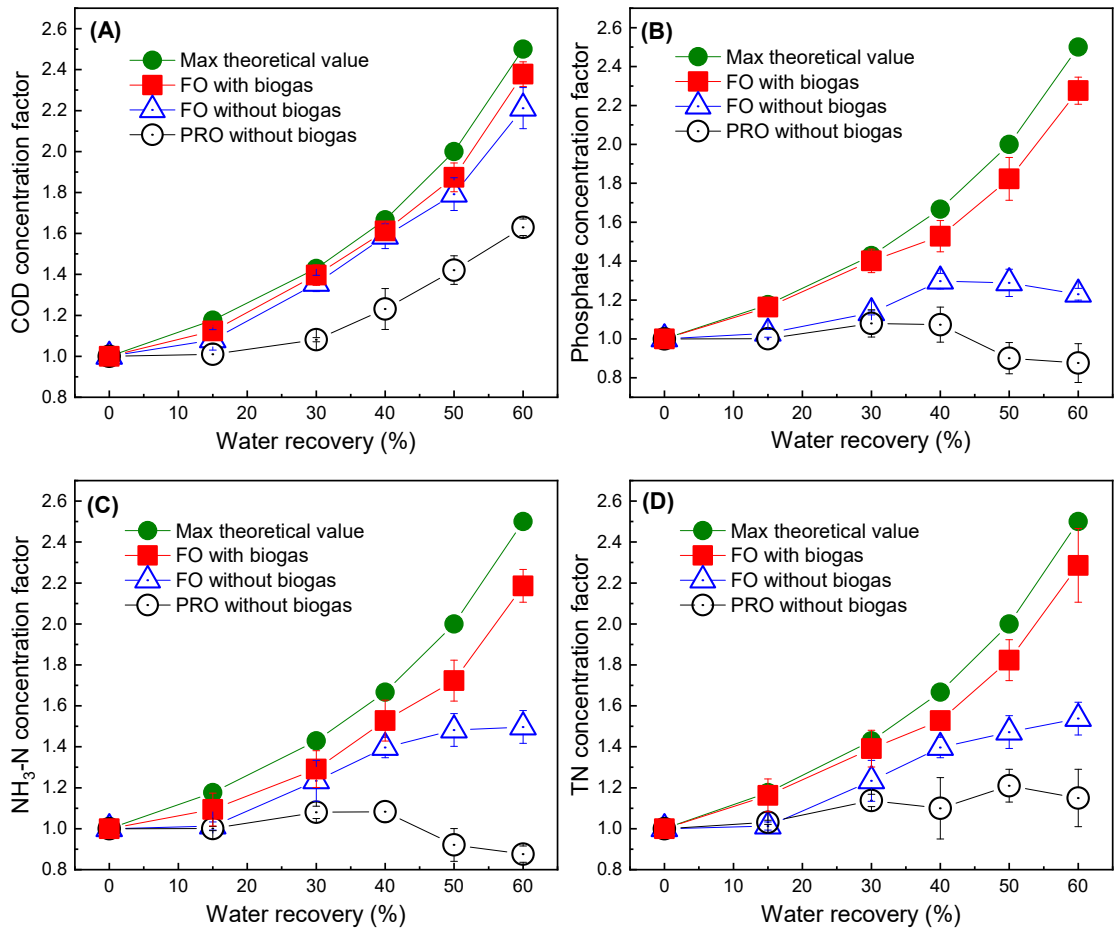
Figure 24: The enrichment of (A) bulk organic carbon, (B) phosphate, (C) ammonia and (D) TN during seawater-driven FO pre-concentration of sludge centrate with and without biogas sparging in different membrane orientations. The maximum theoretical value of each constituent as a function of water recovery was calculated based on a mass balance assuming complete rejection by the membrane (actual rejection values are shown in Table 5). Values and error bars are the mean and standard deviation of two replicate experiments.
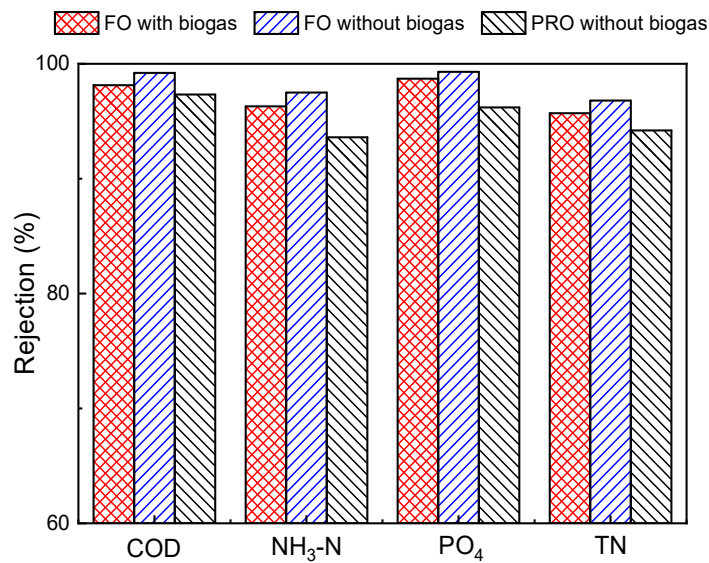
Figure 25: Rejection of bulk organic carbon and nutrients by the FO membranes during seawater-driven FO pre-concentration of sludge centrate with and without biogas sparging in different membrane orientations.

Without biogas sparging, the efficiency of nutrient enrichment during FO pre-concentration of sludge centrate was decreased significantly (Figure 24B-D). This observation appeared to be contrary to the expectation that the concentrations of nutrients are supposed to increase since the FS is concentrated during the filtration according to mass balance and high nutrient rejection by the FO membrane (Figure 25). The decrease in nutrient enrichment coincided with increase in pH of the FS (Figure 26) and decrease in the amount of calcium ions in sludge centrate (Figure 27). These observations suggest that low efficiency of nutrient enrichment can be ascribed to the formation of precipitates (e.g. calcium phosphate ($Ca_3(PO_4)_2$), magnesium phosphate ($Mg_3(PO_4)_2$) and struvite ($MgNH_4PO_4$)), and the conversion of ammonium ions to ammonia gas at high pH. Indeed, the formation of these precipitates is likely to occur due to the positive values of mineral saturation index (SI) [22] calculated for each precipitate (Table 8). Calcium phosphate precipitation is likely to happen first with higher SI value (Table 8). This statement is also

consistent with the EDS analyses further discussed later. In addition to volatilisation, the significant decrease in ammonia enrichment is due to the low rejection of the FO membrane upon the monovalent ion (i.e. NH_4^+ ions) (Figure 25), and electrostatic attraction between the negatively charged membrane surface (Table 5) and ammonium ions.
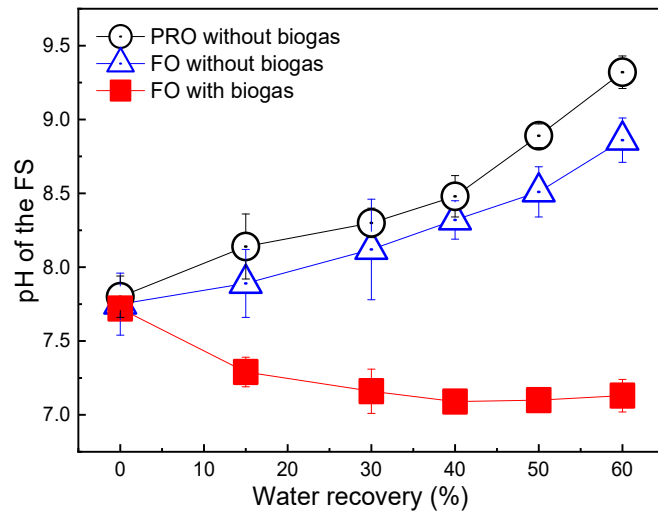
Figure 26: Variation in pH of the FS during seawater-driven FO pre-concentration of sludge centrate with and without biogas sparging in different membrane orientations. Values and error bars are the mean and standard deviation of two replicate experiments.
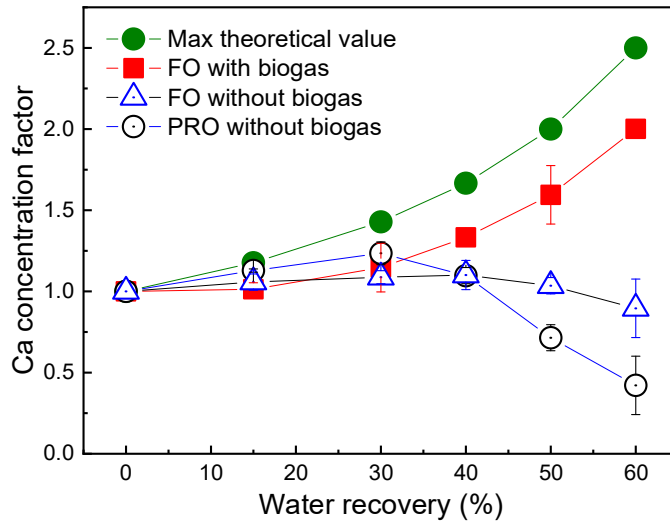
Figure 27: Variation in Ca concentration in the FS during seawater-driven FO pre-concentration of sludge centrate with and without biogas sparging in different membrane orientations. The maximum theoretical value of Ca as a function of water recovery was calculated based on a mass balance assuming complete rejection by the membrane (actual rejection values are shown in Table 5). Values and error bars are the mean and standard deviation of two replicate experiments.

Table 8. The evaluation of saturation index to predict the potential formation of precipitates from existing ions in the FS.

Precipitate type	Ion activity products (IAP)	Solubility (K_{sp})	Saturation index (SI)
Calcium phosphate ($Ca_3(PO_4)_2$)	3.61×10^{-14}	$10^{-32.63}$	19.19
Magnesium phosphate ($Mg_3(PO_4)_2$)	2.77×10^{-16}	$10^{-25.2}$	9.64
Struvite ($MgNH_4PO_4$)	6.81×10^{-8}	$10^{-13.26}$	6.08

Note: $IAP_{calcium\ phosphate} = [Ca^{2+}]^3 \times [PO_4^{3-}]^2$; $IAP_{magnesium\ phosphate} = [Mg^{2+}]^3 \times [PO_4^{3-}]^2$; $IAP_{struvite} = [Mg^{2+}] \times [NH_4^+] \times [PO_4^{3-}]$; $SI = \log(IAP/K_{sp})$.

By contrast, FO mode with biogas sparging demonstrated a remarkable improvement in nutrient enrichment (Figure 24B-D). With this technique, the enrichment of phosphate, ammonia and TN was almost similar to the theoretical enrichment curve. This observation is due to the inhibition of P precipitation, and the decreased conversion of ammonium ions to ammonia gas via volatilisation at decreased FS pH when using biogas buffering. Indeed, the pH of the FS decreased gradually and remained stable at around pH 7 during the filtration process (Figure 26). This pH value was not sufficiently favourable for the occurrence of phosphorous precipitation. In addition, the introduction of biogas into the system could increase the alkalinity of the FS via the dissolution of CO_2 into the aqueous solution. Carbonate ions can result in a competitive consumption of calcium ions, which hampers the formation of calcium phosphate precipitates [110]. This result is consistent with the changes in the nature of precipitates discussed later.

The difference in nutrient enrichment behaviour between with and without biogas sparging could be elucidated through changes in pH of the FS, Ca concentration in the FS and filtration time during FO pre-concentration of sludge centrate (Figure 26-28). The increased FS pH (Figure 26) was concurrent with the decreased Ca concentration (Figure 27). This result indicated the formation of precipitates, which causes low nutrient enrichment without biogas sparging. The increase of the FS pH promoted precipitation that caused membrane fouling and more prolonged the filtration time (Figure 28). The results revealed that FO mode with biogas sparging demonstrated approximately eightfold decrease in filtration time, compared to PRO mode without biogas sparging at water recovery of 60% (Figure 28).
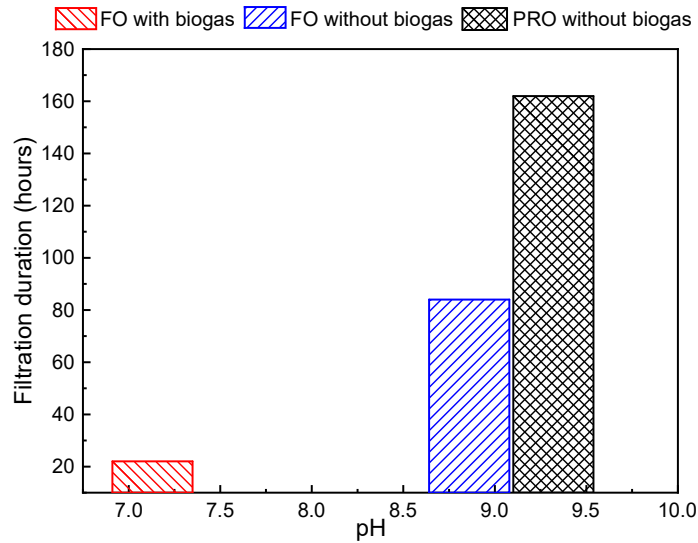
Figure 28: The correlation between FS pH and filtration duration towards different experimental conditions at water recovery of 60%.

3.3.3. Fouling characterisation and fouling mitigation mechanisms

The microscopic analysis and elemental mapping of the fouling layer confirm the formation of Ca-P precipitates on the membrane surface during seawater-driven FO pre-concentration of sludge centrate (Figure 29A-D). The coarse membrane surface after enrichment process indicated the deposition of organic materials and precipitates on the membrane surface (Figure 29A and C). The fouling layer appeared to be more compact in PRO mode in comparison to FO mode without biogas. This observation is consistent with the explanation discussed in the previous section. The presences of Ca, P and O elemental peaks on the membrane surface indicated the composition of calcium phosphate precipitates. The observed stronger elemental peaks and denser distribution of Ca and P (Figure 29B and D) indicated more fouling in PRO mode, compared to FO mode without biogas sparging. In addition, the observed round-shaped particles on the membrane surface are amorphous form of calcium phosphates when compared to the literature [153].
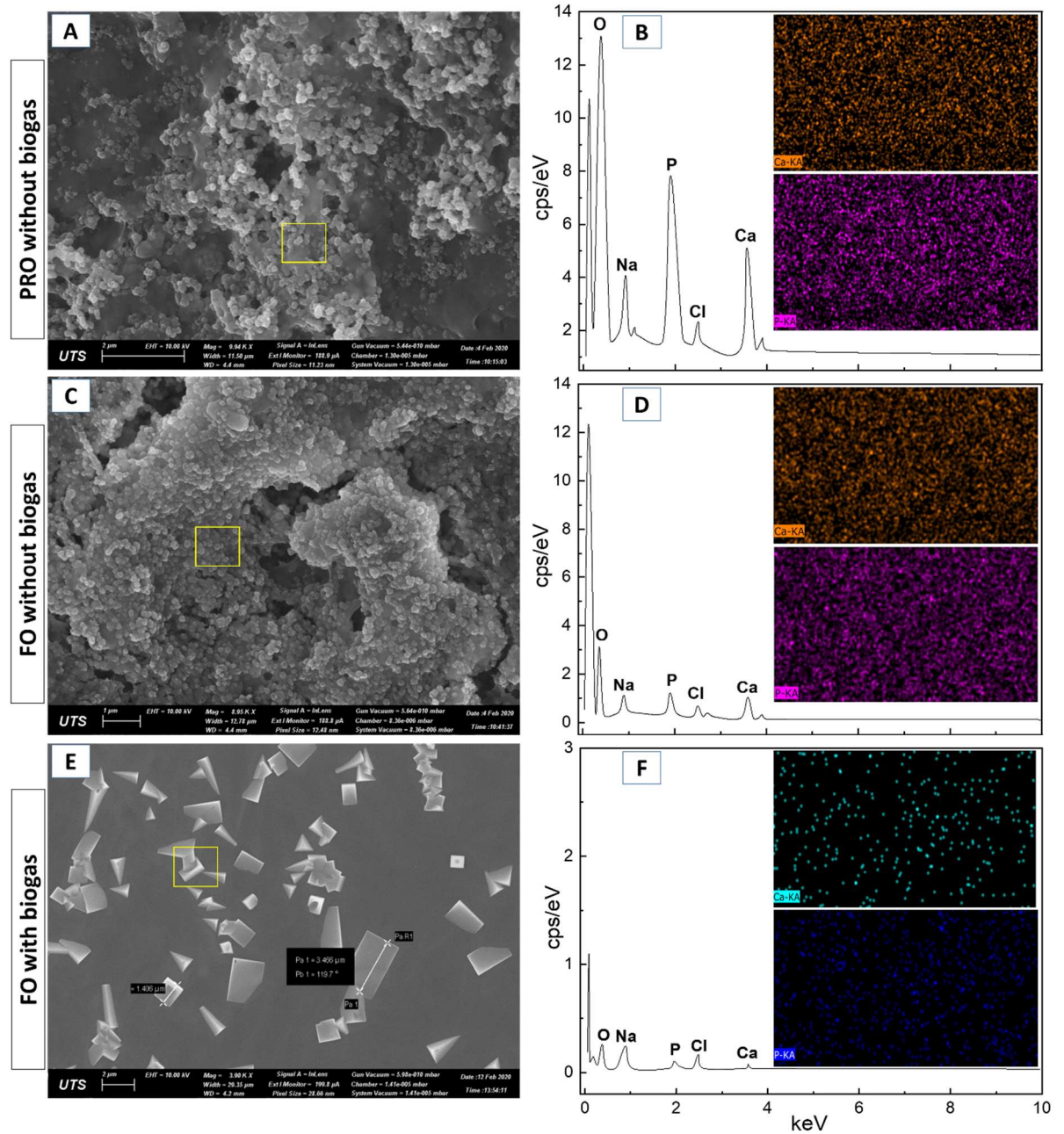
Figure 29: SEM and EDS mapping analyses of fouling layer on the membrane surface facing the FS towards without biogas sparging in PRO mode (A and B, respectively); without biogas sparging in FO mode (C and D, respectively) and with biogas sparging in FO mode (E and F, respectively). The EDS mapping was within the yellow squares.

The introduction of biogas into the FS resulted in the significant changes in morphology and elemental composition of fouling layer on the membrane surface (Figure 29E-F). Instead of a coarse fouling layer with sphere-like precipitates in the case of no

biogas sparging, the membrane surface in FO mode with biogas sparging was covered by a smooth fouling layer scattered with ikaite-like crystals. The formation of ikaite at low pH in the presence of phosphate were reported by Hu et al. (2015) [154]. The EDS elemental analysis (Figure 29F) revealed that biogas buffering significantly decreased the amounts of Ca, P and O content in the composition of the fouling layer. This result is strongly supported by the sparse distribution of Ca and P on the membrane surface via the mapping analysis (Figure 29F).

The above observations suggested possible mechanisms of using biogas buffering to mitigate fouling and improve the efficiency of seawater-driven FO enrichment of nutrients in sludge centrate. Biogas buffering controls the increase in the FS pH, thus minimizing the formation of phosphorous precipitates. This first mechanism is rigorously discussed in the previous section as well as strongly evidenced through the SEM and EDS mapping images shown above. In addition, the dissolution of CO_2 in biogas into the FS could increase its alkalinity, which may lead to the competitive reaction with phosphate. This mechanism is consistent with the results reported by Song et al. that the precipitation rate of phosphate was hindered significantly in the presence of carbonate at pH 8 or lower [101]. The formation of ion pairs between calcium and carbonate and the decrease of free calcium ions were shown to be the reasons for the decreased phosphate precipitation rate [101]. Indeed, the observation of ikite-like crystals in the fouling layer on the membrane surface in the conclusion of the filtration could confirm this mechanism.

3.4. Conclusions

This study demonstrated the feasibility of biogas sparging to control membrane fouling and improve the enrichment efficiency of a seawater-driven forward osmosis (FO) system that was used to pre-concentrate sludge centrate for subsequent nutrient and energy

recovery. Biogas from anaerobic co-digestion of sewage sludge and beverage waste was used for this purpose. Without biogas sparging, severe membrane fouling and low organic and nutrient enrichment efficiency were observed. The observed low enrichment efficiency was due to the conversion of ammonium to ammonia, and the deposition of organic matter and Ca-P precipitates on the membrane surface at high feed solution pH during the enrichment process. By sparging biogas into sludge centrate, membrane fouling was significantly reduced, and the efficiency of organic matter and nutrient enrichment was close to theoretical values. In other words, organic and nutrient contents in sludge centrate increased proportionally against water recovery. FO membranes with biogas sparging demonstrated high fouling reversibility with almost 90% pure water flux recovery using only physical flushing. The enhanced nutrient enrichment and reduction in membrane fouling by sparging sludge centrate with biogas could be ascribed to the solubilisation of phosphate and ammonium at neutral pH due to carbonate buffering.

Chapter 4. Phosphorus recovery from sludge centrate using forward osmosis and steel-making slag

This chapter has been published as: *M.T. Vu, L.N. Nguyen, I. Ibrahim, M. Abu Hasan Johir, N. Bich Hoang, X. Zhang, L.D. Nghiem, Nutrient recovery from digested sludge centrate using alkali metals from steel-making slag, Chemical Engineering Journal 450 (2022) 138186.*

4.1. Introduction

Sludge centrate is the liquid fraction from digestate dewatering to produce biosolids [155, 156]. Compared to wastewater discharge, sludge centrate is small in volume but rich in phosphate and ammonium. The phosphate and ammonium contents are in the range of 421 - 1387 mg/L and 949 - 1141 mg/L, respectively [7, 155, 157]. The high nutrient content and small volume of the sludge centrate stream make it an ideal source for nutrient recovery.

Chemical precipitation followed by crystallisation is a widely used commercial technology for nutrient recovery from sludge centrate [158-161]. Examples of commercial processes using these technologies for Precovery from sludge centrate include Ostara Pearl, MagPrex^{TM}, Crystallactor^{TM}, and Phosnix [158, 159]. The main products that are recovered in these processes and used as fertilisers for agricultural production are struvite and calcium phosphate [158, 159].

Nutrient recovery via precipitation requires additional chemicals such as magnesium, calcium, and other alkaline metals for pH adjustment and forming the precipitate [159]. The high cost of these chemicals is a major obstacle to more wide spread applications of nutrient recovery from sludge centrate [162]. As a result, two major approaches have been explored for further cost reduction. They include enrichment of nutrient content in sludge

centrate prior to chemical addition [140] and utilising alkaline metals from waste such as steel making slag [106, 109].

Forward osmosis (FO) separation has recently emerged as a promising technology for handling highly complex waste streams due to low membrane fouling tendency and high fouling reversibility compared to pressure-driven membrane processes [163-165] as well as possibility for integration with other processes such as electrolysis [166] and biological treatment [167]. In fact, the application of FO to downsize the volume of sludge centrate and enrich its nutrient content for subsequent recovery has been demonstrated in previous studies [7, 11, 168]. During nutrient enrichment by FO, P precipitation must be avoided to prevent membrane fouling and nutrient loss [7, 11]. Innovative techniques have been proposed such as using CO_2 from biogas to lower the feed solution pH to maintain P in the aqueous phase [7, 11]. Membrane fouling (and thus filtration time) can also be reduced by enhanced scouring at the membrane surface for improving P retention [169].

Steel-making slag is a by-product of the steel-making industry [106, 150, 170]. It is the residue from iron ores and additives such as lime and dolomite [106]. Steel-making slag typically consists of CaO (32 – 49%), MgO (5. – 7%), Fe_2O_3 (28 – 32%), Al_2O_3 (4 – 6%), and SiO_2 (8 – 16%) [106, 170]. Approximately 400 Mt tons of steel-making slag are produced annually [106]. Given this enormous volume, steel-making slag must be beneficially reused for applications such as road-base construction [113, 171] and filtration media for wastewater treatment [172, 173] to save space and avoid landfilling. The high CaO content in steel making slag makes it highly reactive when used as aggregates for construction. Thus, the slag must be weathered to leach out alkaline materials to prevent unwanted swelling (or structure expansion) as these materials can undergo further chemical reactions over time. Natural weathering can take up to one year and may release alkaline materials into the water environment [106].

The steel-making slag has high calcium and alkaline contents. It is also a large volume waste product from steel making. The Australasian Slag Association estimated that almost 3 Mt tons of steel-making slag was produced in Australia and New Zealand in 2019. The use of steel-making slag for nutrient recovery from waste streams such as sludge centrate could bring many benefits. The steel industry can reduce waste disposal and management costs significantly. In addition, it is expected that after the precipitation process, the nutrient levels remaining in sludge centrate could be alleviated. As such, WWTPs can minimise the adverse impacts from sludge centrate on treatment efficiency and operation, such as struvite pipe blockages and excess nutrients in the final treated water [174]. After calcium leaching, the slag can be used immediately for road construction, resulting in shortened storage time and lower management costs. The benefits outlined above for the industry stakeholders make this approach highly practical and cost-effective as it can take advantage of all their wasted resources for their beneficial use.

In a previous work, we have demonstrated the potential of steel-making slag as filtration media (or adsorbent) to remove P from aqueous solution [106]. This approach focused on removing low concentration P from treated wastewater effluent to prevent eutrophication. Unlike treated effluent, sludge centrate is a nutrient-rich waste stream. P and N recovery from sludge centrate in a way that would allow also allow for beneficial use of steel-making slag is a win-win solution for steel manufacturing, WWTPs, and the construction industry. This study aims to investigate for the first time the feasibility of using steel-making slag to recover nutrients from sludge centrate. Calcium and alkali metals are weathered out from steel-making slag to produce liquor for nutrient recovery. Factors affecting the leaching process, such as the mass of steel-making slag, particle sizes, and leaching time are examined to optimise the level of calcium ions and pH of the

slag liquor. Prior to the nutrient recovery process, sludge centrate is pretreated using rapid sand filtration and then pre-concentrated using a seawater-driven FO system to enrich nutrients therein to increase the recovery efficiency. Seawater is a low cost draw solution (DS) as it is readily and freely available in coastal areas where steel works and most WWTPs are located. Moreover, the DS regeneration process in this case is not necessary as the diluted seawater after the enrichment process can be immediately discharged into the sea without further treatment. The efficacy of the sand filtration pre-treatment to control membrane fouling and enhance nutrient enrichment during FO pre-concentration of sludge centrate is demonstrated. The limiting factors that affect the nutrient recovery efficiency using slag liquor and concentrated sludge centrate are indicated. The recovery mechanisms are also discussed thoroughly in this study.

4.2. Materials and method

4.2.1. Materials and chemicals

Steel-making slag was from an electric arc furnace at a steel mill in Sydney (Australia). The composition of this slag has been reported in a previous study [106]. The slag was rinsed thoroughly using tap water, dried at 105 °C for 24 hours, and then crushed and sieved into two sizes namely <0.3 mm and 0.3 – 0.6 mm. The resulted slag particles were stored in closed containers and purged using N_2 gas to prevent any reaction with CO_2 from the air. Silica sand at two different size ranges (0.5 mm and 1 – 2 mm) from a commercial supplier was cleaned thoroughly using DI water before use.

Digested sludge centrate was obtained from a high speed centrifuge dewatering system at a WWTP in Sydney (Australia). The sludge centrate was filtered through 150 μm stainless steel mesh to remove large solid particles and then preserved at 4 °C for further use.

Sludge centrate (feed solution, FS) with and without sand filtration pre-treatment was pre-concentrated by a FO system. Seawater from Sydney (Australia) was used as a DS. The obtained seawater was pre-treated through 0.45 μm filter paper before use. The characteristics this seawater were available in a previous study [7]. Flat-sheet thin film composite polyamide (TFC PA) membranes from Porifera, Inc. (Hayward, California, USA) were used to pre-concentrate the sludge centrate. Membrane samples were soaked into DI water over night for complete hydration before use. Key transport properties of this membrane have been reported in a previous study [7].

Sulphuric acid (2 M) was used to adsorb ammonia (NH_3) from volatilisation. The working acid solution was made by diluting a predetermined amount of analytical grade 98% H_2SO_4 (Merck, Germany) with Milli-Q water.

4.2.2. Experimental design

4.2.2.1. Sand filtration pre-treatment

The sand filtration system to pre-treat the sludge centrate was schematically described in Figure 30. The system consisted of one vertical filtration column, two variable speed gear pumps (Micropump, Vancouver, Washington, USA), and two pressure gauges (Process Systems Pty Ltd., Australia). The filtration column was 1,000 mm in length and 26.6 mm in diameter. The cleaned silica sands were loaded into the filter column to form different layers (Figure 30A). The filtration of the sludge centrate was operated in downflow mode under two different conditions corresponding to two flow velocities (i.e. 10 and 20 m/h) for comparison. After filtering 20 L of sludge centrate, the column was backwashed at twice the operational flow velocity for 3 min.
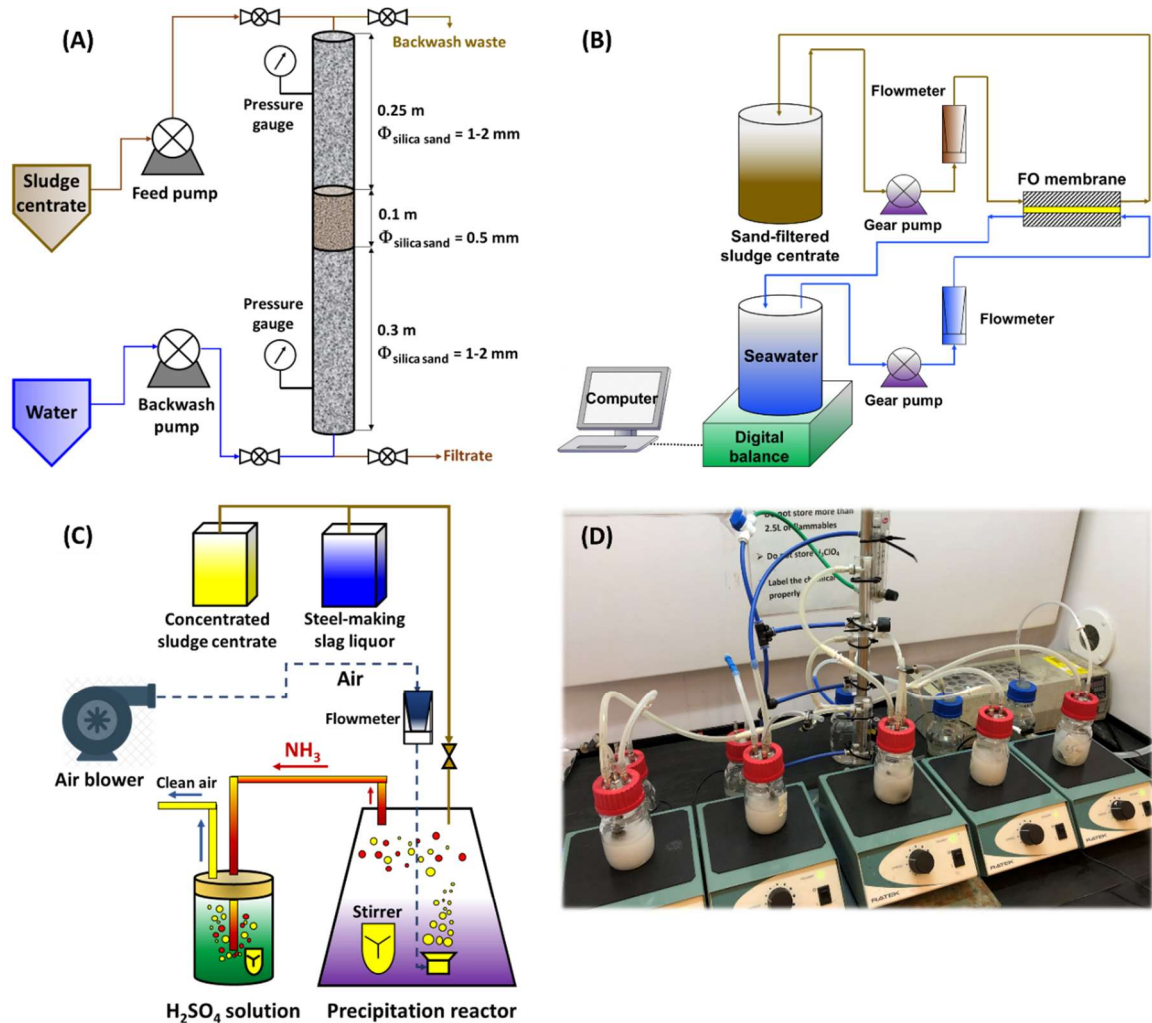
Figure 30: (A) A schematic diagram of a sand filtration system for sludge centrate pre-treatment, (B) A schematic diagram of a forward osmosis system for nutrient enrichment, (C) A schematic diagram of an experimental system for nutrient recovery via precipitation from concentrated sludge centrate and slag liquor, and (D) A photo of the nutrient recovery set-up.

4.2.2.2. Nutrient enrichment by forward osmosis

A lab-scale FO system (Figure 30B) was used to enrich nutrients in the pre-treated sludge centrate. This FO system consisted of an acrylic glass cross-flow membrane cell, two variable speed gear pumps (Micropump, Vancouver, Washington, USA), two flowmeters, and a digital balance to measure the flux. The feed and draw solutions were circulated through the two symmetric rectangular semi-cells of the FO membrane module

at the same cross-flow velocity of 12 cm/s in a counter-current mode. The internal dimensions of each semi-cell were 10 cm in length, 2 cm in width, and 0.2 cm in height. In other words, the effective membrane area was 20 cm^2. The FO membranes were oriented in active layer facing the FS.

FO experiments were performed in two steps at room temperature (22 °C). First, the membrane pure water flux was determined for 1 h using DI water as the FS and seawater as the DS. Next, sludge centrate (with or without pre-treatment) and fresh seawater were used as the FS and DS, respectively. All FO experiments were conducted until 70% water recovery. At specific time intervals, 5 mL sample was collected from the FS for analysis. In all FO experiments, the initial volumes of the feed and draw solutions were 0.5 and 1.5 L, respectively. The used high ratio of DS to FS volume was to minimise the dilution effect of the DS during FO operation. The pH and conductivity of the FS were regularly monitored. At the conclusion of the experiments, the concentrated sludge centrate solutions were stored in closed glass containers in the fridge at 4 °C and ready to be used as a first feedstock for nutrient recovery experiments.

4.2.2.3. Steel-making slag liquor preparation

Leaching experiments were conducted in a range of conditions to obtain slag liquors for nutrient recovery. Steel-making slag of < 0.3 mm and 0.3 – 0.6 mm in particle size was added to 200 mL DI water to achieve desirable steel-making slag mass to water volume ratios from 100 to 800. The mixture was agitated at 200 rpm for 2 h using an orbital shaker. Aqueous samples were taken for analysis at a specific time interval to find out impacts of agitating time on the quality of the slag liquor. The liquor (supernatant) was decanted and stored in enclosed containers purged with N_2 gas until further used.

4.2.2.4. Nutrient recovery

Each recovery module included a glass reactor on a magnetic stirrer for mixing, an air flow-meter connected to an air blower, and a H_2SO_4 bottle (Figure 30C). The pre-concentrated sludge centrate and slag liquor were transferred into the reactor and continuously agitated and aerated. The precipitate was then removed for P recovery. Ammonia was purged by aeration and recovered by absorption to the H_2SO_4 solution as ammonium sulfate. The nutrient recovery efficiency was determined based on the difference between the initial nutrient concentrations and their residual concentrations in the supernatant at the end of the experiment.

A range of volume ratios of the pre-concentrated sludge centrate and slag liquor ($V_{concentrated\ sludge\ centrate}$/ $V_{slag\ liquor}$ from 0.3 to 3) were used to investigate the impacts of initial molar ratios of calcium and phosphate ions on the nutrient recovery efficiency. This allowed for a systematic assessment of the impact of initial nutrient concentration and calcium content on the nutrient recovery. All experiments were conducted at contact time of 120 min, temperature of 20 °C, and aeration of 1 L/min. The recovery efficiency was evaluated based on the phosphate and ammonia levels in the solution before and after the reaction. Furthermore, the phosphate and ammonia amounts in the precipitate and the acid solution were also determined at the end of the experiments to establish the mass balance of each constituent for the confirmation of recovery mechanisms. To determine the phosphate content in the recovered precipitate, 50 mL of the precipitate solution after the reaction was filtered through 0.45 μm paper filters. The precipitate on the filter paper was then rinsed thoroughly with DI water before drying until the mass remained unchanged. The dried precipitate was dissolved with 0.1 M HCl acid solution for subsequent phosphate analysis. The phosphate mass balance was established based on the initial input phosphate content from sludge centrate, phosphate content remaining in the

supernatant after the precipitation reaction, and phosphate content transferred into the recovered precipitates.

In addition to nutrients (i.e. phosphate and ammonium), calcium content in the solution before and after the reaction was also determined to understand the recovery behaviour. Preliminary experimental data showed that P precipitation was governed by not only calcium and phosphate content in the system but also the solution pH. Since the slag liquor was highly alkaline, initial pH of the sludge centrate was less relevant. In this study, the impact of final pH on the recovery efficiency was investigated. All experiments were performed in replicate.

4.2.3. Analytical methods

pH and temperature were measured using an HACH HQ40d portable pH meter (HACH, USA). Ammonium concentration was determined using the US-EPA Standard Method 10205 using ammonium kits and a HACH DR3900 spectrophotometer. Orthophosphate (PO_4^{3-}) was measured using ion chromatography (IC) (Thermo Fisher, Australia). The system was equipped with a Dionex AS-AP auto-sampler, Dionex IonPac AG19-4μm guard column (2 x 50 mm) and Dionex IonPac AS19-4μm analytical column (2 x 250 mm). The sample injection volume was 10 μL. The analysis was conducted using potassium hydroxide eluent with the following gradient (time [min]: concentration [mM]) (0-10: 10; 10-25: 45; 25-27: 45; 27-30: 10; 31: stop run). Metals in the sample were analysed using an Inductively Coupled Plasma – Mass Spectroscopy system (ICP-MS, Agilent 7900). The total suspended precipitate that was formed during the recovery process was determined by gravimetric analysis. In detail, 5 mL of the precipitate suspension was filtered through a 1.1 μm pre-weighed glass filter paper. The filter paper was then dried at 105 °C for 8 h to a constant mass.

Morphology and elemental composition of phosphate precipitates were characterised using a scanning electron microscopy (SEM) and energy-disperse X-ray spectroscopy (EDS) system (i.e. a Zeiss Supra 55VP SEM and Oxford EDS system). In addition, the crystallographic structure of the precipitate was determined using X-ray diffraction analysis using a Bruker D8 Discover XRD instrument.

4.3. Results and discussion

4.3.1. Sand filtration pre-treatment of sludge centrate

Pre-treatment of sludge centrate by sand filtration resulted in a significant reduction in TSS without any observable nutrient loss (Table 9). The TSS content decreased eightfold after sand filtration pre-treatment. On the other hand, pH, nutrient content, and composition of all other dissolved constituents in the sludge centrate were unchanged after sand filtration. Small differences before and after sand filtration in Tab were within measurement errors. Results in Table 9 confirmed the feasibility of sand filtration to pre-treat sludge centrate for fouling control in the subsequent seawater-driven FO pre-concentration process. Experimental results also showed negligible head loss and complete pressure recovery of the sand filtration column after backwashing (Table 10).

Table 9. Comparison in the properties of raw sludge centrate and sand-filtered sludge centrate (values indicated average ± standard deviation of at least three samples).

Parameters	Raw sludge centrate	Sand-filtered sludge centrate
pH	8.02 ± 0.07	8.05 ± 0.07
TSS (mg/L)	250.2 ± 11.3	30.2 ± 5.7
PO_4^{3-} (mg/L)	596.4 ± 15.5	579.8 ± 14.1
NH_3-N (mg/L)	913.2 ± 36.1	902.7 ± 21.1
Ca (mg/L)	42.8 ± 3.1	43.5 ± 0.5
Mg (mg/L)	13.2 ± 1.1	15.2 ± 2.3

Table 10. Comparison in the sand column operation and the properties of sand-filtered sludge centrate at different sand filtering conditions.

Parameters	Scenario 1	Scenario 2
Filtration velocity (m/h)	10	20
Backwash velocity (m/h)	22.5	45
Bed expansion (%)	7	20
Head loss after filtering 20 L of sludge centrate (kPa)	2	2
Recovered filtration pressure after backwash (%)	100	100
pH	8.07	8.05
TSS (mg/L)	28.7	30.2
PO_4^{3-} (mg/L)	576	580
NH_3-N (mg/L)	901	903
Ca (mg/L)	44.2	43.5
Mg (mg/L)	15.0	15.2

4.3.2. FO pre-concentration

Sand filtration pre-treatment effectively mitigated membrane fouling during FO pre-concentration of the sludge centrate using seawater as the DS (Figure 31A). Without sand filtration, the maximum water recovery was 70% when the water flux decreased to almost zero. The observed rapid flux decline was attributed to the deposition of suspended solids on the membrane surface. Without sand filtration, the feed solution pH increased significantly to above pH 9 (Figure 31B), leading to unintended phosphate precipitation on the membrane surface and N loss due to ammonia volatilisation (Figure 31C and D, respectively). Previous research has shown that alkaline condition is favourable to calcium phosphate precipitation and transforming ammonium to gaseous ammonia (pK_a = 9.25). By contrast, sludge centrate pre-treatment using sand filtration resulted in a linear flux decline; and well above 70% water recovery could be achievable (Figure 31A). In this case, flux decline was governed mostly by the decrease in osmotic pressure gradient

70

across the FO membrane due to dilution of the DS, reverse salt flux, and salt concentration increase in the FS.

Sand filtration pre-treatment resulted in significantly lower nutrient loss during FO pre-concentration (Figure 31C and D). When pre-treated sludge centrate was pre-concentrated, the increase in phosphate concentration closely resembled the theoretical value during the FO enrichment process according to mass balance assuming 100% PO_4^{3-} retention by the FO membrane (Figure 31C). Ammonia pre-concentration was also observed as the volume concentration factor increased to two (Figure 31D). By contrast, without sand filtration pre-treatment, phosphate enrichment by FO was 70% lower (Figure 31C) and no ammonia enrichment was observed (Figure 31D). The decrease in nutrient enrichment coincided with increase in pH in the feed (Figure 31B), leading to possible phosphate loss via struvite and calcium phosphate precipitation. Indeed, even with sand filtration, calcium enrichment did not occur during the pre-concentration of raw sludge centrate (data not shown). Mineral saturation index calculation also confirmed super saturation condition with respect to calcium phosphate (Table 11).

Table 11. The evaluation of saturation index to predict the potential formation of precipitates from existing ions in the FS.

Precipitate type	Ion activity products (IAP)	Solubility (K_{sp})	Saturation index (SI)
Calcium phosphate ($Ca_3(PO_4)_2$)	2.79×10^{-13}	$10^{-32.63}$	20.1
Magnesium phosphate ($Mg_3(PO_4)_2$)	2.71×10^{-12}	$10^{-25.2}$	13.6
Struvite ($MgNH_4PO_4$)	2.40×10^{-6}	$10^{-13.26}$	7.6

Note: $IAP_{calcium\ phosphate} = [Ca^{2+}]^3 \times [PO_4^{3-}]^2$; $IAP_{magnesium\ phosphate} = [Mg^{2+}]^3 \times [PO_4^{3-}]^2$; $IAP_{struvite} = [Mg^{2+}] \times [NH_4^+] \times [PO_4^{3-}]$; $SI = \log(IAP/K_{sp})$.

As discussed above, N loss was attributed to ammonia volatilisation and permeation through the FO membrane [5, 143]. The problem was more severe for raw sludge centrate due to pH increase and cake-enhanced concentration polarisation at the membrane surface due to TSS deposition. Although ammonia loss was significant in this study, N recovery from sludge centrate was a less pressing need compared to P. P is a non-renewable resource [175]; whereas, N fertilizer can be synthesised from N_2 gas in the air.
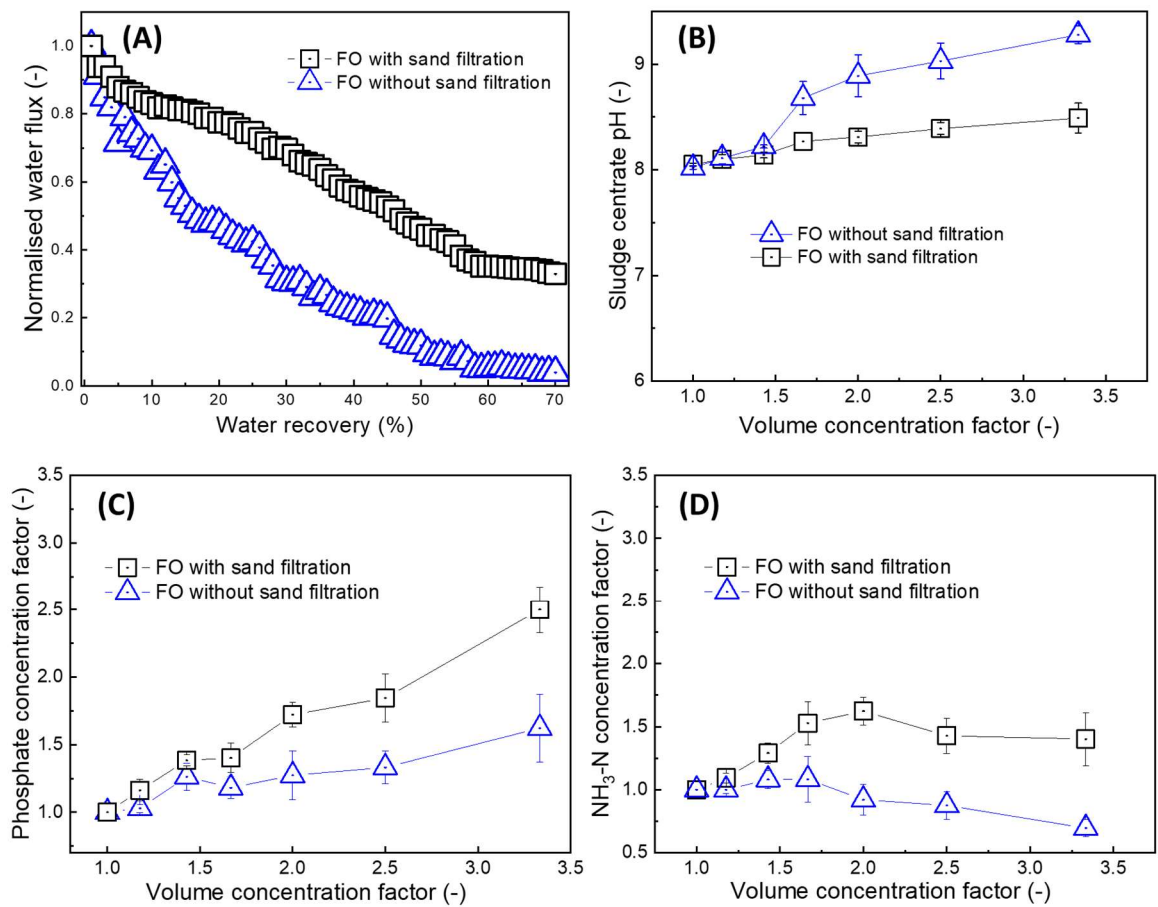
Figure 31: Changes in water flux (A) and FS pH (B) and the enrichment of (C) phosphate and (D) ammonium during the seawater-driven FO pre-concentration of sludge centrate with and without sand filtration pre-treatment. Values and error bars are the mean and standard deviation of two replicate experiments.

4.3.3. Steel-making slag liquor preparation

Calcium and alkalinity were two key ingredients from steel making slag for P recovery from sludge centrate. Thus, a series of leaching experiments was conducted to determine suitable slag mass and particle size.

Increasing the mass of slag and decreasing slag particle size resulted in more calcium and alkali release into the liquor (Figure 32). This observation could be attributed to the increased surface area and alkaline content for calcium oxide release to the water as the smaller particle size and more slag were used. The hydrolysis of alkali oxides resulted in

a higher number of hydroxyl and calcium ions released into the liquor. High calcium content and high pH in slag liquor were essential for the subsequent P recovery. Results in Figure 32 showed that steel-making slag could release calcium and other alkaline materials to significantly increase the liquor pH value. Calcium content in the liquor was proportional to the mass of slag used to produce liquor. On the other hand, the release of alkaline materials (indicated by liquor pH) was less impacted by the mass of slag and particle size. pH value of the slag liquor only increased by 5% when the steel-making slag mass increased by eight folds (Figure 32). In all cases, the liquor pH from either slag particle size was well above pH 11.5, which was sufficient to facilitate calcium phosphate precipitation for P recovery.
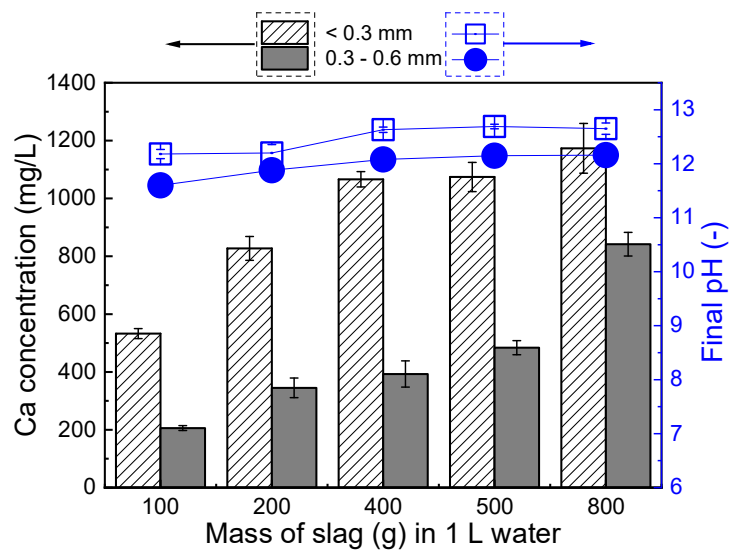
Figure 32: Effects of particle sizes and slag mass on the properties of slag liquor. Values and error bars are the mean and standard deviation of two replicate experiments.

Similar to the impacts of steel-making slag mass and particle size, prolonged leaching (or mixing) time resulted in higher calcium content but had insignificant impacts on the pH of the slag liquor (Figure 33). Overall, calcium content increased almost fourfold as the leaching time increased from 0.5 to 48 h, especially at smaller mass of steel-making slag, while the pH value of the slag liquor reached around 12.5 within 2 h and did not

significantly increase further. Based on results in Figure 32 and Figure 33, steel-making slag of 400 g/L and particle size of <0.3 mm was used to produce a suitable slag liquor for the subsequent nutrient recovery experiments.
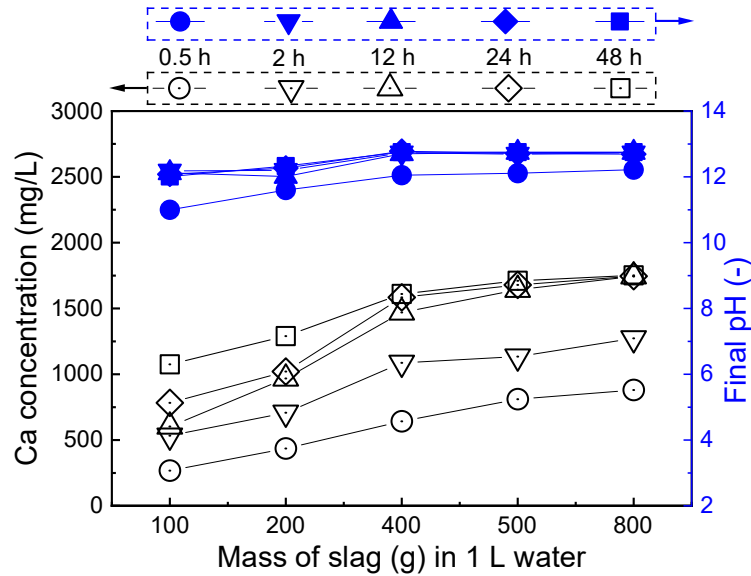
Figure 33: Effects of leaching time on the properties of slag liquor (mixing at 200 rpm by an orbital shaker). Values and error bars are the mean and standard deviation of two replicate experiments.

4.3.4. Nutrient recovery

4.3.4.1. Impacts of sludge centrate to slag liquor volume ratio on nutrient recovery

The volume ratio of sludge centrate to slag liquor governed the nutrient recovery efficiency (Figure 34A and B). As expected, using more slag liquor (higher Ca^{2+} and alkaline content) led to higher nutrient recovery. The increase in phosphate recovery efficiency was consistent with the increase in calcium over phosphate molar ratio (Figure 36). These results confirmed calcium phosphate precipitation as a major mechanism for P recovery. As such, calcium phosphate precipitation could be enhanced by a stronger alkaline environment and higher calcium concentration when more slag liquor was added to concentrated sludge centrate. This result is in good agreement with higher calcium phosphate precipitation efficiency at a high Ca/PO_4 molar ratio previous reported by Lei

et al. [176]. Likewise, ammonia stripping was also more effective at elevated pH when using more slag liquor (i.e. 71% ammonia recovery at the volume ratio of 0.3 with final pH 10.3). Indeed, the phosphate and ammonia recovery efficiency increased ninefold and sevenfold, respectively as the volume ratio reduced by 10 times.
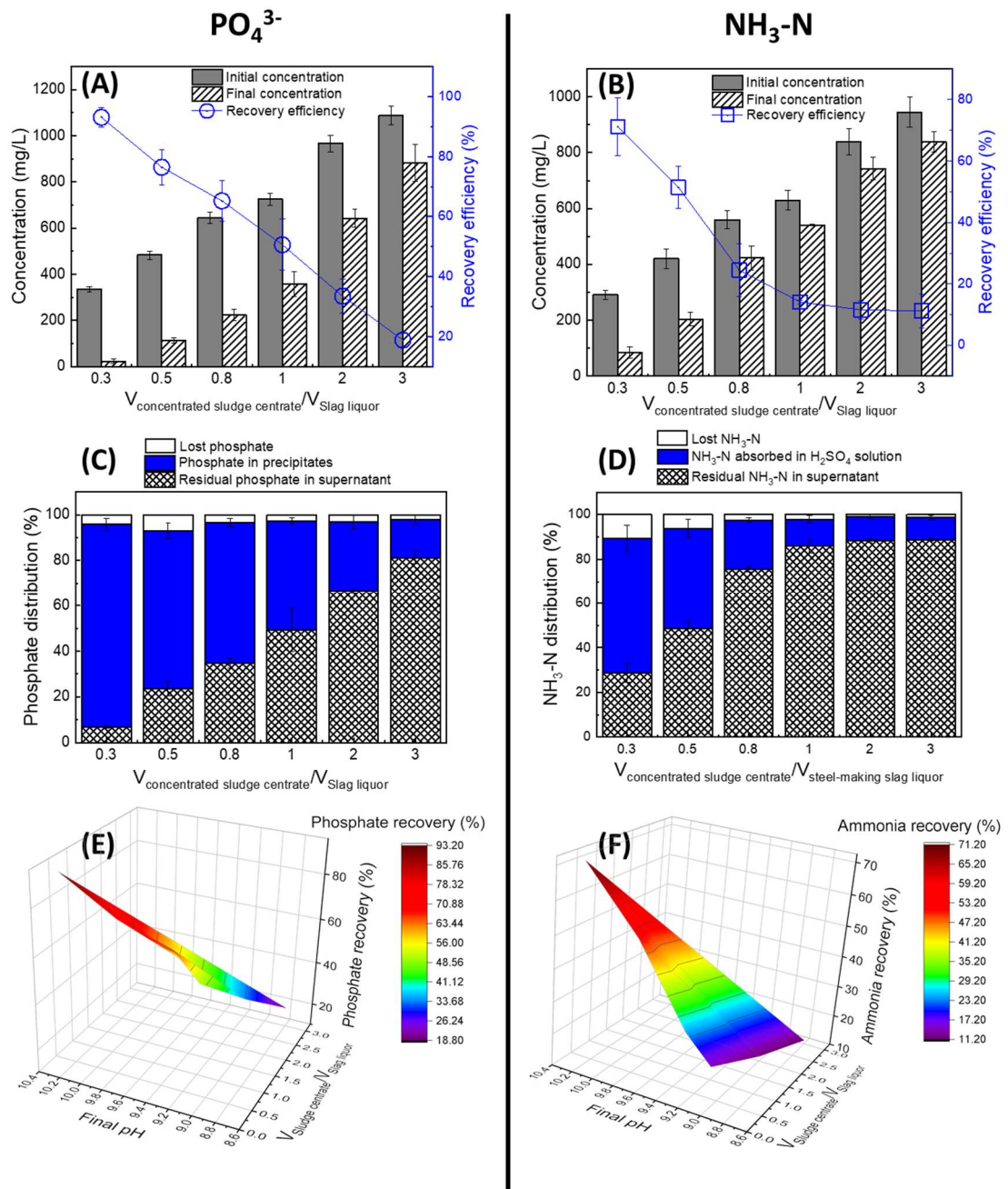
Figure 34: Impacts of pre-concentrated sludge centrate volume to slag liquor volume ratios on (A and B) nutrient recovery efficiency, (C and D) mass balance, and (E and F) final pH of the solution towards phosphate and ammonia, respectively. The recovery efficiency was calculated based on the nutrient concentration in the supernatant of the mixture before and after the precipitation and stripping process. The experiment was carried out at contact time of 120 min, temperature of 20 °C, and aeration of 1 L/min. Values and error bars are the mean and standard deviation of two replicate experiments.

Mass balance calculation confirmed precipitation and volatilisation as the main mechanisms for the nutrient recovery from the sludge centrate using the slag liquor (Figure 34C and D). The formation of more precipitate (measured by TSS level of the solution at the end of the precipitation experiment) was observed when more slag liquor was used at lower $V_{\text{concentrated sludge centrate}}/V_{\text{slag liquor}}$ ratios (Figure 35). At the volume ratio of 0.3, the formed precipitate content could reach approximately 2,000 mg/L (Supporting Information). In other words, 1 m^3 of the mixture of sludge centrate and slag liquor at their volume ratio of 0.3 could produce 2 kg of calcium phosphate precipitate. Elementary analysis of the recovered precipitates confirmed phosphate precipitation as a main P recovery mechanism. Ammonia was recovered as ammonium sulphate in the acidic quenching solution, confirming the conversion of ammonium ions to ammonia gas via volatilisation process.
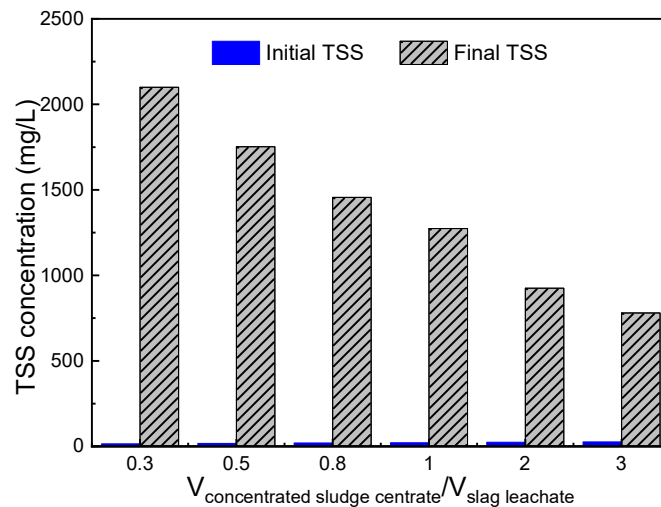
Figure 35: Changes in the amount of precipitate (measured by TSS content) formed in the solution during the recovery process. The experiment was carried out at contact time of 120 min, temperature of 20 °C, and aeration of 1 L/min.

During phosphate and ammonia recovery, the solution pH was a key factor affecting the nutrient recovery efficiency (Figure 34E and F). pH could be regulated by the volume

ratio of concentrated sludge centrate to slag liquor. Using more sludge centrate and less slag liquor at the high volume ratio decreased the solution pH, resulting in reduced recovery efficiency. This result might be due to the less effective precipitation and volatilisation reactions at a low final pH. Elevated solution pH and high Ca/PO_4 molar ratio could increase P recovery efficiency [176]. The interplay between alkalinity (indicated by pH) and the volume ratio of sludge centrate over slag liquor on the recovery efficiency of phosphate and ammonia were presented as surface plots in Figure 34E and F, respectively.

More calcium was removed from the solution as the volume ratio of sludge centrate to slag liquor decreased (Figure 36A). The consistency of calcium removal efficiency with nutrient recovery efficiency plus the presence of phosphate in the recovered precipitates (via mass balance) confirmed that P in sludge centrate was recovered as calcium phosphate precipitates. This conclusion was also supported by the elemental characterisation of recovered precipitates further discussed in section 4.3.4.3. Using more slag liquor could promote the formation of calcium phosphate precipitates, thus higher calcium removal efficiency. Indeed, the calcium removal efficiency increased by ninefold as the $V_{concentrated\ sludge\ centrate}/V_{slag\ liquor}$ ratio decreased 10 times.

P recovery efficiency was dependent on the initial $Ca:PO_4$ molar ratio and final pH (Figure 36B). Increased initial $Ca:PO_4$ molar ratios as a result of using more slag liquor and less concentrated sludge centrate and elevated final pH resulted in a better nutrient recovery (Figure 36A and B). The specific impacts of each parameter on the nutrient recovery efficiency were discussed further in the next section.
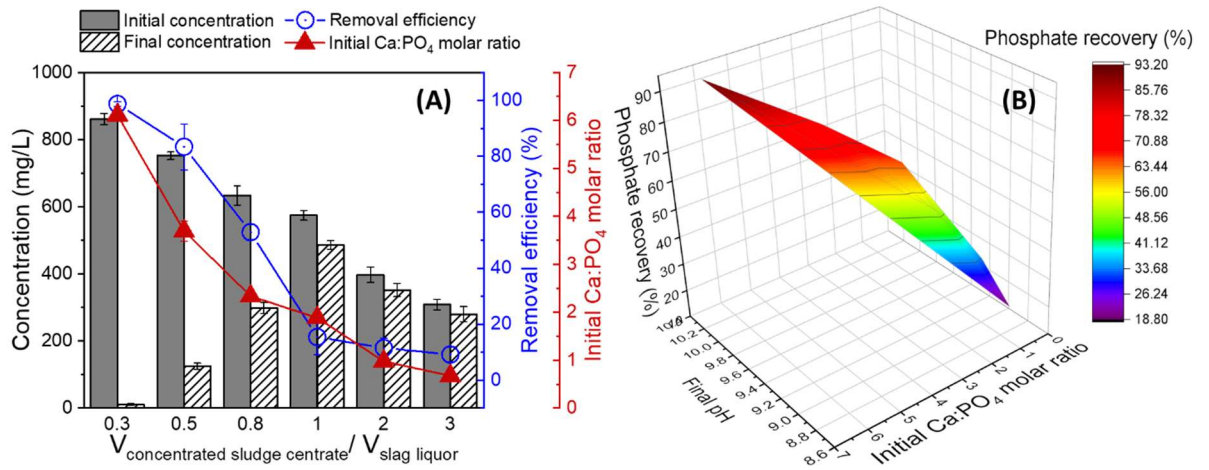
Figure 36: (A) Changes in calcium content in the bulk solution and (B) a correlation between initial Ca:PO$_4$ molar ratios, final pH, and phosphate recovery during the recovery process. Values and error bars are the mean and standard deviation of two replicate experiments.

4.3.4.2. Impacts of final pH on the nutrient recovery performance

Elevated final pH increased ammonia recovery significantly, but only enhanced phosphate recovery slightly (Figure 37). These results suggested that final pH was a limiting factor to ammonia recovery as the conversion of ammonium to ammonia gas was predominantly regulated by the pH of the solution. However, in addition to pH, the phosphate precipitation efficiency was also significantly dependent on the initial molar gradients of constituents. Indeed, only 64% phosphate was recovered at the initial Ca:PO$_4$ molar ratio of 1.88 and final pH 13 (Figure 37A), while over 96% phosphate recovery could be achieved at the initial Ca:PO$_4$ molar ratio of 6 and final pH 10.3 (Figure 34A). As such, the efficiency of phosphate recovery was more dependent on the initial Ca:PO$_4$ molar than the final pH.
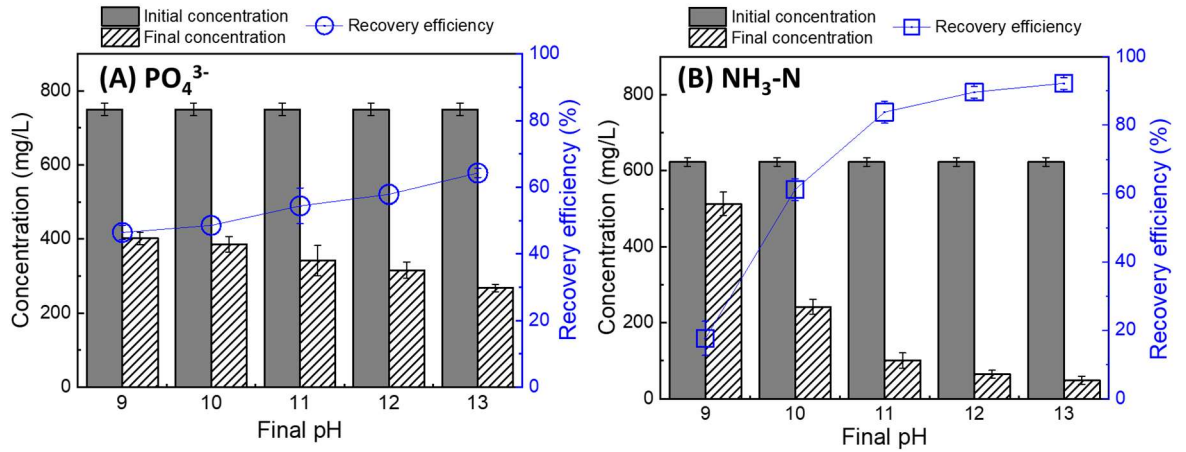
Figure 37: Impacts of final pH of the mixture on (A) phosphate and (B) ammonia recovery (Experimental conditions: $V_{\text{concentrated sludge centrate}}$/ $V_{\text{slag liquor}}$ = 1 corresponding to initial Ca:PO$_4$ molar ratio = 1.88; contact time = 120 min; aeration = 1 L/min). Values and error bars are the mean and standard deviation of two replicate experiments.

4.3.4.3. Precipitate characterisation

The microscopic analysis and elemental mapping of the recovered precipitates confirmed the formation of calcium phosphate during the recovery process (Figure 38). This observation was consistent with the explanation discussed in section 4.3.4.1. The dominant Ca, P, and O elemental peaks in the Energy Dispersive X-ray spectrum of precipitate samples were consistent with the composition of calcium phosphate (Figure 38B). This result was further supported by the uniformly distributed Ca and P in the SEM image of the recovered precipitate (Figure 38C and D). In addition, the observed round-shaped particles of the recovered precipitates were an amorphous form of calcium phosphates when compared to the literature. Specifically, the recovered precipitate might be $CaHPO_4 \cdot 2H_2O$ with XRD characteristic peaks at 2θ = 11.6°, 21.0°, and 29.3° [177] (Figure 39).
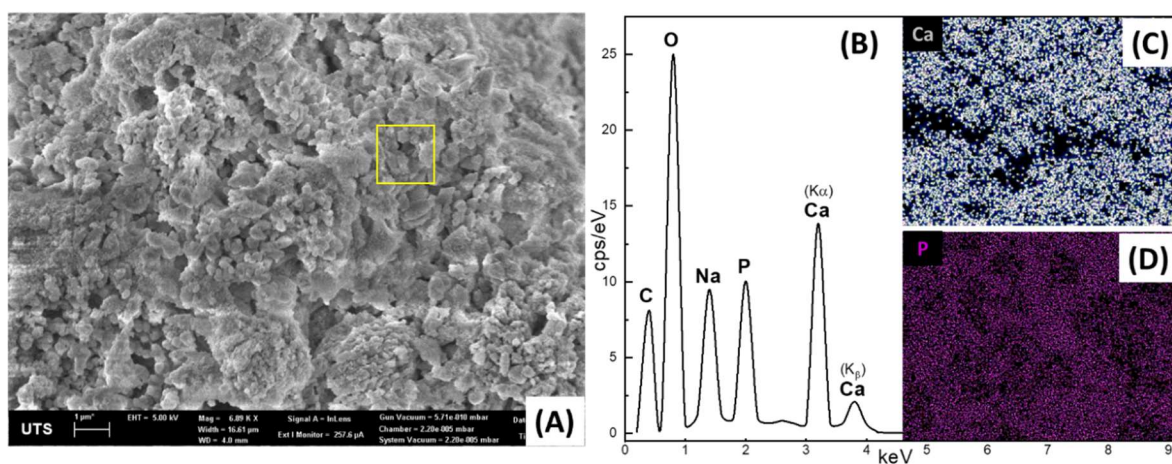
Figure 38: Microscopic and compositional analysis of the recovered precipitate: (A) SEM image; (B) EDS spectrum; (C) calcium and (D) P distribution mapping.
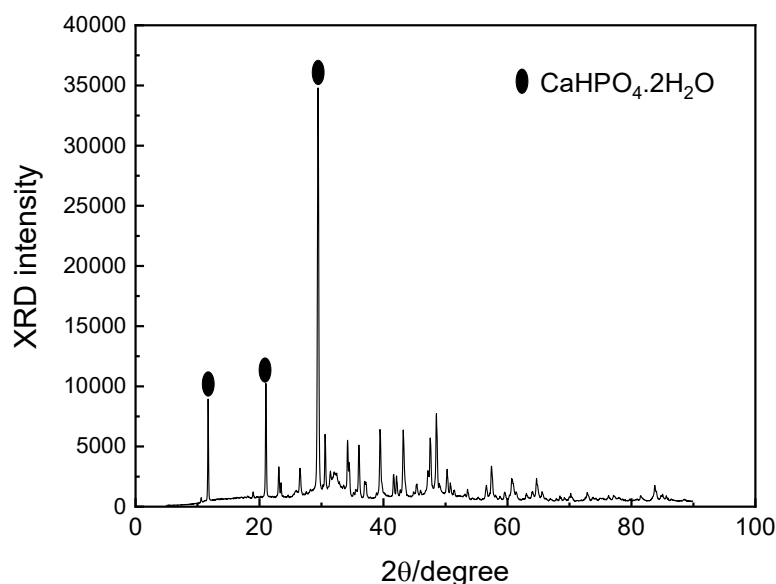
Figure 39: The XRD patterns of the recovered precipitate.

4.4. Conclusions

This study demonstrated the potential for utilising calcium and other alkali metals from steel-making slag to recover nutrients from anaerobically digested sludge centrate. Steel-making slag was successfully used to produce slag liquor containing high calcium and alkaline material contents for nutrient recovery from sludge centrate. The results indicated that up to 96% phosphate and 71% ammonia in sludge centrate could be recovered using

slag liquor at the optimum condition. P and N were recovered via calcium phosphate precipitation and ammonia volatilisation, respectively. In this study, the effectiveness of sludge centrate pre-treatment methods (i.e. sand filtration and FO enrichment) in facilitating nutrient recovery was demonstrated. Sand filtration pre-treatment decreased total suspended solid of sludge centrate by eightfold, resulting in significantly less membrane fouling and nutrient loss during FO pre-concentration. The study also demonstrated that final pH was a limiting factor for N recovery while the initial $Ca:PO_4$ molar ratio was more important to P recovery. This study has demonstrated a complete proof-of-concept system to recover nutrients from sludge centrate using steel-making slag. Further research on pilot scale is needed to examine the techno-economic feasibility of this approach. Post-treatment of liquid phase after nutrient recovery should also be considered in future work.

Chapter 5. Feasibility of using steel-making slag for removing residual phosphorus from an aqueous solution

5.1. Feasibility of using steel-making slag to remove P from an aqueous solution as a polishing step

5.1.1. Introduction

P is both an important resource and a major pollutant in the aquatic environment [102]. P is a key fertilizer ingredient and is also widely used in the high-tech industry [10]. On the other hand, P release from municipal and industrial wastewater is strictly regulated because it is responsible for eutrophication which results in harmful blue green algal bloom and oxygen depletion of the waterway [178]. Thus, P removal and recovery from wastewater is essential for resource conservation as well as environmental protection [179-181].

Several options for P removal and recovery from various wastewater have been explored in recent years. They include biological treatment [70, 182, 183], ion exchange [184, 185], chemical precipitation [186, 187], membrane separation [10, 11, 188] and adsorption [110, 189-191]. P removal by adsorption is probably the most extensively investigated and widely used in full-scale operations. However, the cost of adsorbent materials and/or adsorbent regeneration remain a major hurdle to more wide spread and large scale applications [192]. Research efforts to use secondary or by-products from

industry as absorbents will provide multiple benefits including i) reduction in cost, ii) repurpose waste materials for beneficial applications.

Steel-making slag is a major by-product of steel industry. It is a dense rock-like product generated through the addition of lime and dolomite to steel scrap during the steelmaking process [193]. The molten solution of silicates and oxides (i.e. slag) is poured from the furnace and allowed to slowly air cool, forming a crystalline material [193]. According to the World Steel Association, the steel industry annually produced over 400 Mt of steel-making slag [194]. Steel-making slag can be utilised for a range purposes. About 76% is currently beneficially reused in a range of applications such as aggregate supplement for concrete production and road construction [111]. Given its shearing resistance and high density, steel-making slag can be used as aggregates for civil engineering works, such as backfill, earth cover, and embankment [171]. In addition, given a rich content of Fe_2O_3, CaO, SiO_2 and MgO, steel-making slag can be used for cement production, fertilizer production, and soil improvement. The utilisation of steel-making slag in cement production can reduce energy consumption and CO_2 emission by approximately 40% compared to ordinary cement [195] as well as conserve resource (e.g. limestone, crushed stone and sand), thus ensuring clean production of steel and cement industry.

The application of steel-making slag in civil engineering, especially in asphaltic pavements has been accelerated in recent years [113]. In its virgin form, steel-making slag is highly reactive. Chemical reaction between metal oxides in steel-making slag and moisture and carbon dioxide in the air can cause swelling and structural damage when using as aggregates for construction [113]. Thus, steel making slag must be aged or weathered prior to any utilization as construction aggregates [196]. The current natural

weathering is time consuming and can take up to one year [113]. In addition, during the weathering process, alkaline materials may be released into natural waterbody [109].

Steel-making slag is an alkaline material composed primarily of metal oxides, namely CaO, SiO_2, Fe_2O_3, Al_2O_3 and MgO [109, 197]. Given its rich alkaline content, steel making slag can potentially be used to remove CO_2 from flue gas [150] and P from wastewater or storm water runoff [109, 111, 198, 199]. Previous studies have used steel-making slag to remove P from aqueous solution [109, 197, 199-201]. The results to date mainly have not clearly distinguished the P removal mechanisms (i.e. adsorption and chemical precipitation) using steel-making slag. Therefore, the removal behaviour of steel-making slag in aqueous solution and the process to enhance the removal efficiency have been often overlooked. It is expected that once P removal mechanism of using steel-making slag is fully elucidated, further performance optimisation can be achieved.

In this study, P removal by electric arc furnace slag was investigated. Operating conditions affecting P removal were elucidated for process optimisation. Isotherms and kinetics of the removal process were also determined to establish the adsorption capacity and the limit of mass transfer. Underlying P removal mechanisms by steel-making slag were revealed. A possible measure to improve the P removal efficiency of using steel-making slag that was derived from the understanding of removal mechanism were proposed and investigated. It is envisaged that steel-making slag can be used as a polishing step (i.e. tertiary treatment step) for further reduction of P from secondary treated effluent. The contact between steel-making slag and effluent encourages the release of calcium from this material can accelerate the weathering effect. Once calcium oxide has been depleted and the steel-making slag is fully weathered, it can be used for construction applications.

5.1.2. Materials and methods

5.1.2.1. Materials

The steel-making slag in this study was from an electric arc steel-making furnace (InfraBuild, Rooty Hill NSW 2766 Australia). The information regarding typical elemental composition of this steel-making slag was sourced from the product sheet of the steel manufacture (Table 12). The steel-making slag was rinsed with DI water to get rid of dust impurities and then dried at 105 °C for 24 hours. Then, the steel-making slag was crushed and sieved into four different particle sizes (0.15 – 0.6; 0.6 – 1.0; 1.0 – 2.0; and 2.0 – 4.5 mm). The steel-making slag particles were stored in airtight containers, which were purged with N_2 gas to prevent any potential reactions with the ambient air.

Table 12. Elemental composition of the steel-making slag in this study.

Component	CaO	Fe_2O_3	SiO_2	MgO	Al_2O_3	MnO	Cr_2O_3	TiO_2	SO_3
% weight	32	32	16	7	6	6	3	< 1	< 1

The analytical grade chemicals were used in this study. KH_2PO_4 was dissolved in deionized (DI) water to make synthetic aqueous solution, which simulates secondary treated effluent. An acetate buffer consisting of CH_3COOH (0.1 M) and CH_3COONa (0.1 M) was used to maintain a desirable pH when necessary.

5.1.2.2. Experimental design

5.1.2.2.1. Batch experiments

A series of batch experiments was conducted to assess the performance of P removal using the steel-making slag under a range of operating conditions. Unless otherwise stated, 1 g of the steel-making slag was added to 200 mL aqueous solution in each experiment (i.e. the steel-making slag mass to liquid volume ratio of 5 kg/m^3) at room temperature. The mixture was agitated continuously at 200 rpm on a flat shaker. The

aqueous phase was then filtered using 1.2 μm glass fiber syringe filters for subsequent analysis. Experiments to investigate the effects of initial pH on the P removal efficiency were performed at a range of pH from 2 to 13. pH of the P solution was adjusted to the desired value using 0.1 M HCl and 0.1 M NaOH solutions. The duration of these experiments was 72 hours. P concentration was determined to calculate the amount of P removed per unit mass of the steel-making slag and P removal efficiency as presented in Eqs. (4-6):

$$q_t = \frac{V(C_0 - C_t)}{m} \tag{4}$$

$$q_e = \frac{V(C_0 - C_e)}{m} \tag{5}$$

$$\eta = \frac{C_0 - C_t}{C_0} \times 100\% \tag{6}$$

Where q_t and q_e are the P removal capacity of the steel-making slag at time t and equilibrium state, respectively (mg/g); η stands for P removal efficiency (%); C_0, C_t and C_e are the P concentrations at the beginning, at time t and equilibrium state, respectively (mg/L); V is the volume of solution (L) and m is the mass of steel-making slag (g). All experiments were conducted in duplicate.

5.1.2.2.2. Adsorption isotherm

The adsorption isotherm was determined at a constant dosage of the steel-making slag (5 kg/m^3) and varying P concentration in the range from 5 to 50 mg/L. This range was selected based on the concentration of P in wastewater and for accurately establishing the adsorption isotherm models according to our preliminary experiments. The experiment lasted 72 hours to ensure that apparent equilibrium has been achieved. Four isotherm adsorption models that include Langmuir, Freundlich, Temkin and Dubinin-

Radushkevich (D-R) were employed to describe the adsorption behaviour of steel-making slag as presented in Eqs. (7-10) in Table 13 [199, 202, 203].

Table 13. Adsorption isotherm models evaluated in this study.

Model	Equation	Parameter	
Langmuir	$\dfrac{1}{q_e} = \dfrac{1}{q_m} + \dfrac{1}{q_m K_L}\dfrac{1}{C_e}$	q_m, K_L	(7)
Freundlich	$\ln q_e = \ln K_F + \dfrac{1}{n}\ln C_e$	K_F, n	(8)
Temkin	$q_e = \dfrac{RT}{b_T}\ln K_T + \dfrac{RT}{b_T}\ln C_e$ $$B = \dfrac{RT}{b_T}$$	b_T, K_T, B	(9)
D-R	$\ln q_e = \ln Q - 2B_D R^2 T^2 \ln\left(1 + \dfrac{1}{C_e}\right)$ $$E = \dfrac{1}{\sqrt{B_D}}$$	Q, B_D, E	(10)

Note: q_m is the maximum uptake capacity of the steel-making slag (g/Kg); K_L and K_F are the Langmuir and Freundlich adsorption constants, respectively; n is the heterogeneity factor; K_T is the equilibrium binding constant (L/mol); R is the universal gas constant (8.314 J/K.mol); T is the temperature (K); b_T is Temkin isotherm constant (kJ/mol); B is constant related to heat of sorption (J/mol); Q is the maximum adsorption capacity (mol/g); B_D is a constant related to the adsorption energy (mol^2/kJ^2); E is the mean free energy of adsorption (kJ/mol).

5.1.2.2.3. Adsorption kinetics

The adsorption kinetics of P removal reaction were fitted to Lagergren pseudo-first order, pseudo-second order, Elovich and intraparticle diffusion (IP) models as described in Eqs (11-14) in Table 14 [202-204]. The initial P concentration was 85 mg/L. This high

initial P concentration was to ensure that the maximum P uptake capacity of steel-making slag (equilibrium state) could be accurately assessed. Aqueous samples were taken for analysis at a specific interval to calculate the adsorption capacity and establish the kinetic models.

Table 14. Kinetic adsorption models used in this study.

Model	Equation	Parameter	
Pseudo-first order	$\ln(q_e - q_t) = \ln q_e - k_1 t$	q_e, k_1	(11)
Pseudo-second order	$\dfrac{t}{q_t} = \dfrac{1}{k_2 q_e{}^2} + \dfrac{t}{q_e}$	q_e, k_2	(12)
Elovich	$q_t = \dfrac{1}{\beta}\ln[\alpha\beta] + \dfrac{1}{\beta}\ln t$	α, β	(13)
Intraparticle diffusion	$q_t = K_p\sqrt{t} + C$	K_p, C	(14)

Note: k_1 and k_2 are the equilibrium rate constants of pseudo-first order and pseudo-second order models, respectively; α is the initial adsorption rate (mg/g.min); β is desorption constant (g/mg); K_p is a rate constant (mg/g.min$^{0.5}$); C is boundary layer thickness. Other parameters are similar to those presented above.

5.1.2.2.4. Phosphorus removal mechanisms

To differentiate between adsorption and chemical precipitation as key P removal mechanisms, an additional set of experiments was conducted. Instead of adding the steel-making slag directly into aqueous solution at the beginning of the experiment, the steel-making slag was agitated in DI water to allow for the release of leachate containing chemicals that may react and precipitate with P. The duration of leachate release was similar to that of direct reaction between the steel-making slag and the aqueous solution. As a result, the released alkaline materials that were readily available for the reaction with

P in these two cases were approximately the same. The aqueous phase was then filtered using 1.2 μm glass fiber syringe filters prior to reacting with P. It is noted that the certain amount of P was added into the aqueous phase to ensure the initial P concentration of 85 mg P/L. The difference in residual P concentration between the presence and absence of the steel-making slag particles after the reaction could be used to achieve the objective stated earlier.

5.1.2.3. Analytical methods

Physical surface characteristics of the steel-making slag including specific surface area and mean pore size were measured using a Brunauer-Emmette-Teller (BET) instrument (autosorb iQ model, Quantachrome Instruments). Its morphological structure and elemental composition before and after removal process were characterized using scanning electron microscopy (SEM, Zeiss EVO LS15) and energy dispersive X-ray mapping spectroscopy (EDS, Bruker SDD XFlash 5030) analysers. Fourier transform infrared (FTIR) spectroscopy of steel-making slag samples before and after adsorption was characterized using a Bruker V70 FTIR spectrometer. The wavenumber range was from 4000 to 600 cm^{-1}. In addition, the point of zero charge (PZC) of steel-making slag was determined following the salt addition method reported elsewhere [205].

P and Ca concentrations were measured using an Inductively Coupled Plasma – Mass Spectroscopy system (ICP-MS, Agilent 7900). pH was measured using an HACH HQ40d portable pH meter.

5.1.3. Results and discussions

5.1.3.1. Steel-making slag particle characterisation

Previous studies have demonstrated effective P removal by steel-making slag via adsorption [197, 199]. Thus, in this study, surface properties of steel-making slag particles were characterised to further elucidate the adsorption behaviour of P. Results in Table 15

show an increase in key parameters favourable for adsorption including specific surface area, pore volume, and pore radius as the steel-making slag particle size decreases. In all particle sizes investigated in Table 15, the pore radii are less than 20 Å indicating a microporous structure of the steel-making slag internal surface. Results in Table 15 also highlight the importance of pre-treatment and grinding steel-making slag into a small particle size for P adsorption. It is noteworthy that surface properties of steel-making slag particles were not systematically characterised in most previous studies. The only exception is a study by Blanco et al., [197] who reported the specific surface area and pore volume of their steel-making slag particles. Their data are consistent with those obtained from this study. However, Blanco et al., (2016) did not fractionate and confirm the microporous internal pore structure of their steel-making slag particles (Table 15) [197].

Table 15. Physical characteristics of the steel-making slag including particle size, specific surface area (S_{BET}), pore volume (V_T) and pore radius (values indicated the average $\pm$ standard deviation of three samples).

Reference	Particle size (mm)	S_{BET} (m^2/g)	V_T (cm^3/g)	Pore radius (Å)
This study	0.15 – 0.60	4.04 $\pm$ 0.21	0.048 $\pm$ 0.004	7.837 $\pm$ 0.458
	0.60 – 1.00	3.44 $\pm$ 0.12	0.012 $\pm$ 0.002	6.183 $\pm$ 0.115
	1.00 – 2.00	1.95 $\pm$ 0.32	0.007 $\pm$ 0.002	5.814 $\pm$ 0.327
	2.00 – 4.50	1.24 $\pm$ 0.05	0.004 $\pm$ 0.001	4.732 $\pm$ 0.009
Blanco et al., (2016)	0.10 – 10.0	0.64	0.340	Not available

5.1.3.2. Adsorption isotherm and kinetics

The Langmuir and Freundlich isotherms can describe P adsorption to the steel-making slag (Table 16), confirming adsorption as a major P removal mechanism. Both isotherms shows better P adsorption to the smaller slag particle size, evidenced by the increasing maximum uptake capacity (q_m) or adsorption constant (K_F) of the Langmuir and Freundlich isotherms respectively as the particle size decreases (Table 16). According to Langmuir model, the maximum P adsorption capacity of particle size of 0.15 – 0.6 mm is 10.21 mg/g, which is comparable to that of recycled concreate aggregate (6.88 mg/g) in the literature [206]. The Langmuir isotherm is based on an assumption that the adsorption surface is homogenous. In the Freundlich isotherm, this assumption is relaxed by incorporating the heterogeneity factor (n) to account for an uneven surface. Considering the fitting coefficient (R^2), the Langmuir isotherm can describe the adsorption of P to steel-making slag better than the Freundlich isotherm especially for

steel-making slag with particle sizes of less than 2 mm (Table 15). Results in Table 15 suggest that the steel-making slag with a particle size (2.0 – 4.5 mm) has a heterogeneous surface, unsuitable for the Langmuir isotherm (R^2 = 0.53). Indeed, the Freundlich isotherm can better describe P adsorption by steel-making slag with large particle size. The high heterogeneity factor (n) of the Freundlich isotherm ranging between 2.71 and 4.45 also indicate the heterogeneity of the steel-making slag surface. The complementarity between the Langmuir and Freundlich isotherms to describe P adsorption to steel-making slag of different particle sizes also suggests another removal mechanism additional to adsorption.

In addition to Langmuir and Freundlich models, the experimental data, especially for small particle sizes also fitted well to Temkin and D-R models with high correlation coefficient values (R^2 > 0.8) (Table 16). Both Temkin and D-R models reflected higher adsorption capacity of smaller particle sizes with higher K_T and Q values. The B values related to heat of sorption in Temkin model are positive, which indicates that the adsorption process is exothermic [202]. These values are higher for smaller particle sizes. The mean sorption free energy (E) values (i.e. < 8 kJ/mol) in D-R model suggested the possibility of physical adsorption [207].

Table 16. Adsorption isotherms of P to steel-making slag of different particle sizes.

Isotherm model	Parameter	Particle size (mm)			
		0.15 – 0.6	0.6 – 1.0	1.0 – 2.0	2.0 – 4.75
Langmuir	q_{max} (mg/g)	10.21	2.9	1.34	0.56
	K_L (L/mg)	0.49	0.23	0.74	0.32
	R^2	0.94	0.94	0.92	0.53
Freundlich	n	2.89	3.64	4.45	2.71
	K_F	2.21	1.75	0.63	0.16
	R^2	0.51	0.83	0.99	0.76
Temkin	K_T (L/mol)	24.86	7.06	12.04	0.87
	b_T (J/mol)	2685	5865	10767	13178
	B (J/mol)	0.92	0.42	0.23	0.19
	R^2	0.83	0.82	0.99	0.71
D-R	Q (mol/g)	6.77	2.51	1.33	0.58
	B_D (mol^2/kJ^2)	8.6×10^{-8}	1.8×10^{-7}	1.1×10^{-7}	2.6×10^{-7}
	E (kJ/mol)	2.41	1.64	2.11	1.40
	R^2	0.88	0.96	0.89	0.48

Two particle sizes including 0.15 – 0.6 mm and 0.6 – 1.0 mm were selected for further kinetic study given their high P uptake capacities (Table 16). The kinetic results indicate that P removal process using the steel-making slag can be presented well by pseudo-first order and pseudo-second order models, followed by Elovich and IP models since the values of the correlation coefficients in all cases were high (≥ 0.85) (Table 17). However, for the entire particle sizes studied, the pseudo-second order kinetics illustrated the best

fittings to the experimental data, suggesting the sorption mechanism via chemical reaction (i.e. precipitation). In other words, precipitation can also be a major P removal mechanism according to the assumption of the pseudo-second-order kinetic model that the rate-limiting step may be chemical sorption involving valence forces through sharing or exchange of electrons between absorbents and absorbates [199, 208]. Moreover, the good fit of Elovich model is consistent with the chemisorption mechanism [202]. These results support the aforementioned hypothesis that precipitation could be an additional removal mechanism apart from adsorption. In addition, the correlation coefficient (R^2) of 0.15 – 0.6 mm particle size is higher than that of 0.6 – 1.0 mm in IP model, indicating that the greater contribution of the surface sorption in the rate limiting step in the case of small particle size adsorption [209].

Table 17. Kinetic modelling of different particle sizes.

Kinetic model	Parameter	Particle size (mm)	
		0.15 – 0.6	0.6 – 1.0
Pseudo-first order	q_e (mg/g)	4.03	1.83
	k_1	1×10^{-3}	3.6×10^{-3}
	R^2	0.98	0.94
Pseudo-second order	q_e (mg/g)	11.16	2.62
	k_2	2×10^{-3}	2.6×10^{-3}
	R^2	0.99	0.96
Elovich	α (mg/g.min)	1497	0.08
	β (g/mg)	1.51	2.41
	R^2	0.88	0.87
IP	K_p (mg/g.min$^{0.5}$)	0.07	0.07
	C	6.83	0.24
	R^2	0.96	0.85

5.1.3.3. Effects of operational conditions on P removal using steel-making slag

The steel-making slag releases alkali and thus increases final pH of the aqueous solution significantly (Figure 40). Elemental analysis (Table 12) shows a large fraction of calcium oxide (32%) in the steel-making slag in this study. In aqueous solution, calcium oxide can dissolve into the water and releases Ca^{2+} and hydroxyl ions via dissolution to increase in pH of the aqueous solution.

Small steel-making slag particles release alkaline materials into the aqueous solution faster, resulting in higher final pH of the aqueous solution compared to large steel-making

slag particles (Figure 40). pH of the 10 mg P/L aqueous solution at equilibrium state could reach 11 when using the particle size from 0.15 – 0.6 mm, while that only increased to approximately 9 as the particle size of 2.0 – 4.5 mm was used (Figure 40). This is because the smaller slag particle sizes result in more surface (Table 15) for calcium oxide exposure to the aqueous environment. The hydrolysis of these oxides leads to the higher number of hydroxyl ions released into the aqueous solution, thus higher pH of the aqueous solution at the end of the adsorption experiment.
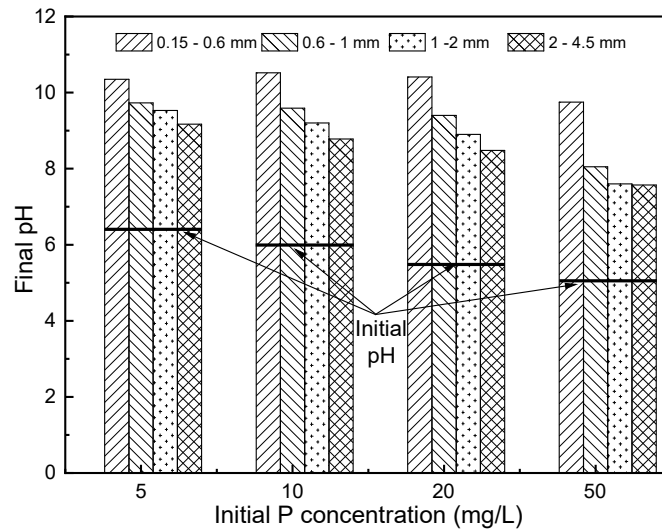
Figure 40: Effects of initial P concentration and particle size on final pH. Experimental conditions: $V_{aqueous\ solution}$ = 0.2 L; steel-making slag mass/ aqueous solution volume = 5 kg/m^3; time = 72 hours; mixing speed = 200 rpm.

P removal efficiency is higher with the smaller steel-making slag particle size (Figure 41). This observation can be explained by two possible mechanisms. Firstly, the decreased size of steel-making slag led to a larger active area with more adsorptive sites, thus increase in the effectiveness of the adsorption of P into the steel-making slag particles and the adsorption rate. In addition, as discussed in section 5.1.3.2, precipitation can also

be a major removal mechanism using the steel-making slag. The smaller particle size can lead to more Ca^{2+} release for P precipitation, thus higher removal efficiency.

Results in Figure 41 demonstrates the potential of steel-making slag for polishing aqueous solution with a low P content. In detail, P removal efficiency of 90% could be achieved using steel-making slag particle size of 0.15-0.6 mm at initial P concentration of 5 mg/L. This result suggested that it might be feasible to use this steel-making slag to polish a typical secondary treated effluent with typical P concentration of 1-2 mg/L [210] to meet stringent discharge limit of P at 0.1 mg/L.
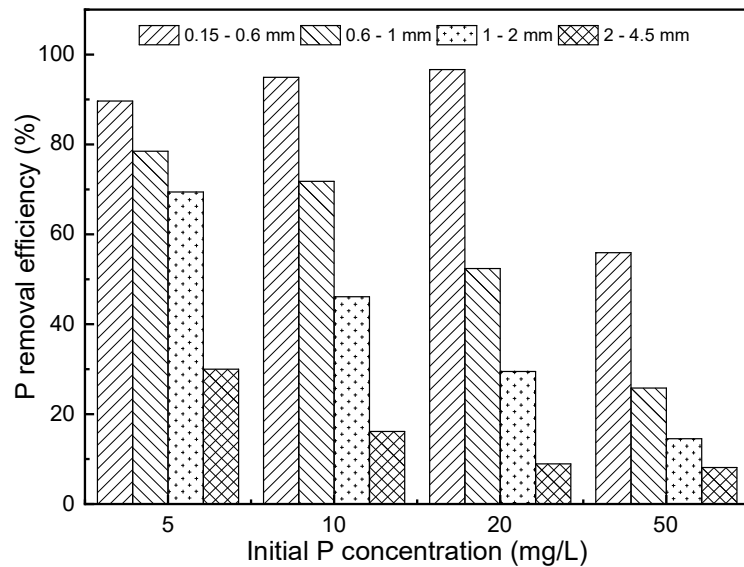
Figure 41: Effects of initial P concentration and particle size on P removal efficiency. Experimental conditions: $V_{aqueous\ solution} = 0.2$ L; steel-making slag mass/ aqueous solution volume = 5 kg/m^3; time = 72 hours; mixing speed = 200 rpm.

P removal efficiency is governed by the initial pH of aqueous solution (Figure 42). Effects of initial pH on P removal using steel-making slag could be divided into two distinctive ranges, regardless of particle sizes. At initial pH up to the pH_{pzc}, P removal efficiency declined as pH increased from 2 to 11 (Figure 42). This observation could be explained via the relationship between pH_{pzc} and electrostatic force. The obtained pH_{pzc}

of steel-making slag was 11.5 (Figure 43). At a low pH value, electrostatic attraction between positively charged steel-making slag surface and phosphate ions can be favourable for adsorption process [211]. Increase in pH close to pH_{pzc} results in a decrease in the surface charge of steel-making slag, thus reducing attractive force and lowering the efficiency of P removal. However, at the second stage when initial pH was above pH_{pzc}, there was again an increase in P removal towards both particle sizes (Figure 42). This phenomenon could be attributed to the direct formation of Ca phosphate precipitates on the steel-making slag surface at high pH [212] as also evidenced from EDS spectra in section 5.1.3.6.
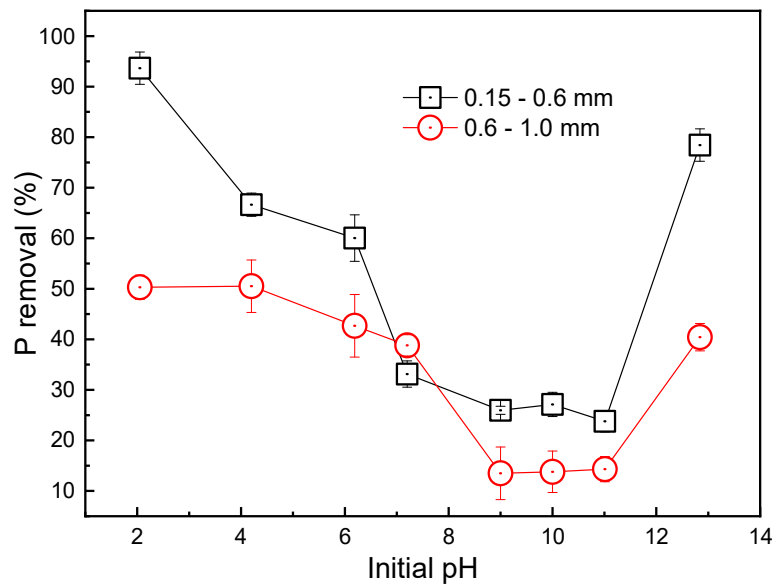
Figure 42: Effects of initial pH of aqueous solution on P removal efficiency. Experimental conditions: $V_{aqueous\ solution}$ = 0.2 L; Initial P concentration = 50 mg/L; steel-making slag mass/ aqueous solution volume = 5 kg/m^3; time = 72 hours; mixing speed = 200 rpm. Values and error bars are the mean and standard deviation of two replicate experiments.
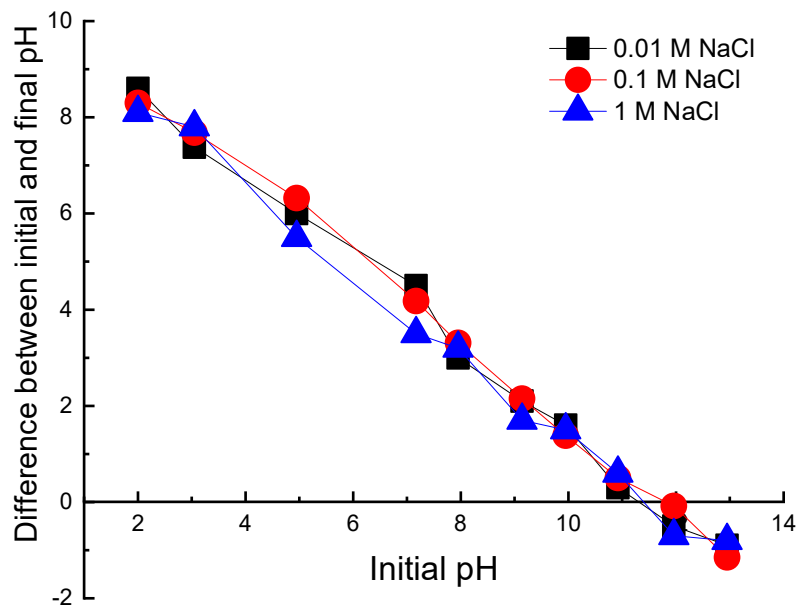
Figure 43: Average point of zero charge for triplicate samples of steel-making slag

P removal is also affected by the aqueous solution volume loading, defined here as the steel-making slag mass to aqueous solution volume ratio (Figure 44). P removal increases as the steel-making slag mass to aqueous solution volume ratio increases. This increase is due to the increase in pH and adsorption sites as well as the produced alkali (liberation of OH⁻ ions into the solution) for P removal.
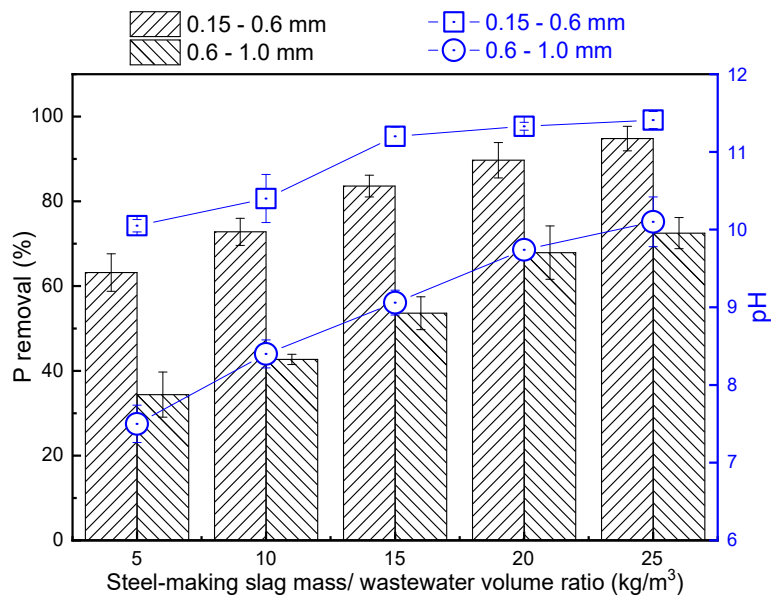
Figure 44: Effects of steel-making slag mass/ aqueous solution volume ratios on changes in final pH and P removal efficiency. Experimental conditions: $V_{aqueous\ solution}$ = 0.2 L; initial P concentration of aqueous solution = 50 mg/L; time = 72 hours; mixing speed = 200 rpm. Values and error bars are the mean and standard deviation of two replicate experiments.

5.1.3.4. Effects of using buffer system on P removal capacity of steel-making slag

Calcium release from the steel-making slag significantly influenced the aqueous solution alkalinity. As calcium was released to the aqueous phase, there was also a pH increase over time (Figure 45). As reported in section 5.1.3.1, steel-making slag with small particle size has a larger surface area, leading to more calcium release into the aqueous phase (Figure 45).

To assess the impact of pH on calcium release, the results from initially buffered and unbuffered aqueous solution are compared (Figure 45). Ca^{2+} concentration increased much faster when the aqueous solution was buffered compared to unbuffered aqueous solution (Figure 45). This is because the hydrolysis of calcium oxide from the steel-making slag is more favourable at a low pH.

102

Due to the reaction between phosphate and calcium to form Ca-P precipitates, the presence of P in aqueous solution also hindered the increase in Ca^{2+} concentration in the aqueous phase as the experiments progressed (Figure 45). This observation confirms the reaction between Ca^{2+} ions and phosphate P to form Ca-P precipitates as a major P removal mechanism. The formation of some of these precipitates (e.g. hydroxyapatite) consumes OH^- ions via the following reaction [197, 201], thus, lessen the increase in pH.

$$5Ca^{2+} + 3PO_4^{3-} + OH^- \rightarrow Ca_5(PO_4)_3(OH)\downarrow$$
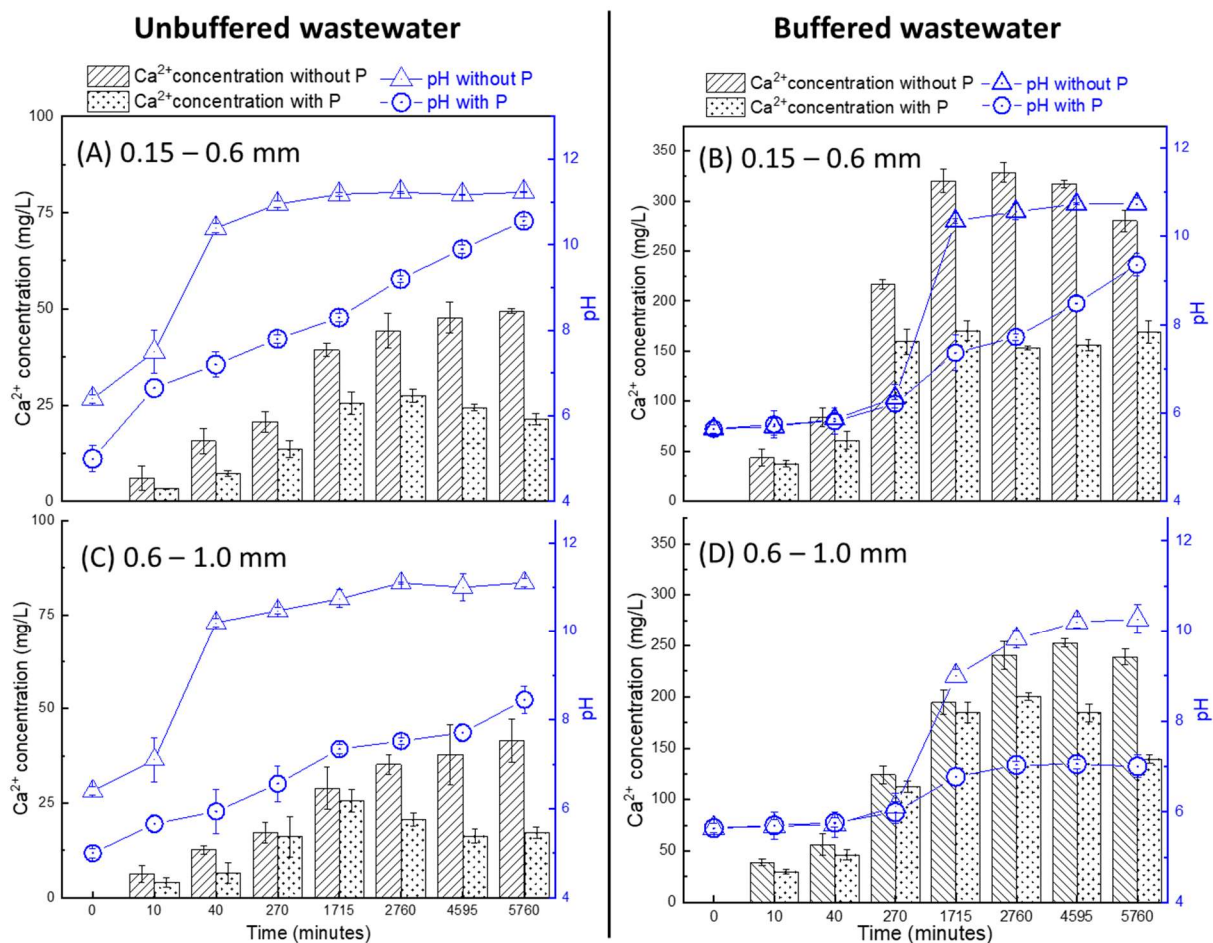
Figure 45: Changes in calcium content and pH using unbuffered and buffered aqueous solution with and without P at different particle sizes over time. Experimental conditions: $V_{aqueous\ solution} = 0.2$ L; initial P concentration of aqueous solution = 85 mg/L; mixing speed = 200 rpm; steel-making slag mass/ aqueous solution volume ratio of 5 kg/m^3. Note: The time value on the X-axis is not on a linear scale. Values and error bars are the mean and standard deviation of two replicate experiments.

Results in Figure 46 show the significant role of pH in the removal of P by steel-making slag. Buffering the aqueous solution resulted in a significantly enhanced P removal. Under optimised condition, near complete P removal can be achieved using steel-making slag size of 0.15 – 0.6 mm (Figure 46). A similar trend can be observed with

larger steel-making slag particle size of 0.6 – 1.0 mm between buffered and unbuffered aqueous solution (Figure 46).
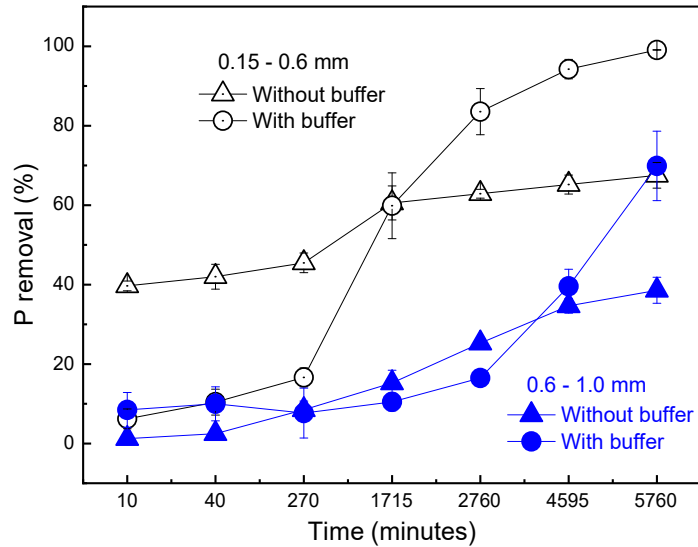
Figure 46: Changes in P removal using different steel-making slag particle sizes with and without the buffer system over time. Experimental conditions: $V_{aqueous\ solution}$ = 0.2 L; initial P concentration of aqueous solution = 85 mg/L; mixing speed = 200 rpm; steel-making slag mass/ aqueous solution volume ratio of 5 kg/m^3. Note: The time value on the X-axis is not on a linear scale. Values and error bars are the mean and standard deviation of two replicate experiments.

5.1.3.5. P removal mechanisms by the steel-making slag

To differentiate between adsorption and precipitation, alkaline materials were first weathered out from the steel-making slag into an aqueous solution (section 5.1.2.2). Spent steel-making slag was then removed. The obtained aqueous solution was mixed with aqueous solution containing P. Results from Figure 47 show chemical precipitation as a major but not the only P removal mechanism. In the presence of steel-making slag, both adsorption and precipitation can occur. The presence of steel-making slag resulted in higher P removal efficiency particularly at the beginning of the experiment (Figure 47).

It is also noteworthy that difference in P removal between the combination of adsorption and precipitation (in the presence of steel-making slag) and only precipitation decreased over time. This observation suggests that at the beginning, P removal was dominated by adsorption but adsorption was also driven by the interaction between calcium and P to eventually form Ca-P precipitates on the surface of the steel-making slag particles. This is further discussed in the next section.
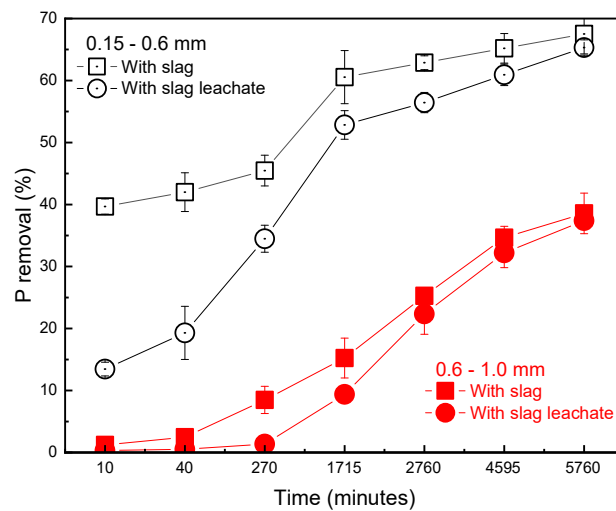
Figure 47: Comparison in P removal between presence and absence of steel-making slag towards different steel-making slag particle sizes. Experimental conditions: $V_{aqueous\ solution}$ = 0.2 L; initial P concentration of aqueous solution = 85 mg/L; mixing speed = 200 rpm; steel-making slag mass/ aqueous solution volume ratio of 5 kg/m^3. Note: The X-axis is on a logarithmic scale. Values and error bars are the mean and standard deviation of two replicate experiments.

5.1.3.6. Characterisation of steel-making slag after P removal

Microscopic analysis, elementary mapping and chemical bonding characterization of the steel-making slag surface before and after adsorption confirm the presence of Ca-P precipitates at the surface of steel-making slag particles (Figure 48 and Figure 49). In agreement with the steel-making slag composition previously reported in Table 12, Ca,

Si, Fe, Mg and O were abundant at the coarse surface of fresh steel-making slag (Figure 48A-B). The observation of the peaks in the FTIR regions of 400 – 800 cm^{-1} and 991 cm^{-1} (Figure 49) also confirmed the presence of M-O (M = Mg, Al, Fe), and Ca-O bonds, respectively [213, 214].
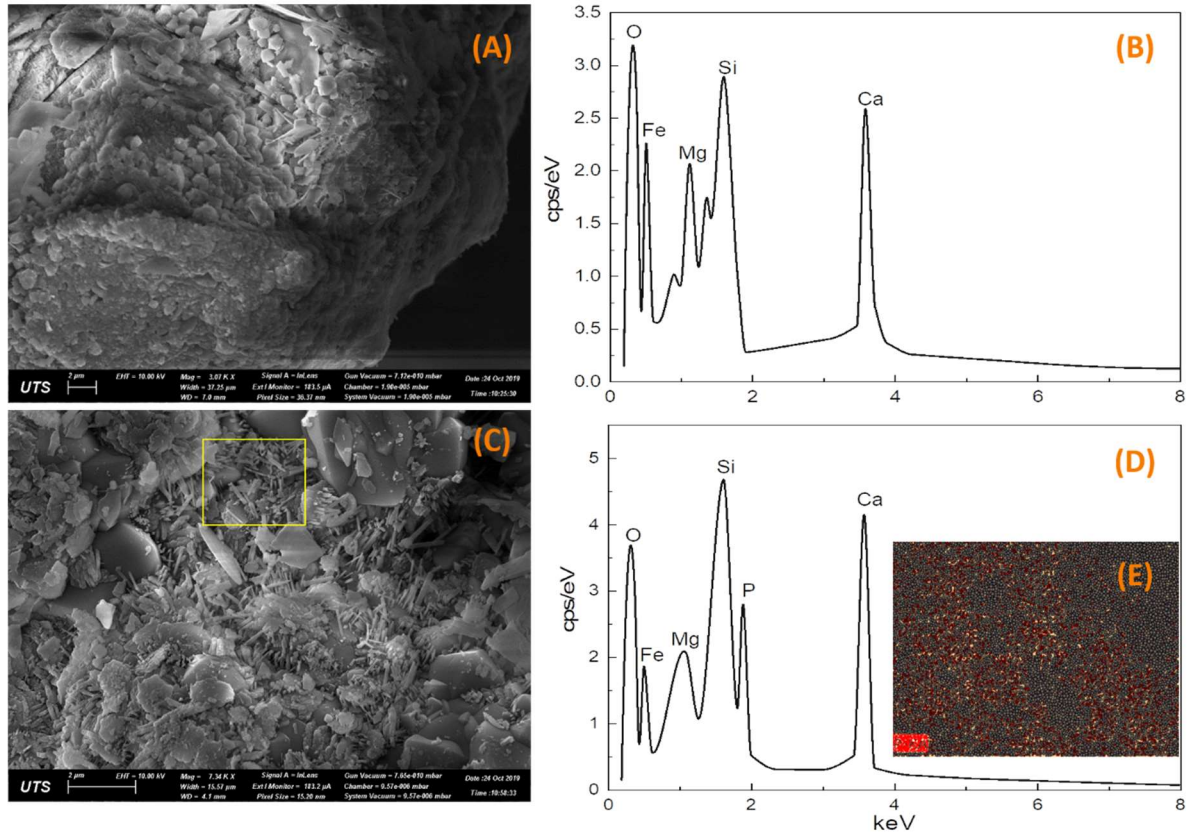
Figure 48: SEM and EDS mapping measurements of steel-making slag surface (A and B) before and (C and D) after P removal. In the image of EDS mapping (E), red dots represent the distribution of P on the surface of steel-making slag (EDS mapping was within the box in Figure 8C).

After adsorption, the surface was covered by a layer of needle-like crystals consistent with the morphology of hydroxyapatite (HAP) (Figure 48C). The HAP crystals observed on the surface of the steel-making slag in this study had a similar shape to those observed by Neira et al. [215]. The energy dispersive X-ray spectroscopy (EDS) analysis demonstrated that the crystalline layer consisted of Ca and P (Figure 48D), indicating

crystallization of HAP. This result is in good agreement with the FTIR spectra of steel-making slag surface with the observation of the band around 1080 cm^{-1} (Figure 49) that represents the vibration of O-P-O bond of HAP [213]. Uniform distribution of P on the steel-making slag surface after adsorption is also confirmed through EDS mapping analysis (Figure 48E).
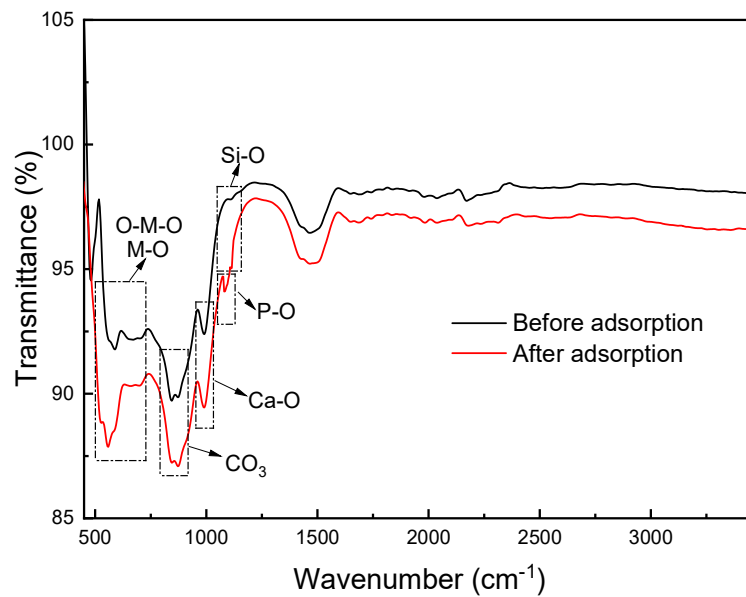
Figure 49: FTIR spectra of steel-making slag before and after P removal.

It is noteworthy that both before and after adsorption, there was the appearance of the band close to 860 cm^{-1} (Figure 49). This peak resulted from the bending effect of the interlayer carbonate group [213]. The presence of carbonate group in steel-making slag composition is possibly due to the CO_2 adsorption from the atmosphere. In addition, the intensity of peak decreased after adsorption, which could be attributed to the reduction of free alkali in samples.

5.1.4. Conclusions

The potential of steel-making slag to remove P from treated aqueous solution as a polishing step was demonstrated in this study. Up to 90% can be removed using 5 kg

steel-making slag with particle size of 0.15 – 0.6 mm for each m^3 of simulated effluent. The adsorption isotherm and kinetics of P to steel-making slag were established for a detailed examination of P removal mechanism. The results demonstrate for the first time that both adsorption and precipitation can be major P removal mechanisms by steel-making slag. Adsorption is initially the dominant removal mechanism, followed by Ca-P precipitation as alkali and calcium content are released from the steel-making slag at a later stage. The results indicate that an alkaline environment and high Ca^{2+} concentration are essential for achieving high efficiency of P removal via precipitation. Of particular note, a significant increase in P removal by using steel-making slag can be achieved by buffering aqueous solution at pH of 5.6 and near complete P removal (>99%) can be achieved. Particle size of steel-making slag is an important parameter governing P removal efficiency. The proposed P removal application is particularly useful to steel-making slag fines from the grinding of slag to aggregates. These results show the potential of steel-making slag as adsorbent in a passive and inexpensive process to remove the residual P from wastewater treatment effluents prior to discharge to the environment. However, further research especially at pilot scale is necessary to evaluate the economic viability of this proposed application.

5.2. Application of the steel-making slag to quench residual phosphorus from the recovery process effluent

This chapter has been published as: *M.T. Vu, H.C. Duong, Q. Wang, Z. Cai, N.B. Hoang, N.T.T. Viet, L.D. Nghiem, A low-cost method using steel-making slag to quench the residual phosphorus from wastewater effluent, Environmental Technology & Innovation (2023) 103181.*

5.2.1. Introduction

Sludge centrate, a liquid phase obtained from dewatering digested sludge of anaerobic digesters in WWTPs, is a P-rich stream [155, 216]. A high concentration of P in this stream offers an opportunity for the recovery process [74]. Indeed, a previous study already demonstrated the possibility of using calcium and alkali metals from steel-making slag to recover P via precipitation under the form of calcium phosphate precipitates [74]. However, the research efforts were only made to maximise the efficiency of the recovery process. Little attention has been paid to downstream processing. The fact is that the residual nutrient concentration in the recovery process effluent could be abundant [74]. The discharge of this stream into the waterway without proper post treatment can cause negative impacts on the surrounding environment (e.g. eutrophication and algae bloom phenomenon) [217, 218]. Hence, the post treatment of the recovery process effluent is of necessity.

Several possible methods could be used to remove P from wastewater. Examples include biological treatment [219, 220], ion exchange [221, 222], adsorption [223-225], chemical precipitation [74, 226, 227], and membrane separation [228, 229]. However, given usually low concentration of residual P (i.e. less than 50 mg/L PO_4-P) in the recovery process effluent, treatment technologies such as wetlands, adsorption, and microalgae cultivation are preferred as the economic aspects of treatment are taken into

account [18, 109]. Of these methods, adsorption is the most straightforward method in large scale operations for P removal [230, 231]. However, the cost of adsorbent materials and/or desorption process are limitations to hinder the wide applications of this technology [231]. To address these challenges, using secondary or by-products (e.g. steel-making slag and red mud) from steel and aluminium industries to remove P from wastewater can be a solution due to multiple advantages including reduced treatment costs and beneficial use of waste materials [106]. Due to the presence of metal oxides, (e.g. CaO, MgO, Fe_2O_3, and SiO_2) in the composition, steel-making slag could be capable of capturing P [106, 231]. The feasibility of using steel-making slag to remove P from an aqueous solution has been demonstrated [106]. The weathered steel-making slag or weathered slag after the removal process could be used directly for road base construction.

In a previous study, steel-making slag was used as a source of calcium and alkali metals for the P recovery process [74]. In this process, the calcium and alkali metals were extracted from steel-making slag and then reacted with phosphate ions in pre-concentrated sludge centrate to form calcium phosphate precipitates for recovery [74]. It is hypothesised that steel-making slag after the recovery process with the residual content of metal oxides might still have the capability of capturing P, suggesting a promising approach to using this kind of weathered slag to quench the residual P from the recovery process effluent. This approach can simultaneously maximise the use of this material and further accelerate the weathering of steel-making slag for beneficial use. The intensively weathered slag is less chemically reactive when applied to road construction. In addition, sludge centrate is of high alkalinity (i.e. bicarbonates) [232]. It was reported that the presence of inorganic carbon (e.g. bicarbonates) in the solution could cause competing adsorption effects and reduce the P removal efficiency [101, 233]. Given the high

alkalinity of sludge centrate (i.e. $1,000 - 5,000$ CaCO$_3$ mg/L) [232], the impacts of inorganic carbon in the recovery process effluent on P removal by steel-making slag also need to be taken into account.

This study aims to investigate the feasibility of reusing the weathered slag from the recovery process to quench the residual P from the recovery process effluent. The P removal performance of the weathered slag is determined in parallel with that of fresh slag for comparison. Impacts of the effluent pH on the removal efficiency are examined. In addition, the weathered slag dosage is optimised to ensure the best performance of the removal process. The removal mechanisms are also discussed in this study. Furthermore, the effects of inorganic carbon in the recovery process effluent on the removal performance are disclosed herein.

5.2.2. Materials and methods

5.2.2.1. Materials

In this study, the steel-making slag was used as a source of calcium for the P recovery process. The steel-making slag was collected from an electric arc furnace (InfraBuild, Rooty Hill NSW 2766 Australia). The compositional characteristics of this steel-making slag were presented in a previous study [106]. The steel-making slag was rinsed using distilled water to remove dirt and impurities. The rinsed steel-making slag was then dried at 105 °C overnight. After that, the dried steel-making slag was crushed and sieved to obtain a particle size of less than 0.3 mm. The ground steel-making slag was then stored in an airtight container which was purged using N$_2$ gas to prevent any potential reactions with the ambient air.

Sludge centrate was collected from a dewatering system at a WWTP in Sydney (Australia). Sludge centrate was filtered through 150 μm stainless steel mesh to remove large solid particles and then stored at 4 °C for further use. Seawater as a draw solution

(DS) for a FO system was taken from a beach in Sydney, Australia. The collected seawater was filtered through 0.45 μm filter paper before use. The composition of this seawater was found in a previous study [78].

The lab-scale sand filtration and FO systems to pre-treat and pre-concentrate sludge centrate, respectively were described in detail in Chapter 4. A lab-scale system to perform the P recovery process has been also found in Chapter 4 as well. A 0.1 M hydrochloric acid (HCl) solution was used to adjust the pH of the recovery process effluent.

5.2.2.2. Experimental design

In this study, two sets of experiments were conducted in sequence to investigate the feasibility of using steel-making slag to quench the residual P from the recovery process effluent. The first experiment was to release the process effluent and the weathered slag from the P recovery process. The experimental procedures in this first step were similar to those in Chapter 4. The second experiment focused on using the weathered slag to quench the residual P in the recovery process effluent. It is noted that both the weathered slag and the recovery process effluent were obtained from the first experiment.

In the first experiment, sludge centrate was pre-treated using the sand filtration system at a filtration rate of 20 m/h. The sand filtered sludge centrate was then pre-concentrated using the FO system until 70% water recovery. The operating conditions of the FO enrichment system were found in Chapter 4. The concentrated sludge centrate was used as the first feedstock for the P recovery process. A slag liquor as the second feedstock for the P recovery process was produced by adding steel-making slag of <0.3 mm in particle size into DI water at the dosage of 400 g/L. The slag liquor was obtained by decanting the supernatant of this mixture after being agitated at 200 rpm for 2 hours using an orbital shaker. The slag liquor was then stored in an enclosed and N_2-purged container for further use in the subsequent P recovery process. The solid phase called weathered slag in the

bottom of the glass container after the agitation process was collected and dried at 105 °C for 24 hours and stored in an enclosed and N_2-purged container for further use in a subsequent post-treatment process. Next, the recovery process was conducted at the sludge centrate to slag liquor volume ratio of 0.3, reaction time of 120 min, temperature of 20 °C, and aeration rate of 1 L/min. At the end of the recovery experiments, the precipitate mixture was kept still for gravity-driven clarification for 1 hour. The settling efficiency of the precipitate particles was determined using a 1 L volumetric cylinder. The recovery process effluent was obtained by decanting the supernatant of the separated precipitate mixture. An aqueous sample of this solution was taken for analysis. The settling efficiency of the formed precipitates was important to evaluate the solid-liquid separation of the mixture solution. This parameter was determined by comparing the volume of the precipitates deposited over time with the initial volume of the mixture (i.e. 1 L) in the volumetric cylinder.

In the second test, a series of batch experiments were performed to evaluate the performance of P removal from the recovery process effluent using the weathered slag under different experimental conditions. The impacts of weathered slag dosages, defined as the slag mass to the recovery process effluent volume ratio, on the removal efficiency were investigated. These experiments were conducted with the range of slag dosage from 1 to 10 g/L at room temperature. Experiments to investigate the impacts of the solution pH on the removal efficiency were performed at a pH range from 7.5 to 10.4. The pH of the recovery process effluent was adjusted to desired values using 0.1 M HCl acid solution. Unless otherwise stated, the mixture of weathered slag and the recovery process effluent was agitated continuously at 200 rpm on a flat shaker. The duration of these experiments was 72 hours. The aqueous phase was then filtered using 1.2 μm glass fiber syringe filters for subsequent analysis.

The compliance with adsorption isotherm models was also examined to understand the removal mechanism. The adsorption isotherm was determined at a constant P concentration (i.e. the default P level of the recovery process effluent) and varied dosage of the weathered slag from 1 to 10 g/L. The experiment lasted 72 hours to ensure that apparent equilibrium has been achieved. In this study, two isotherm adsorption models including Langmuir and Freundlich were employed to describe the adsorption behaviour of the weathered slag. The details of these two models could be found in section 5.1.2.

To evaluate the impacts of inorganic carbon in the recovery process effluent on the removal efficiency, P removal experiments were also performed using a de-carbonated recovery process effluent. This solution was produced by adjusting its pH to 3.5 using 0.1 M HCl solution followed by aeration at the flow rate of 1 L/min for 30 min. The composition of the recovery process effluent after de-carbonation was characterised to determine the efficiency of the inorganic carbon stripping process.

5.2.2.3. Analytical methods

pH and turbidity were measured using a portable HACH HQ40d pH meter and a portable HACH 2100Q IS turbidity meter (HACH, USA), respectively. Ammonium concentration was determined using the US-EPA Standard Method 10205 using ammonium kits and a HACH DR3900 spectrophotometer. In addition, the point of zero charge (PZC) of steel-making slag was determined following the salt addition method reported elsewhere [205]. In detail, three NaCl solutions at three different concentration values (i.e. 0.01 M, 0.1 M, and 1 M) were prepared by dissolving corresponding amounts of analytical grade sodium chloride salt into DI water. For each prepared solution, a series of conical flasks containing 50 mL of NaCl solution was set up and adjusted pH to 2, 3, 5, 7, 8, 9, 10, 11, 12, and 13 using 0.1 M NaOH and 0.1 M HCl solutions. To each different pH solution, 0.5 g of steel-making slag was added and agitated at 150 rpm for 24 hours

using an orbital shaker. The initial and final pH values of each solution were measured. The correlation in the difference between final and initial pH against the initial pH was plotted for three different molar NaCl solutions. The x-intercept value was denoted as PZC.

P and Ca concentrations in the sample were analysed using an Inductively Coupled Plasma – Mass Spectroscopy system (ICP-MS, Agilent 7900). The total suspended solid (TSS) content was determined by gravimetric analysis. In detail, 5 mL of the precipitate suspension was filtered through a 1.1 μm pre-weighed glass filter paper. The filter paper was then dried at 105 °C for 8 hours to a constant mass. Inorganic carbon was measured using a total/dissolved organic carbon analyser.

5.2.3. Results and discussions

5.2.3.1. Characterisation of the recovery process effluent

The nutrient levels (i.e. total P and NH_3-N) in the recovery process effluent were significantly lower compared to those in fresh sludge centrate but still abundant (Table 18). As explained in the previous study, the decrease in total P and ammonia in sludge centrate after the recovery process was attributed to the formation of Ca-P precipitates and the conversion of ammonium ions to ammonia gas under the alkaline environment [74]. After the recovery process, total P and ammonia levels (i.e. 5.55 and 113 mg/L, respectively) were still excessive although the removal efficiencies for each achieved 96.8 and 90%, respectively. According to the Environmental Protection Agency in the United States, the recommended level of total P and NH_3-N for aquatic life should be less than 0.1 and 17 mg/L, respectively. The current levels of total P and NH_3-N in the recovery process effluent are approximately 50 and 10 times higher than the regulated values. Therefore, this stream must be treated before being discharged into the environment.

Gravity-driven clarification was capable of separating the formed precipitates effectively from the solution (Figure 50). The separation step is critical for further treatment of the recovery process effluent. The precipitate settling efficiency increased significantly to 70% during the first 20 min of settling time before gradually reaching 80% after 60 min (Figure 50). The recovery process effluent was almost transparent as the turbidity decreased to 0.28 NTU, equivalent to 99.7% removal efficiency, compared to the turbidity of fresh sludge centrate. The results suggested that the recovery process effluent could be removed from the mixture solution easily only by the decanting method after the gravity-driven settling of precipitates.

Table 18. The properties of sludge centrate after different treatment processes (values indicated average ± standard deviation of three samples).

Parameters	Sludge centrate	Sand filtered	Concentrated sludge centrate	Slag liquor	Recovery process effluent	De-carbonated effluent
pH (-)	8.02 ± 0.03	8.07 ± 0.06	8.31 ± 0.07	12.7 ± 0.3	10.4 ± 0.1	4.2 ± 0.1
TSS (mg/L)	198 ± 18.4	37.0 ± 11.3	17.0 ± 7.9	-	-	-
Turbidity (NTU)	82.0 ± 9.1	24.0 ± 6.2	13.0 ± 4.7	0.25 ± 0.10	0.28 ± 0.07	0.28 ± 0.06
Total P (mg/L)	177.2 ± 11.5	175.0 ± 5.9	487.2 ± 5.8	-	5.55 ± 0.24	5.61 ± 0.13
NH_3-N (mg/L)	1124 ± 41	1105 ± 37	1278 ± 14	-	113 ± 11	116 ± 10
Inorganic carbon (mg/L)	516.2 ± 23.5	527.8 ± 18.7	1432 ± 72	53.0 ± 2.8	113.2 ± 11.3	0
Ca (mg/L)	36.8 ± 10.5	39.2 ± 6.9	47.3 ± 4.4	1078 ± 18	13.8 ± 1.8	14.2 ± 2.0
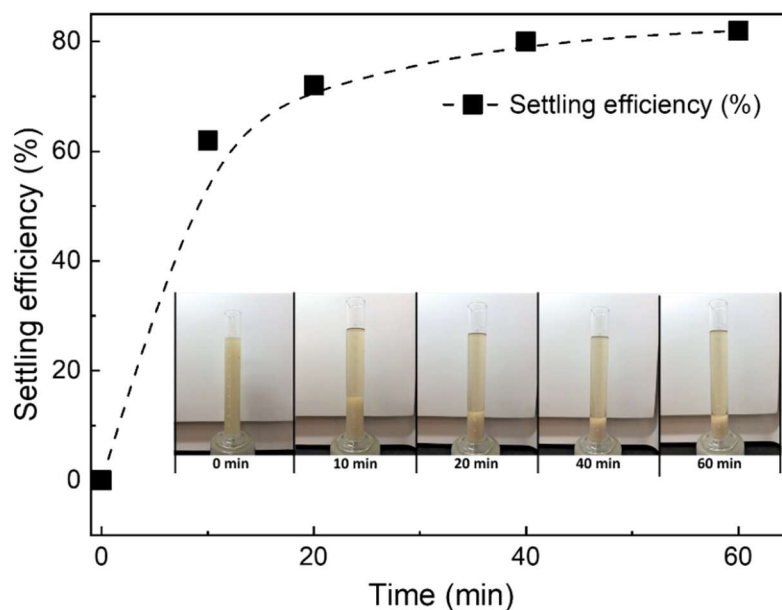
Figure 50: Settling performance of formed precipitates after the recovery process.

5.2.3.2. Impacts of initial pH of the recovery process effluent on the removal efficiency

Overall, weathered slag and raw slag showed similar (or almost identical) performance in P removal (Figure 51). Regardless of the solution pH, weathered slag always showed similar P removal efficiency to raw slag. This observation suggests that after the weathering process, the P removal capability of slag remained unchanged. This is probably due to the high content of Ca remaining in weathered slag after the leaching process. Indeed, only 0.7% of total Ca in raw slag was released into the slag liquor (data not shown).

Decreased initial pH of the recovery process effluent increased the P removal efficiency significantly (Figure 51). In addition, it appeared that pH also affected the impacts of slag dosage on the P removal efficiency. At high pH 10.4, the maximum P removal efficiency was approximately 50%. Moreover, at this pH value, an increase in the slag dosage of above 5 g/L did not enhance the removal efficiency. At lower pH, the

119

impacts of slag dosage on the removal efficiency were more significant as increased efficiencies were observed at elevated slag dosage. The results demonstrated that P could be almost completely removed from the solution using weathered slag when pH was adjusted to be lower than 8.5 (Figure 51). This phenomenon could be explained via pH_{pzc} of weathered slag (i.e. approximately 11.2) (Figure 52). At lower pH, leach slag was more negatively charged, encouraging the attractive electrostatic force between the slag surface and phosphate ions in the solution. This force could promote the P removal mechanism via physical adsorption. This result could be supported by the isotherm results discussed further in section 5.2.3.4. The results in Figure 51 demonstrated that a further decrease in pH to less than 8.5 was unnecessary as no improvements in P removal were observed.
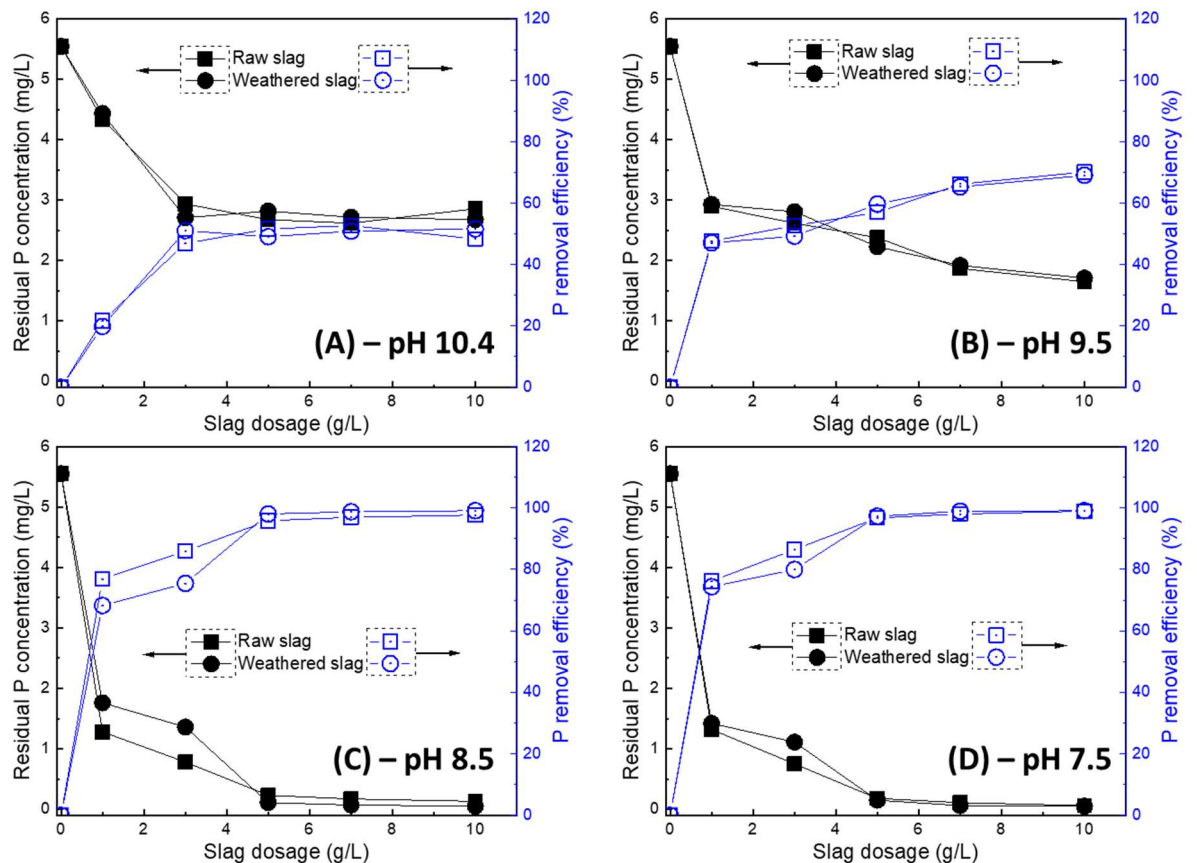
Figure 51: Impacts of steel-making slag dosage and solution pH: (A) – pH 10.4, (B) – pH 9.5, (C) – pH 8.5, and (D) – pH 7.5 on P removal efficiency. The experimental conditions: contact time = 72 hours, mixing speed = 200 rpm.
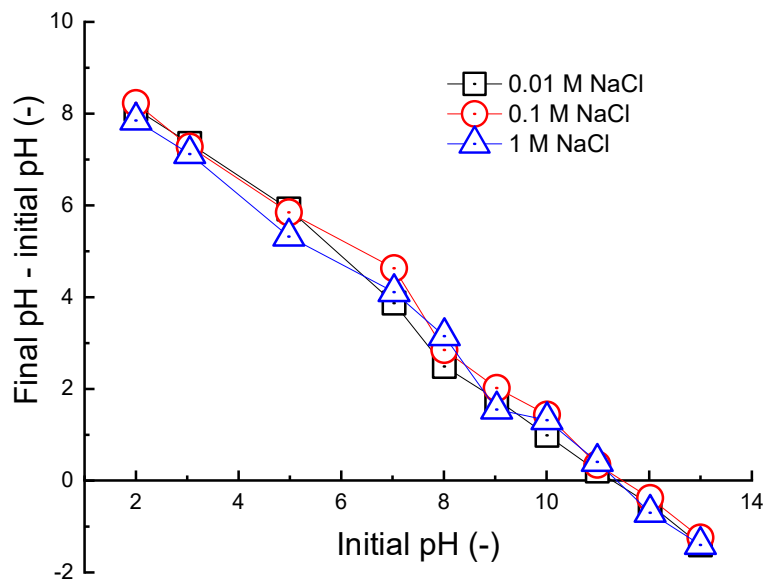
Figure 52: Average point of zero charge of the weathered slag determined by using NaCl solution at different concentrations.

5.2.3.3. Impacts of mixing time on the removal efficiency

Prolonged mixing time was necessary for better P removal efficiency (Figure 53). The removal efficiency increased significantly during the first 25 min then decelerated. Given the discussions from the previous study, this result could be explained by the involvement of different removal mechanisms at different reaction time periods. In detail, at the early stage of the reaction, the dominant removal mechanism was adsorption as this mechanism was facilitated at a favourable solution pH (i.e. 8.5). Hence, the reaction rate was fast. Over time, when more Ca was released into the solution with increasing pH, the removal mechanism via Ca-P precipitation prevailed. This mechanism explained the slow reaction kinetics at this reaction stage.
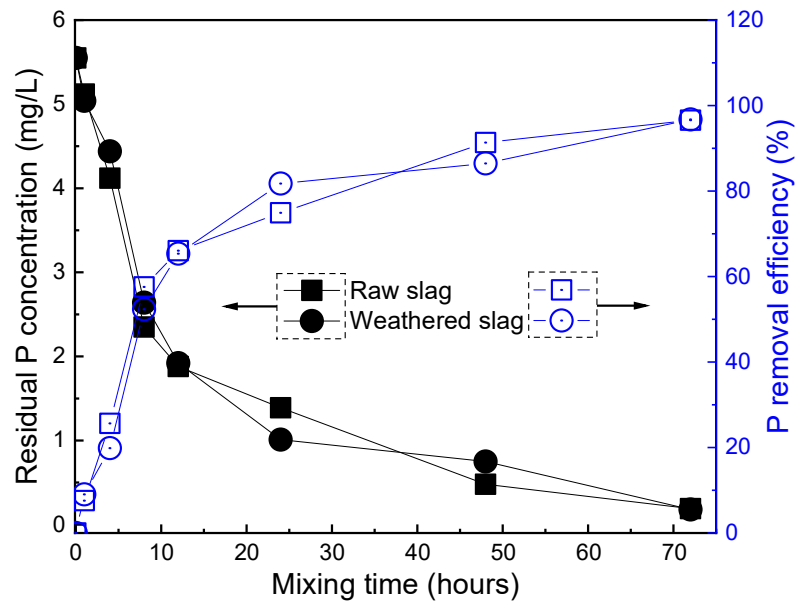
Figure 53: Impacts of mixing time on P removal efficiency by different types of slag. The experimental conditions: slag dosage = 5 g/L, solution pH = 8.5, mixing speed = 200 rpm.

5.2.3.4. Adsorption isotherm and removal mechanisms

The solution pH could govern the P removal mechanism by raw and weathered slag (Table 19). The adsorption behaviour of raw slag and weathered slag was described by fitting two basic isotherm models (i.e. Langmuir and Freundlich). The results from Table 19 demonstrated that the adsorption behaviours of raw slag and weathered slag were comparable and dependent on the solution pH. At pH 8.5, the P adsorption to raw and weathered slag could be described by the Langmuir and Freundlich isotherms (Table 19), confirming adsorption as a major P removal mechanism. However, both isotherm models could not be used to describe the adsorption behaviour at pH 10.4 as all fitting coefficients (R^2) were very low. The results are consistent with the observations in the previous section. In consideration of R^2 values, the adsorption of P to both types of slag can be modelled better by the Langmuir isotherm rather than the Freundlich isotherm.

Table 19. Adsorption isotherms of P to different types of slag at different solution pH values.

Isotherm model	Parameters	pH 10.4		pH 8.5	
		Raw slag	Weathered slag	Raw slag	Weathered slag
Langmuir	q_{max} (mg/g)	-0.68	-0.73	5.68	2.45
	K_L (L/mg)	-0.14	-0.14	0.86	6.22
	R^2	0.29	0.34	0.95	0.91
Freundlich	n	0.49	0.59	1.32	2.64
	K_F	0.06	0.09	2.77	2.03
	R^2	0.50	0.42	0.91	0.77

5.2.3.5. Impacts of inorganic carbon in the recovery process effluent on the removal efficiency

Results from this study show that bicarbonate content in the solution can affect P removal. In fact, de-carbonation of the recovery process effluent decreased the P removal by the weathered slag. In other words, the presence of inorganic carbon in the recovery process effluent facilitated the P removal performance (Figure 54). The results from Figure 54 demonstrated that regardless of the type of slag used, the P removal efficiency decreased by approximately 20% when inorganic carbon was removed completely from the recovery process effluent. This observation could be probably due to the non-participation of the co-precipitation of calcium carbonate and calcium phosphate in the absence of inorganic carbon in the de-carbonated recovery process effluent. When the recovery process effluent was used, the co-precipitation of calcium carbonate and calcium phosphate could be evidenced by the coincidence of high P and inorganic carbon removal

behaviours and low final calcium content in the solution at the end of the experiment (Figure 55). Moreover, a significant increase in the final calcium content was observed in the absence of inorganic carbon, confirming no occurrence of calcium carbonate precipitation (Figure 55). The promoted P removal efficiency by adsorption by the co-precipitation in the presence of carbonate ions has also been reported in the literature [234].
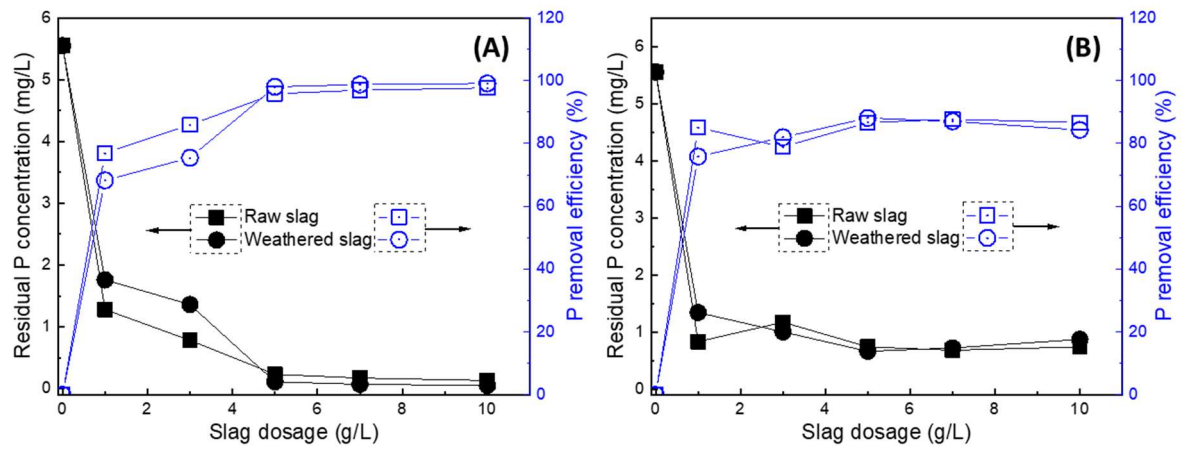
Figure 54: Impacts of the presence of inorganic carbon on P removal efficiency by different types of slag using (A) the recovery process effluent and (B) the de-carbonated recovery process effluent). The experimental conditions: initial solution pH = 8.5, contact time = 72 hours, mixing speed = 200 rpm.
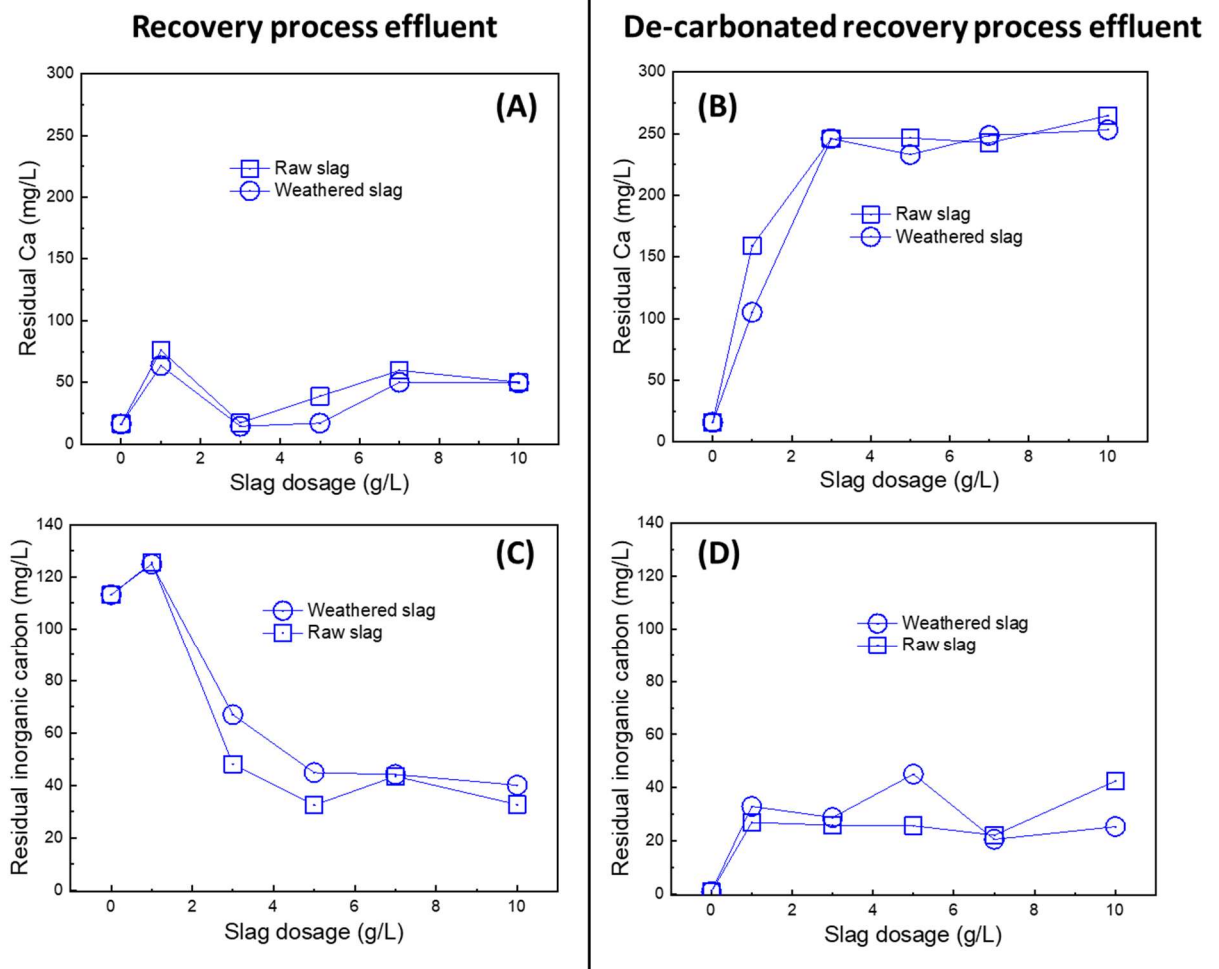
Figure 55: Changes in (A and B) residual Ca and (C and D) residual inorganic contents in the process effluent and the de-carbonated process effluent, respectively during the post treatment under different dosages of slag. The experimental conditions: initial solution pH = 8.5, contact time = 72 hours, mixing speed = 200 rpm.

5.2.4. Conclusions

The feasibility of using weathered slag after the recovery process to quench residual P from the recovery process effluent has been demonstrated in this study. The results showed that the P removal efficiency was low without the adjustment of the recovery process effluent pH. Decreased pH of the recovery process effluent resulted in increased removal efficiency. At the optimal conditions (i.e. pH 8.5 and steel-making slag dosage of 5 g/L), approximately 98% P removal could be achieved with the output level of less

than 0.1 mg/L. The results also demonstrated that enhanced P removal by pH adjustment resulted from the involvement of adsorption in the removing process. This observation was evidenced via the compliance with Langmuir isotherm of the adsorption of P to slag at decreased pH. In addition, the results indicated that the presence of inorganic carbon in the recovery process effluent could facilitate P removal via co-precipitation effects.

Chapter 6. Phosphorus removal and biomass production from sludge centrate using a sequencing batch membrane photo-bioreactor

6.1. Introduction

Municipal wastewater is a valuable resource in a circular economy because it can be used to recover and reuse energy, nutrients, and clean water [7, 10, 235]. In WWTPs, most of the organic input from wastewater is anaerobically digested to produce biogas which is a source of clean energy and digestate (a mixture of solid and liquid residue from anaerobic digestion) [4]. Sludge centrate is the liquid fraction after digestate dewatering that has been reported as the concentrated source of nutrients (i.e. N and P). The ammonia and phosphate contents in sludge centrate can reach up to 1 and 0.5 g/L, respectively [5-8]. The high N and P content in a small volume of sludge centrate offers an excellent opportunity for nutrient recovery.

Nutrient recovery from sludge centrate is a win-win solution for nutrient management in WWTPs. Even if only 30% of nutrients in sewage end up in sludge centrate, the standard practice of returning this stream to the headwork for further treatment can have a negative impact on WWTPs [9]. Examples include nutrient organic carbon imbalance, struvite blockage, and failure to meet stringent effluent discharge standards [10, 11]. Thus, nutrient recovery from sludge centrate can simultaneously improve compliance with effluent discharge standards while also lowering maintenance costs due to the

significant reduction in struvite blockage. At the same time, valuable fertilizers can be made from the recovered nutrients.

To date, a number of techniques have been studied and applied to recover nutrients from wastewater, such as sludge centrate. Examples include direct stripping [236], ion exchange [237], electrodialysis [86], chemical precipitation [10, 22], membrane filtration [10, 238], and microbial electrochemical processes [155, 239]. They have proven their efficacy and potential in recovering nutrients from wastewater. However, majority of these processes are primarily focused on P recovery rather than a combination of both N or P [155]. Furthermore, high chemical and energy consumptions continue to be major barriers to commercialisation of these technologies [10, 86, 240]

Microalgae-based treatment has recently emerged as a cost-effective and environmentally-friendly method of removing and recovering nutrients from wastewater [9, 241]. Microalgae use sun light as the energy source, carbon dioxide from the atmosphere as the carbon source, and N and P from wastewater to grow. Microalgae based wastewater treatment has numerous advantages including low operating costs [241], carbon capture [242, 243], the production of biochemical feedstock [244], and biofuel from algal biomass [245].

Microalgae-based treatments for removing nutrients from wastewater and producing biomass in photobioreactors have been demonstrated in several studies [124, 246]. Zhou, Li, Gao and Zhao [246] reported that *Spirulina platensis* in saline wastewater could remove 80% of total N and 93% of total P, and achieve 0.76 g/L in biomass content. In a more recent study, Sayedin, Kermanshahi-pour, He, Tibbetts, Lalonde and Brar [124] showed N and P removal efficiencies of 95% and 78% from anaerobic digestate, respectively, by *Chlorella sorokiniana*. However, microalgae-based technology has a

high space requirement, thus, it has been rarely commercially applied for removing nutrients from wastewater [247]. A major technical challenge is to increase the microalgae content in the reactor for process intensification and reduction in space requirement [247, 248].

The aforementioned challenge can be addressed by incorporating a submerged ultrafiltration membrane with the bioreactor to form a membrane photobioreactor (MPR). In the MPR, a high algal biomass concentration can be achieved at a low hydraulic retention time allowing for process intensification. Furthermore, this method can be easily scaled up.

Therefore, this study aims to evaluate the effectiveness of an MPR following an ingenious operation cycle in simultaneously recovering nutrients and producing microalgal biomass from sludge centrate. The feasibility of continuous operation of the microalgae system is demonstrated via monitoring its stable performance. Additionally, the effects of hydraulic retention duration and the rate of sludge centrate loading on nutrient removal and biomass generation are investigated. The results from this study are expected to be a stepping-stone to valorise sludge centrate via nutrient recovery and microalgal biomass production.

6.2. Materials and methods

6.2.1. Microalgae inoculum and sludge centrate

The freshwater green microalgae strain *C. vulgaris* (CS-41) used in this study was collected from the Australian National Algae Culture Collection, CSIRO Microalgae Research (Hobart, TAS, Australia). The microalgae were incubated in MLA medium at the University of Technology Sydney culture collection [249]. A concentrated microalgae solution was prepared from the culture collection and used as inoculum. This was

accomplished by removing the supernatant from the culture and centrifuging the remainder at 3,000 rpm for 5 min.

Sludge centrate from a high speed centrifuge at a full scale WWTP (located in Sydney, Australia) was used as the nutrient source to cultivate the microalgae. Large particles were removed from sludge centrate using a 75 μm stainless steel filter mesh. The raw sludge centrate is at pH 6.95 and had 253 mg/L COD, 998 mg/L NH_3-N, and 312 mg/L PO_4^{3-}. The TN and total TP were 1012 and 318 mg/L, respectively.

6.2.2. Experimental systems

Three identical 3.5 L glass reactors were used to cultivate microalgae (Figure 56). The internal dimensions of each reactor were 20 cm in length, 4 cm in width, and 45 cm in height. In order to ensure adequate mixing, each reactor's microalgae culture was aerated at a rate of 1 L/min using a stone diffuser positioned at the bottom of the reactor. The air was cleaned using a 0.45 μm cartridge filter. The reactor was illuminated with a surrounding LED strip at a light intensity of approximately 100 $\mu mol/m^2/s$ in a 18:6-hour light:dark cycle. This light/dark cycle condition has been established in our previous work as a favourable condition for *C. vulgaris* growth [248]. These operational conditions were consistent throughout the experiments regardless of the operation modes of the microalgae reactor.

Figure 56: A photo of batch-mode microalgae reactor.

In the MPR, a polyvinylidene difluoride ultrafiltration (UF) hollow fiber membrane module (Mitsubishi Rayon Co., Ltd) was used to withdraw the treated water (Figure 57 and Figure 58A). The nominal pore size and total surface area of the module were of 0.04 μm and 0.073 m^2, respectively. A Masterflex Peristaltic pump (Cole-Parmer, USA) connected to the membrane module was used to extract clean water from the MPR. A pressure transducer (PT30 model, Extech Instruments, United States) was inserted in the suction line of the pump to monitor the changes in transmembrane pressure during operation.

Figure 57: A photo of membrane photobioreactor.

6.2.3. Experimental design

Microalgae growth and nutrient removal were evaluated at two nutrient (sludge centrate) loading rates. The feed solutions to the MPR were prepared by diluting raw sludge centrate 12.5 and 25 times using clean water corresponding to high and low nutrient loading rates, respectively. This work aims to demonstrate the effectiveness of the MPR in maintaining stable performance in terms of microalgae growth and nutrient removal. Therefore, the pre-treated sludge centrate (section 6.2.1) was further filtered through 1 μm filter paper prior to the dilution step in order to minimise any impacts caused by the presence of bacteria and turbidity in the medium.

Each reactor were inoculated by dosing 50 mL of the concentrated microalgae culture (section 6.2.1) into 2950 mL of diluted sludge centrate in order to achieve a biomass content of approximately 145 mg/L. Each reactor had a working volume of 3 L. It is noted that Microalgae cultures in three reactors were inoculated simultaneously using diluted sludge centrate corresponding to each nutrient loading rate presented earlier. During the stationary phase, one reactor remained in batch mode. The other two reactors were switched to the MPRs at HRT of 3 and 5 days, respectively.

Algal biomass extraction and sludge centrate feeding were conducted once a day in four steps (Figure 58B). First, 100 mL of the microalgae culture was collected from each reactor, which was subsequently used for the measurement of biomass content and nutrient removal. Second, 900 and 500 mL of treated water were extracted through the membrane from each reactor over 1 hour corresponding to HRT of 3 and 5 days, respectively. In practice, the treated water from a microalgae system would be mixed with the raw feed solution for the next cultivation cycle. In this study, the treated water was not reused for cultivation so that a constant nutrient loading can be achieved for

systematic comparison. Instead, the above described fresh culture media were used for daily feeding the system. Third, after the filtration process, fresh diluted sludge centrate solution was fed to the reactor to maintain the HRT of 3 and 5 days, respectively. Finally, the microalgae reactor was operated under steady conditions for the remaining duration of the day.
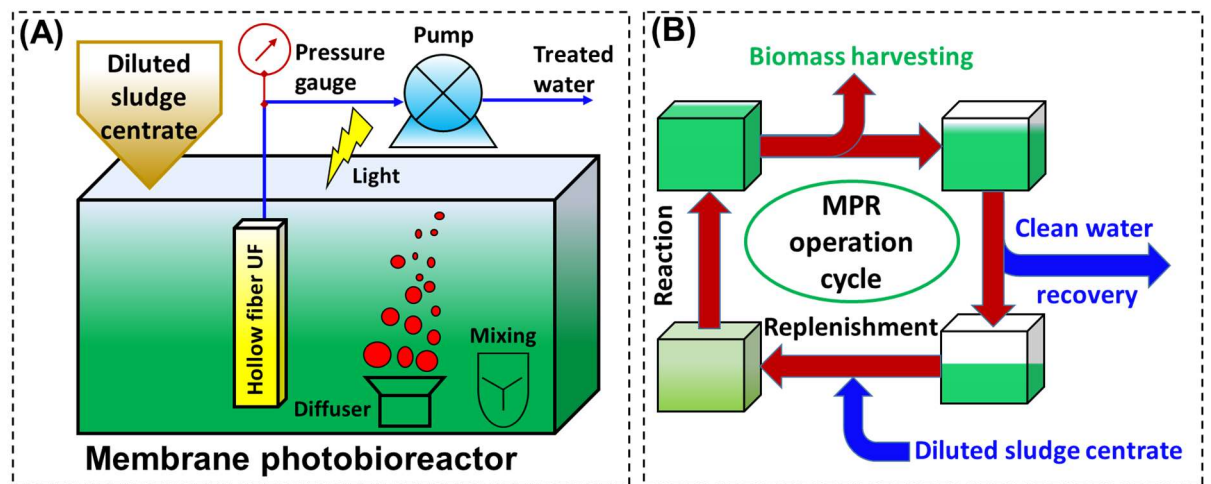
Figure 58: Schematic diagram of experimental systems in this study, which presents (A) membrane photobioreactor and (B) MPR operation cycle.

At the end of the MPR experiment, membrane permeability was measured at the final microalgae content in the reactor. The initial membrane flux was adjusted to 20 L/m^2.h and the transmembrane pressure during filtration was recorded for 150 min for permeability calculation. During the permeability tests, the permeate was returned to the reactor to maintain constant liquid volume and microalgae concentration. The MPR was continuously aerated with air at 1.5 L/min through a diffuser placed in the bottom of the reactor. The permeability test was conducted in replication. At the end of each filtration cycle, the membrane module was backwashed at 40 L/m^2.h using clean water and aerated at 1.5 L/min for 5 min.

6.2.4. Analytical methods

Chemical oxygen demand (COD) was measured by the US-EPA Standard Method 5220 using a HACH DRB200 COD reactor and HACH DR3900 spectrophotometer. Ammonium (NH_3-N), total N (TN) and total P (TP) were determined by HACH standard kits using the HACH DR3900. Orthophosphate (PO_4^{3-}) was measured using ion chromatography (IC) (Thermo Fisher, Australia). The system was equipped with a Dionex AS-AP auto-sampler and a Dionex AS19 IC column (7.5 μm pore size, 4 mm diameter and 250 mm length). The sample injection volume was 10 μL. The analysis conducted using potassium hydroxide eluent with the following gradient (time [min]: concentration [mM]) (0-10: 10; 10-25: 45; 25-27: 45; 27-30: 10; 31: stop run).

The optical density and dry weight of microalgae culture were determined daily using a UV spectrophotometer (UV 6000 Shimadzu; Australia) at a wavelength of 680 nm and by gravimetric analysis, respectively to assess microalgae growth. For the optical density measurement, 3 mL of homogeneous microalgae cell suspension was transferred into a cuvette to measure the optical density. For gravimetric analysis, 50 mL of microalgae cell suspension was filtered through a 1.1 μm pre-weighed glass filter paper. The filter paper was then dried at 60 °C for 4 hours to a constant mass. A linear regression coefficient (R^2) of 0.96 was confirmed between the optical density and dry weight biomass.

6.3. Results and discussions

6.3.1. Biomass production

Results in Figure 59A confirm that microalgae can thrive in sludge centrate. At both nutrient loading rates, there was no observable lag phase, which indicates good adaption of *C. vulgaris* to sludge centrate as the growth medium (Figure 59A). In batch mode, the microalgae grew rapidly and reached a stationary phase with a biomass concentration of

1,100 mg/L at day 6 at both loading rates. The specific growth rates under both nutrient loadings were similar at 0.34 day^{-1} in batch mode. The biomass content and specific growth rate in this study were similar or higher than those reported in previous studies using nutrient rich effluent or aquaculture wastewater as culturing media [247, 250]. Results in this study confirm that sludge centrate was sufficient to maintain high microalgal biomass productivity. Another reason is that biomass production could be promoted by the heterotrophic growth of *C. vulgaris* with the presence of organic carbon in sludge centrate [251].

In batch mode, the microalgae population collapsed after 12-14 days of continuous operation (Figure 59A). This ecological collapse is expected and mainly due to the limited illumination and depletion of limiting nutrients, especially N, as evidenced by the complete removal of ammonia in the effluent in batch mode at the stationary phase (Figure 60). In addition, beyond the stationary phase, the microalgae cultures were highly alkaline at pH 9.35 (data not shown), which was unfavourable for *C. vulgaris* growth [252]. The observed phenomenon is consistent with the growth stages of microalgae (i.e. lag, exponential growth, stationary, and death stages) in previous photobioreactor studies [70, 245].

By contrast to batch mode, the MPR could achieve stable biomass production (Figure 59B&C). In the MPR, regular extraction of microalgal biomass and treated water as well as the replenishment of fresh feed improved the biomass production at both nutrient loading rates. Biomass content in the MPR was 40% higher than that in batch mode (at HRT of 3 days). The observed improved biomass content in the MPR was due to the retention of microalgal biomass by the membrane. The sufficient supply of nutrients from daily fresh feed replenishment to the MPR could also promote the growth of microalgae,

thus increasing biomass content. While the main focus of this study was on microalgae growth in the MPR, additional work is also recommended to examine any long term changes in cell morphology and content caused by sludge centrate.

In the MPR, nutrient loading did not show any discernible impact on biomass growth (Figure 59). The microalgal biomass contents at low and high nutrient loading rates were similar in the MPR (Figure 59B and 58C). This is because in the MPR, the system is not limited by nutrients. Microalgal biomass content in the MPR of approximately 1.6 g/L in this study is much higher than that (i.e. approximately 0.9 – 1.1 g/L) reported in previous works in the literature [247, 248]. Thus, illumination for photosynthesis has probably become the limiting factor in this study. Furthermore, feeding the reactor with high ammonium content (approximately 80 mg/L) on a daily basis may cause toxicity to *C. vulgaris* microalgae, reduce cell viability, and retard the biomass production [253, 254].
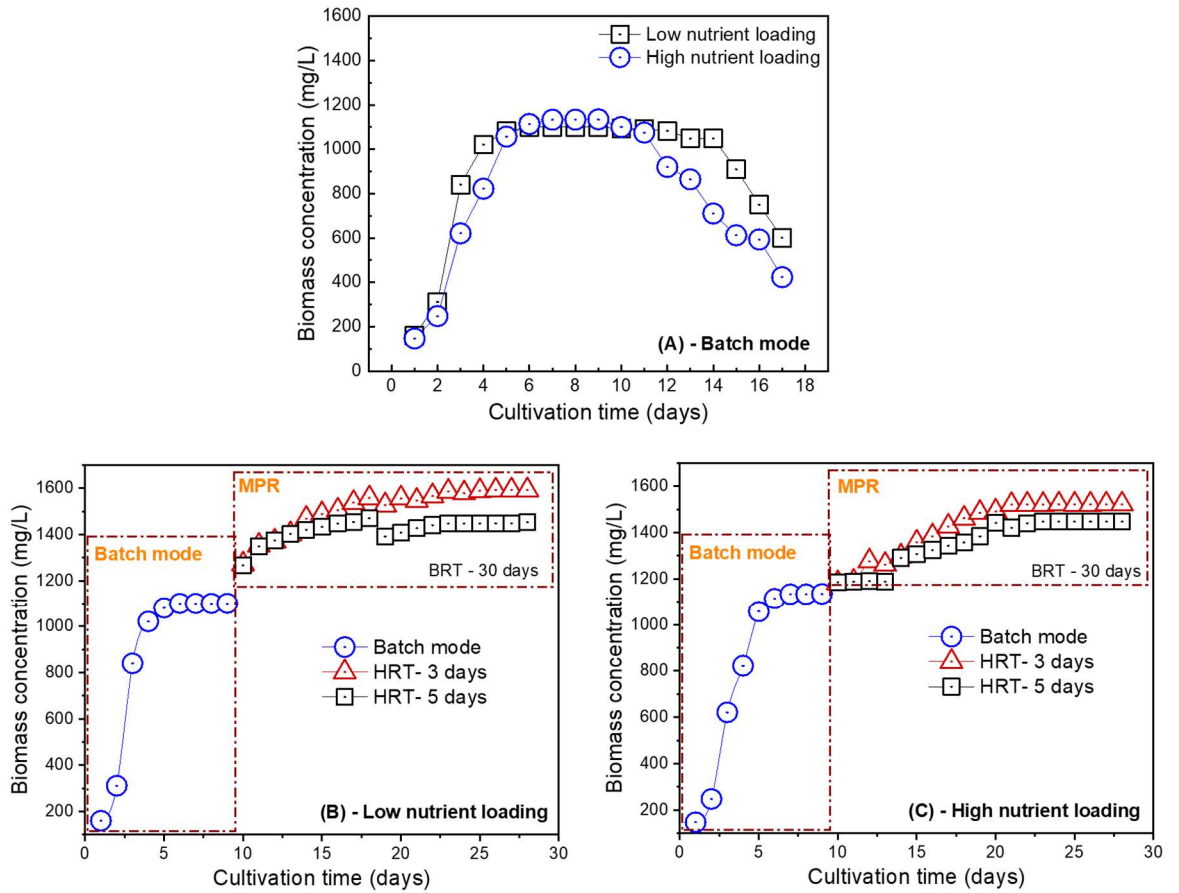
Figure 59: Changes in biomass production of (A) batch mode microalgae reactor and the MPR at (B) low nutrient loading and (C) high nutrient loading.

In MPR mode, microalgal biomass production is regulated by HRT. A low HRT resulted in higher microalgal biomass production (Figure 59B and 58C). The impact of HRT on microalgal biomass production was more profound at the low nutrient loading rate. This is because the larger volume of withdrawal effluent and the replenishment of fresh feed could result in better control of the culture pH and improved illumination for microalgae growth. The obtained pH values of the microalgae culture using the low rate of sludge centrate at HRT of 3 and 5 days after stabilisation of biomass growth were approximately 7.6 and 8.3, respectively.
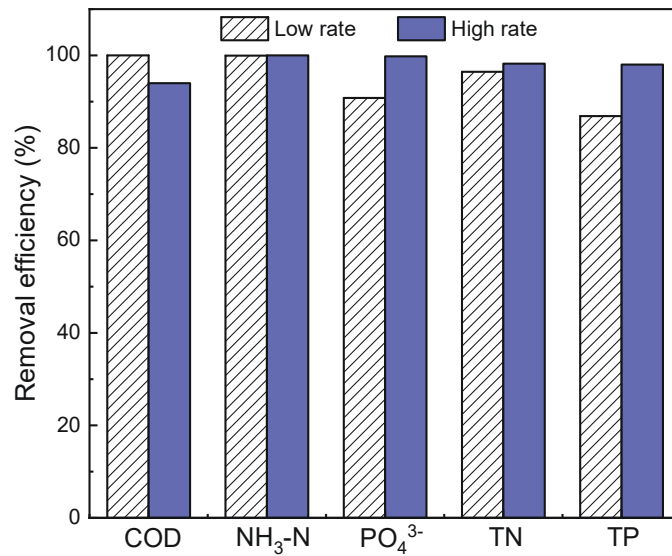
Figure 60: Organic matter and nutrient removal by microalgae at different nutrient loading rates in batch mode cultivation.

6.3.2. Organic matter and nutrient removal from sludge centrate

The removal of COD by *C. vulgaris* microalgae was minimal (Figure 61). This outcome is expected because microalgae are autotrophs, meaning they can obtain energy from light and grow using CO_2 rather than organic carbon to grow. There is an increase in COD residue from sludge centrate addition in the effluent (Figure 61). Nevertheless, the COD residue reached an equilibrium after about four days in the MPR. The observed increase in COD residue is due to the dilution effect at the beginning of the MPR operation and initial chemoautotrophic microalgae growth. In batch mode, COD was removed completely by the microalgae culture, which could be attributed to the chemoautotrophic growth of *C. vulgaris* and enhanced organic carbon metabolism under N-starved conditions [255].
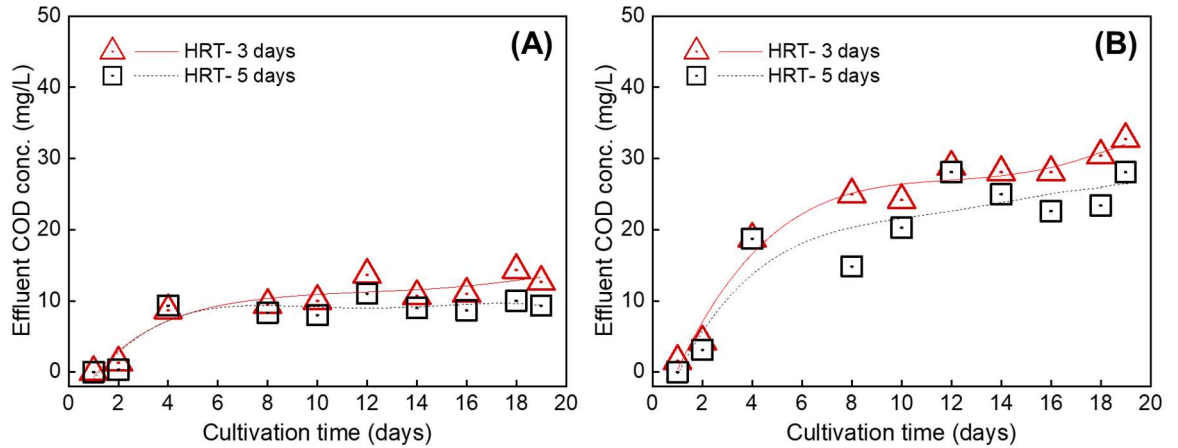
Figure 61: Changes in COD concentration in the MPR effluent (permeate) over time at (A) low and (B) high rate of sludge centrate and different HRTs.

At the beginning of the MPR operation, nutrient content in the treated water remained at a low level as evidenced by the high removal efficiency over the first few days (Figure 62). This initial increase in nutrient removal can also be attributed to the dilution effect discussed above in relation to COD removal. Nutrient removal eventually reached a stable value in all experiments as the equilibrium of nutrient input and output was reached.

Nutrient loading rate has a significant impact on nutrient removal efficiency (Figure 62). Nutrient removal at the high loading rate was only half of that at the low loading rate. As discussed in section 6.3.1, increased nutrient loading did not affect biomass growth. The main mechanism of nutrient removal is mentioned to be biomass production combined with nutrient consumption for microalgae assimilation. Thus, higher nutrient input and low utilisation for biomass growth could result in higher nutrient content in the effluent and decreased removal efficiency.
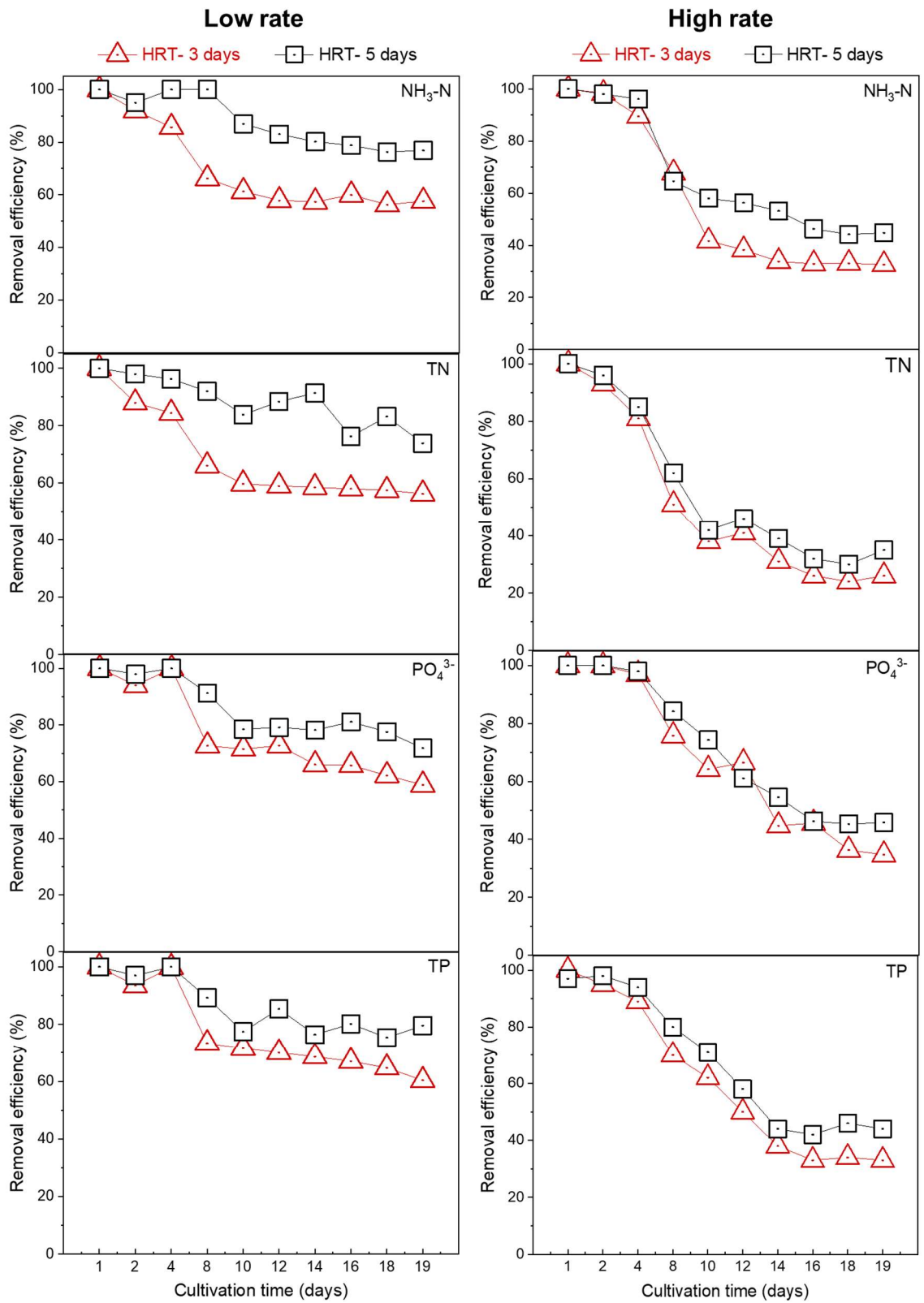
Figure 62: Nutrient removal from sludge centrate in the MPRs at different rate of sludge

centrate and different HRTs.

HRT also has a significant impact on nutrient removal efficiency (Figure 62). On average, 80% ammonia and 72% phosphate could be removed from sludge centrate at low nutrient loading rate with HRT of 5 days. Under low nutrient loading rate, 5 days HRT showed better nutrient removal with approximately 30% increase compared to 3 days HRT. This result could be attributed to more adequate contact time for the nutrient assimilation by microalgae at longer HRT. Furthermore, the elevated pH (i.e. pH 8.3) of the culture after 5 days HRT could promote ammonia volatilisation, thus increasing N removal efficiency.

6.3.3. Membrane permeability

Backwashing completely reversed the membrane water flux. This was demonstrated by insignificant differences in the initial membrane permeability between duplicate experiments regardless of HRTs (Figure 63). The change in the membrane permeability followed a similar pattern throughout the specific filtration process. The membrane permeability decreased significantly during the first 60 min and then remained stable (Figure 63). The rapid deposition of microalgae cells on the membrane surface caused by high hydrodynamic drag force could explain the significant reduction in permeability during the early stages of filtration. The constant permeability after reaching a steady-state value could be attributed to the equilibrium of deposition phenomenon, which occurred as a large number of microalgae cells were swept away from the membrane surface by the shear force generated by the aeration in the reactor.
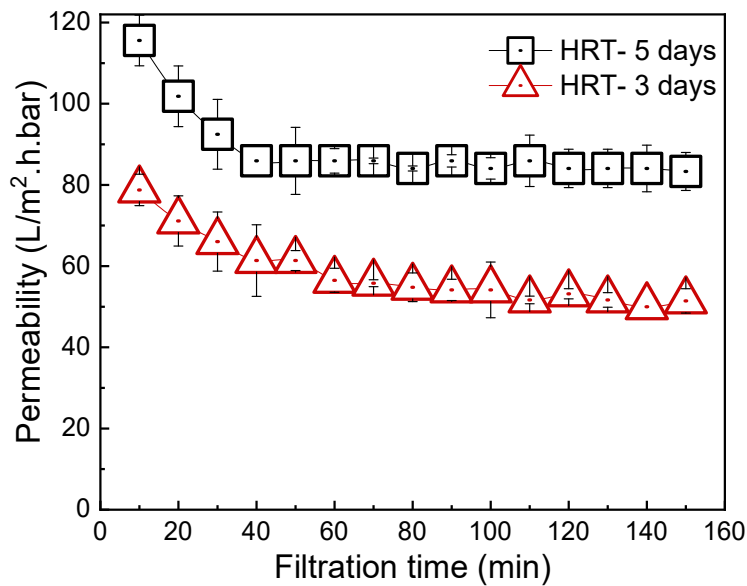
Figure 63: Comparison in membrane permeability of microalgae culture at low loading rate of sludge centrate and different HRTs. Values and error bars are the mean and standard deviation of two replicate experiments.

The permeability of the membrane was determined by the amount of biomass in the reactor (Figure 63). Longer HRT (i.e. 5 days) resulted in higher permeability (Figure 63). The longer HRT with lower biomass concentration, as shown in section 6.3.1, could reduce the severity of microalgae deposition on the membrane, thus improving the permeability. A higher permeability value indicates that the membrane resistance is low and that a larger volume of the medium can be filtered in the same amount of time. These findings imply that operating the MPR at short HRT is recommended due to the low membrane resistance and consequently lower energy consumption.

6.3.4. Biomass harvesting

Overall, the microalgal biomass was effectively harvested from the reactor by the cationic polyacrylamide flocculant (Figure 64). At low dosage of cationic polymers, only microalgal biomass cultivated in the batch mode reactor could be harvested effectively (Figure 64). As the dosage of flocculants increased almost double, the difference in

142

harvesting efficiency among various conditions was negligible (Figure 64). At the same type and dosage of flocculants, especially at low dosage, the harvesting efficiency of microalgae grown in the MPR with longer HRT was always better than that at shorter HRT (Figure 64). This observation is due to changes in charge neutralisation and bridging effects on the microalgae cells. Cationic polymers as flocculants can neutralise the negatively-charged microalgal cells, thus destablising the suspended microalgae cells. Also, the cationic polymers can act as bridging reagents to link the cells together, thus better formation of the flocs. Higher dosage of flocculants with increased charge neutralisation and stronger bridging effects led to the higher harvesting efficiency (Figure 65).
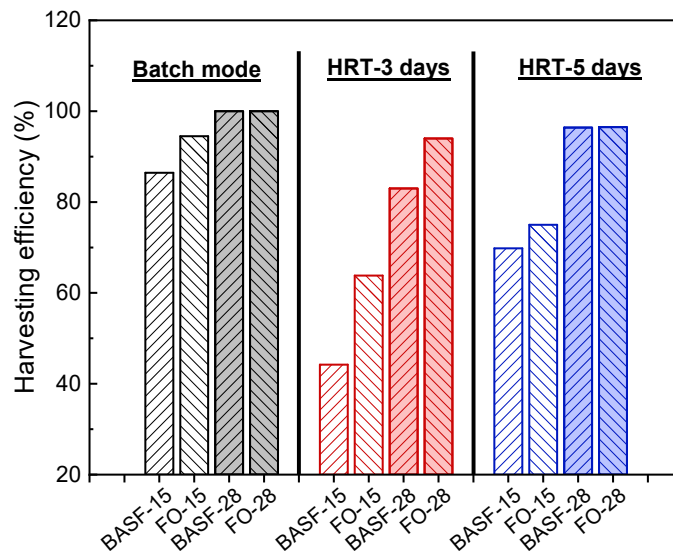
Figure 64: Effects of HRTs and polymer dosages on harvesting microalgal biomass cultivated at high dilution factor of sludge centrate.
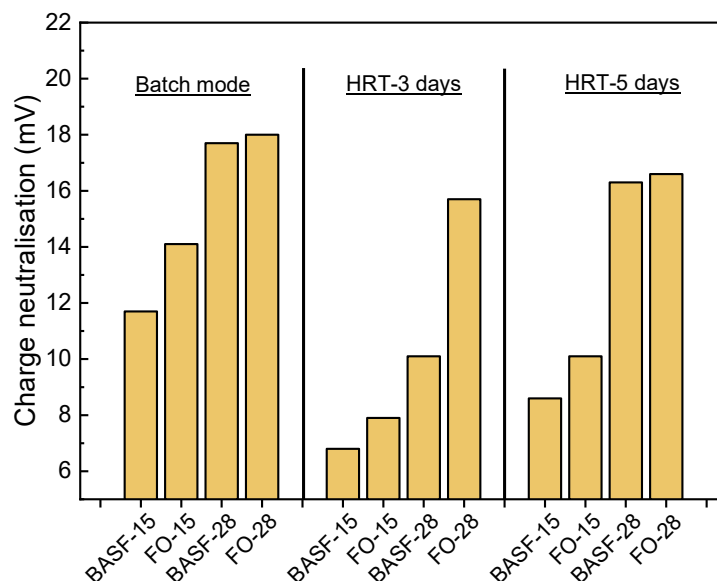
Figure 65: Changes in charge neutralisation of microalgae surface zeta potential using different cationic polymers for harvesting microalgae cultivated at different conditions.

6.3.5. Lipid content

Lipid content of microalgae is governed by the operation mode and HRT of the MPR (Figure 66). Lipid content varied from 17 to 25%. These values of the lipid content of *Chlorella vulgaris* obtained in this study are consistent with those found in the literature [256]. The results indicated that the microalgae cultivated in 5 days HRT MPR showed a higher lipid content than the rests. This might be due to higher removal of N 5 days HRT and the culture was grown under N limitation for a prolonged growing time. Limited N concentration is identified to facilitate the lipid synthesis of microalgae cells. The results also demonstrate that the operation of MPR at high HRT values could increase lipid content of the *Chlorella vulgaris*.
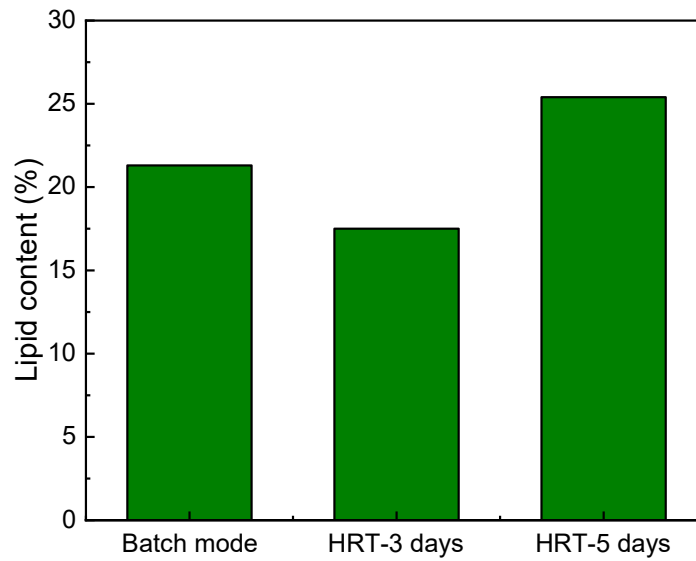
Figure 66: Lipid content of microalgae biomass at stationary phase using sludge centrate at high dilution factor.

6.4. Conclusions

The feasibility of using an MPR for simultaneous nutrient recovery and algal biomass production from anaerobic sludge centrate was demonstrated. In this study, it can be concluded that in comparison to the batch mode reactor, the MPR allows for continuous cultivation of microalgae with 40% higher biomass content. The effects of nutrient loading on biomass growth were negligible. Reduced nutrient loading rate and increased HRT resulted in improved nutrient removal efficiency. The permeability of the membrane was determined by the amount of biomass in the reactor. After backwashing using only water, the water flux could be fully recovered.

Chapter 7. Conclusions and Future Recommendations

7.1. Conclusions

This study has successfully initiated and developed the innovative integrated system using membrane and steel-making slag to remove and recover P from sludge centrate. The developed complete system involved four sequential steps to maximise the P removal and recovery from sludge centrate. These steps consisted of pre-treatment by sand filtration and biogas sparging, enrichment by FO, recovery via Ca-P precipitation, and post-treatment by adsorption and microalgae cultivation technologies pre-treatment, enrichment, recovery, and post treatment via immobilisation and utilisation technologies.

The results from this thesis demonstrated the proof-of-concept of biogas sparging to control membrane fouling during P enrichment in sludge centrate by forward osmosis. Sludge centrate sparging by biogas reduced membrane fouling (measured by flux decline) and filtration time by two and eight times, respectively compared to forward osmosis operation without biogas sparging at the same water recovery of 60%. In addition, the water flux was almost fully recovered by physical flushing when biogas sparging was applied. Biogas sparging also resulted in a significant improvement in the enrichment of organic, ammonia, and phosphate to close to the theoretical value based on mass balance calculation. In other words, organic matter and nutrients were retained in the bulk solution for subsequent recovery. Fouling mitigation and nutrient enrichment improvement by biogas sparging could be attributed to carbonate buffering to maintain a near neutral pH for preventing calcium phosphate precipitation on the membrane surface and ammonia volatilisation.

This thesis work demonstrated the feasibility of using calcium and other alkali metals from steel-making slag to extract and recover P from sludge centrate for fertiliser production. Up to 96% phosphate and 71% ammonia could be recovered from sludge

centrate at the optimal conditions. Mass balance calculation confirmed precipitation and volatilisation as the main mechanisms for phosphate and ammonia recovery, respectively. Morphology and elemental analysis of obtained precipitates confirmed that P was recovered in the form of dicalcium phosphate dihydrate ($CaHPO_4.2H_2O$). The results also showed that sludge centrate pre-treatment by sand filtration and forward osmosis enrichment was essential to achieve high nutrient recovery. Sand filtration pre-treatment decreased the total suspended solid of sludge centrate by eightfold, leading to mitigated membrane fouling and reduced nutrient loss during FO pre-concentration. The production of slag liquor with high calcium and alkaline content from steel-making slag for nutrient recovery was demonstrated. Slag liquor with high pH increased ammonia recovery significantly, but only enhanced phosphate recovery slightly. Phosphate recovery was more dependent on the initial $Ca:PO_4$ molar ratio than the final pH. The process demonstrated in this study has potential and significant practical implications to nutrient recovery from wastewater and beneficial use of steel-making slag.

This study also evaluated a passive inexpensive process to remove P from an aqueous solution. This work differentiated between surface adsorption and chemical precipitation in the bulk solution as key P removal mechanisms by steel-making slag. Experimental results showed that P removal efficiency was governed by steel-making slag particle size, initial P content and ratio of steel-making slag mass to aqueous solution volume. The results demonstrated the potential of steel-making slag for removing dissolved phosphate from wastewater especially as a polishing step. Even at an elevated concentration of P of 5 mg/L, over 90% P removal was achieved using 5 kg steel-making slag with particle size of 0.15 – 0.6 mm for each m^3 aqueous solution. Higher removal efficiency was also achievable through process optimisation. In particular, P removal by steel-making slag could be significantly enhanced, and nearly complete removal (>99%) could be

achievable by buffering the aqueous solution at pH of 5.6. This study also established the isotherms and kinetics of the adsorption of P to steel-making slag to identify key removal mechanisms. Experimental data systematically indicated that P removal by steel-making slag was governed by both adsorption and chemical precipitation. At the early stage of the removal process, adsorption was the dominating removal mechanism, while the P removal via chemical precipitation could occur once the release of Ca^{2+} calcium into the aqueous phase was sufficient to form calcium phosphate precipitates. Overall, P removal by chemical precipitation depended on both pH and Ca^{2+} concentration in aqueous solution.

Following the completed fundamental research on the investigation of the feasibility of using steel-making slag to polish the aqueous solution, the application of steel-making slag in quenching residual P from the recovery process effluent (i.e. liquid phase or supernatant) has been demonstrated in this study. The results showed that the P removal efficiency was low without the supernatant pH adjustment. Decreased pH of the supernatant resulted in increased removal efficiency. At the optimal conditions (i.e. pH 8.5 and steel-making slag dosage of 5 g/L), approximately 98% P removal could be achieved with the output level of less than 0.1 mg/L. The results also demonstrated that enhanced P removal by pH adjustment resulted from the involvement of adsorption in the removing process. This observation was evidenced via the compliance with Langmuir isotherm of the adsorption of P to steel-making slag at decreased pH. In addition, the results indicated that the presence of inorganic carbon in the supernatant could facilitate P removal via co-precipitation effects.

In addition, the study successfully demonstrated the feasibility of using a novel sequencing batch membrane photobioreactor for simultaneous nutrient removal and algal biomass production from diluted sludge centrate. In comparison to the batch mode

reactor, the membrane photobioreactor allowed for continuous cultivation of microalgae with 40% higher biomass content. The effects of nutrient loading on biomass growth were negligible. Reduced nutrient loading rate and increased hydraulic retention time (HRT) resulted in improved nutrient removal efficiency. Cultivation of *Chlorella vulgaris* in the membrane photobioreactor at longer HRT led to higher lipid content of the algal cell. The permeability of the membrane was determined by the amount of biomass in the reactor. After backwashing using only water, the water flux could be fully recovered. The results from this study suggested the feasibility of using the membrane microalgae-based bioreactor to remove P and produce biomass from the recovery process effluent.

7.2. Recommendations for future work

P removal and recovery from waste are an inevitable trend for sustainable development in the context that global P reserves are depleting at an alarming rate. This study has proposed and demonstrated the feasibility of the membrane-based and steel-making slag-based system in recovering and removing P from sludge centrate. However, there are still several issues to be addressed prior to the full-scale deployment of this technology.

In Chapter 3, the proof-of-concept of biogas sparging to control the membrane fouling during FO pre-concentration of sludge centrate was effective. However, the integration of biogas into the FO system may be challenging when biogas, a flammable and harmful gas, is fed continuously into the system. The challenges related to safety issues, mass transfer, and recovery of exhausted biogas after the buffering processes need to be taken into consideration. For this reason, the development of a proper configuration for this purpose is desirable.

Chapter 4 provided a practical way of using steel-making slag as a source of calcium for the P recovery process. The formed calcium phosphate precipitates can be theoretically considered as fertilisers. However, the purity and particle size of these

precipitates needs to be evaluated and optimised to satisfy the requirements of a commercial fertiliser grade for agricultural production. Comparing the life cycle assessment of this alternative with that of the mineral fertiliser from phosphate rock is necessary to have understandings of its impacts on global warming, eutrophication, and energy demand to farmland.

In Chapter 5, an innovative approach of using weathered steel-making slag of the recovery process to quench the residual P in the recovery process effluent was demonstrated to be feasible. The effluent of the recovery process was purified regarding P level and the intensively weathered steel-making slag could be immediately applied to the road construction. Nevertheless, the post treatment of the P-removed effluent still needs to be conducted given the high residual level of ammonia. The treatment of high pH P-removed effluent before discharge is also of necessity.

In Chapter 6, the novel sequencing batch membrane photobioreactor has demonstrated its effectiveness in removing nutrients and producing biomass from diluted sludge centrate. The results suggested the possibility of using this system to remove P and produce biomass from the recovery process effluent. Further research on applying this configuration to polish the real recovery process effluent is needed to confirm the hypothesis.

Upon the above-mentioned improvements of the individual treatment steps, the development, construction, and operation of the initiated framework on a pilot scale are necessary to evaluate the techno-economic feasibility of the whole system. The comprehensive results from the pilot scale are expected to lay the foundation for full-scale adoption.

REFERENCES

[1] D. Mueller, N. Spahr, Water-quality, streamflow, and ancillary data for nutrients in streams and rivers across the nation, 1992 - 2001, in: U.S. Geological Survey data, U.S. Geological Survey, 2005.

[2] D. Puyol, D.J. Batstone, T. Hülsen, S. Astals, M. Peces, J.O. Krömer, Resource recovery from wastewater by biological technologies: Opportunities, challenges, and prospects, Frontiers in Microbiology, 7 (2017) 2106-2106.

[3] M.-L.V. Ravago, A.M. Balisacan, U. Chakravorty, Chapter 1 - The principles and practice of sustainable economic development: Overview and synthesis, in: A.M. Balisacan, U. Chakravorty, M.-L.V. Ravago (Eds.) Sustainable Economic Development, Academic Press, San Diego, 2015, pp. 3-10.

[4] V. Vutai, X.C. Ma, M. Lu, The role of anaerobic digestion in wastewater management, EM (Pittsburgh, Pa.), (2016) 12-16.

[5] Y. Li, Z. Xu, M. Xie, B. Zhang, G. Li, W. Luo, Resource recovery from digested manure centrate: Comparison between conventional and aquaporin thin-film composite forward osmosis membranes, Journal of Membrane Science, 593 (2020) 117436.

[6] H. Liu, X. Li, Z. Zhang, L.D. Nghiem, L. Gao, Q. Wang, Semi-continuous anaerobic digestion of secondary sludge with free ammonia pretreatment: Focusing on volatile solids destruction, dewaterability, pathogen removal and its implications, Water Research, 202 (2021) 117481.

[7] M.T. Vu, L.N. Nguyen, M.A. Hasan Johir, X. Zhang, L.D. Nghiem, M. Elimelech, Biogas sparging to control fouling and enhance resource recovery from anaerobically digested sludge centrate by forward osmosis, Journal of Membrane Science, 625 (2021) 119176.

[8] W. Wang, D.J. Lee, Valorization of anaerobic digestion digestate: A prospect review, Bioresource Technology, 323 (2021) 124626.

[9] I.S.A. Abeysiriwardana-Arachchige, G.W. Chapman, R. Rosalez, N. Soliz, Z. Cui, S.P. Munasinghe-Arachchige, H.M.K. Delanka-Pedige, C.E. Brewer, P.J. Lammers, N. Nirmalakhandan, Mixotrophic algal system for centrate treatment and resource recovery, Algal Research, 52 (2020) 102087.

[10] A.J. Ansari, F.I. Hai, W.E. Price, L.D. Nghiem, Phosphorus recovery from digested sludge centrate using seawater-driven forward osmosis, Separation and Purification Technology, 163 (2016) 1-7.

[11] M.T. Vu, W.E. Price, T. He, X. Zhang, L.D. Nghiem, Seawater-driven forward osmosis for pre-concentrating nutrients in digested sludge centrate, Journal of Environmental Management, 247 (2019) 135-139.

[12] C. Hiet Wong, G.W. Barton, J.P. Barford, 25 - The nitrogen cycle and its application in wastewater treatment, in: D. Mara, N. Horan (Eds.) Handbook of Water and Wastewater Microbiology, Academic Press, London, 2003, pp. 427-439.

[13] Y. Liu, J. Chen, Phosphorus cycle, in: B. Fath (Ed.) Encyclopedia of Ecology (Second Edition), Elsevier, Oxford, 2014, pp. 181-191.

[14] J. Zhang, Q. She, V.W.C. Chang, C.Y. Tang, R.D. Webster, Mining nutrients (N, K, P) from urban source-separated urine by forward osmosis dewatering, Environmental Science & Technology, 48 (2014) 3386-3394.

[15] J. Foct, Future developments and applications of nitrogen-bearing steels and stainless steels, Sadhana, 28 (2003) 731-737.

[16] S.C. Morton, M. Edwards, Reduced phosphorus compounds in the environment, Critical Reviews in Environmental Science and Technology, 35 (2005) 333-364.

[17] S. Daneshgar, A. Buttafava, A. Callegari, A.G. Capodaglio, Economic and energetic assessment of different phosphorus recovery options from aerobic sludge, Journal of Cleaner Production, 223 (2019) 729-738.

[18] J.T. Bunce, E. Ndam, I.D. Ofiteru, A. Moore, D.W. Graham, A review of phosphorus removal technologies and their applicability to small-scale domestic wastewater treatment systems, Frontiers in Environmental Science, 6 (2018).

[19] M.G. Lusk, G.S. Toor, Y.-Y. Yang, S. Mechtensimer, M. De, T.A. Obreza, A review of the fate and transport of nitrogen, phosphorus, pathogens, and trace organic chemicals in septic systems, Critical Reviews in Environmental Science and Technology, 47 (2017) 455-541.

[20] J.I. Inoue, B.K. Biswas, H. Kawakita, K. Ohto, H. Harada, K. Inoue, Removal and recovery of phosphorus from water by means of adsorption onto orange waste gel and pectic acid gel loaded with zirconium, Bioresrouce Technology, 35 (2009) 30-35.

[21] N. Kawasaki, F. Ogata, H. Tominaga, Selective adsorption behavior of phosphate onto aluminum hydroxide gel, Journal of Hazardous Materials, 181 (2010) 574-579.

[22] S. Daneshgar, A. Buttafava, D. Capsoni, A. Callegari, G.A. Capodaglio, Impact of pH and ionic molar ratios on phosphorous forms precipitation and recovery from different wastewater sludges, Resources, 7 (2018).

[23] E. Diamadopoulos, K. Megalou, M. Georgiou, N. Gizgis, Coagulation and precipitation as post-treatment of anaerobically treated primary municipal wastewater, Water Environment Research, 79 (2007) 131-139.

[24] V. Huy Tran, S. Lim, M. Jun Park, D. Suk Han, S. Phuntsho, H. Park, H. Matsuyama, H. Kyong Shon, Fouling and performance of outer selective hollow fiber membrane in osmotic membrane bioreactor: Cross flow and air scouring effects, Bioresource Technology, 295 (2020) 122303.

153

[25] A. Ruiz-Martinez, N. Martin Garcia, I. Romero, A. Seco, J. Ferrer, Microalgae cultivation in wastewater: Nutrient removal from anaerobic membrane bioreactor effluent, Bioresource Technology, 126 (2012) 247-253.

[26] W. Xue, T. Tobino, F. Nakajima, K. Yamamoto, Seawater-driven forward osmosis for enriching nitrogen and phosphorous in treated municipal wastewater: Effect of membrane properties and feed solution chemistry, Water Research, 69 (2015) 120-130.

[27] Z.-r. Hu, M.C. Wentzel, G.A. Ekama, Anoxic growth of phosphate-accumulating organisms (PAOs) in biological nutrient removal activated sludge systems, Water Research, 36 (2002) 4927-4937.

[28] Y.-K. Wang, X.-R. Pan, Y.-K. Geng, G.-P. Sheng, Simultaneous effective carbon and nitrogen removals and phosphorus recovery in an intermittently aerated membrane bioreactor integrated system, Scientific Reports, 5 (2015) 16281.

[29] W. Fan, Y. Li, Q. Sun, F.R. Tay, B. Fan, Quaternary ammonium silane, calcium and phosphorus-loaded PLGA submicron particles against Enterococcus faecalis infection of teeth: An in vitro and in vivo study, Materials Science and Engineering: C, 111 (2020) 110856.

[30] J.L. Jones, Y.G. Yingling, I.M. Reaney, P. Westerhoff, Materials matter in phosphorus sustainability, MRS Bulletin, 45 (2020) 7-10.

[31] S.W. Jung, S.H. Ryu, W.J. Shin, Y. Sohn, M. Huh, R.J. Koch, C. Jozwiak, E. Rotenberg, A. Bostwick, K.S. Kim, Black phosphorus as a bipolar pseudospin semiconductor, Nature Materials, 19 (2020) 277-281.

[32] L. Fernandez, Global consumption of phosphate fertiliser 2009, by country, in, Statista, 2022.

[33] N. Parasana, M. Shah, A. Unnarkat, Recent advances in developing innovative sorbents for phosphorus removal—perspective and opportunities, Environmental Science and Pollution Research, 29 (2022) 38985-39016.

[34] C. Alewell, B. Ringeval, C. Ballabio, D.A. Robinson, P. Panagos, P. Borrelli, Global phosphorus shortage will be aggravated by soil erosion, Nature Communications, 11 (2020) 4546.

[35] D.A. Vaccari, S.M. Powers, X. Liu, Demand-driven model for global phosphate rock suggests paths for phosphorus sustainability, Environmental Science & Technology, 53 (2019) 10417-10425.

[36] A.N. Sharpley, L. Bergström, H. Aronsson, M. Bechmann, C.H. Bolster, K. Börling, F. Djodjic, H.P. Jarvie, O.F. Schoumans, C. Stamm, K.S. Tonderski, B. Ulén, R. Uusitalo, P.J.A. Withers, Future agriculture with minimized phosphorus losses to waters: Research needs and direction, Ambio, 44 (2015) 163-179.

[37] J.R. Mihelcic, L.M. Fry, R. Shaw, Global potential of phosphorus recovery from human urine and feces, Chemosphere, 84 (2011) 832-839.

[38] S. Dahlin, J. Englund, H. Malm, M. Feigel, B. Westerberg, F. Regali, M. Skoglundh, L.J. Pettersson, Effect of biofuel- and lube oil-originated sulfur and phosphorus on the performance of Cu-SSZ-13 and V2O5-WO3/TiO2 SCR catalysts, Catalysis Today, (2020).

[39] O. Zabihi, M. Ahmadi, Q. Li, M.R.G. Ferdowsi, R. Mahmoodi, E.N. Kalali, D.-Y. Wang, M. Naebe, A sustainable approach to scalable production of a graphene based flame retardant using waste fish deoxyribonucleic acid, Journal of Cleaner Production, 247 (2020) 119150.

[40] Z. Zhang, C. Dong, J. Liu, D. Kong, L. Sun, Z. Lu, Preparation of a synergistic reactive flame retardant based on silicon, phosphorus and nitrogen and its application to cotton fabrics, Cellulose, 27 (2020) 1799-1815.

[41] S. Valoriani, C. Eliopoulos, J.D. Irish, M. Borrini, Health and safety issues in the Victorian workplace: An example of mandibular phosphorus necrosis from Gloucester, UK, International Journal of Osteoarchaeology, 30 (2020) 73-79.

[42] M. Smol, M. Preisner, A. Bianchini, J. Rossi, L. Hermann, T. Schaaf, J. Kruopienė, K. Pamakštys, M. Klavins, R. Ozola-Davidane, D. Kalnina, E. Strade, V. Voronova, K. Pachel, X. Yang, B.-M. Steenari, M. Svanström, Strategies for sustainable and circular management of phosphorus in the Baltic sea region: The holistic approach of the InPhos project, Sustainability, 12 (2020).

[43] D. Cordell, J.-O. Drangert, S. White, The story of phosphorus: Global food security and food for thought, Global Environmental Change, 19 (2009) 292-305.

[44] Y. Liu, G. Villalba, R.U. Ayres, H. Schroder, Global phosphorus flows and environmental: Impacts from a consumption perspective, Journal of Industrial Ecology, 12 (2008) 229-247.

[45] C. Vaneeckhaute, V. Lebuf, E. Michels, E. Belia, P.A. Vanrolleghem, F.M.G. Tack, E. Meers, Nutrient recovery from digestate: Systematic technology review and product classification, Waste and Biomass Valorization, 8 (2017) 21-40.

[46] E.M. Barampouti, S. Mai, D. Malamis, K. Moustakas, M. Loizidou, Exploring technological alternatives of nutrient recovery from digestate as a secondary resource, Renewable and Sustainable Energy Reviews, 134 (2020) 110379.

[47] J.P. Sheets, L. Yang, X. Ge, Z. Wang, Y. Li, Beyond land application: Emerging technologies for the treatment and reuse of anaerobically digested agricultural and food waste, Waste Management, 44 (2015) 94-115.

[48] S. Xie, R. Wickham, L.D. Nghiem, Synergistic effect from anaerobic co-digestion of sewage sludge and organic wastes, International Biodeterioration & Biodegradation, 116 (2017) 191-197.

[49] S. Menardo, F. Gioelli, P. Balsari, The methane yield of digestate: Effect of organic loading rate, hydraulic retention time, and plant feeding, Bioresource Technology, 102 (2011) 2348-2351.

[50] A. Tiwary, I.D. Williams, D.C. Pant, V.V.N. Kishore, Emerging perspectives on environmental burden minimisation initiatives from anaerobic digestion technologies for community scale biomass valorisation, Renewable and Sustainable Energy Reviews, 42 (2015) 883-901.

[51] M.L. Christensen, M. Hjorth, K. Keiding, Characterization of pig slurry with reference to flocculation and separation, Water Research, 43 (2009) 773-783.

[52] S. Fouda, S. von Tucher, F. Lichti, U. Schmidhalter, Nitrogen availability of various biogas residues applied to ryegrass, Journal of Plant Nutrition and Soil Science, 176 (2013) 572-584.

[53] A. Limoli, M. Langone, G. Andreottola, Ammonia removal from raw manure digestate by means of a turbulent mixing stripping process, Journal of Environmental Management, 176 (2016) 1-10.

[54] W. Tao, A.T. Ukwuani, Coupling thermal stripping and acid absorption for ammonia recovery from dairy manure: Ammonia volatilization kinetics and effects of temperature, pH and dissolved solids content, Chemical Engineering Journal, 280 (2015) 188-196.

[55] M.T. Vu, L.N. Nguyen, M. Mofijur, M.A.H. Johir, H.H. Ngo, T.M.I. Mahlia, L.D. Nghiem, Simultaneous nutrient recovery and algal biomass production from anaerobically digested sludge centrate using a membrane photobioreactor, Bioresource Technology, 343 (2022) 126069.

[56] P.S. Selvaraj, K. Periasamy, K. Suganya, K. Ramadass, S. Muthusamy, P. Ramesh, R. Bush, S.G.T. Vincent, T. Palanisami, Novel resources recovery from anaerobic digestates: Current trends and future perspectives, Critical Reviews in Environmental Science and Technology, (2021) 1-85.

[57] A.R. Salehiyoun, F. Di Maria, M. Sharifi, O. Norouzi, H. Zilouei, M. Aghbashlo, Anaerobic co-digestion of sewage sludge and slaughterhouse waste in existing wastewater digesters, Renewable Energy, 145 (2020) 2503-2509.

[58] L. Shi, W.S. Simplicio, G. Wu, Z. Hu, H. Hu, X. Zhan, Nutrient recovery from digestate of anaerobic digestion of livestock manure: A review, Current Pollution Reports, 4 (2018) 74-83.

[59] W. Peng, A. Pivato, Sustainable management of digestate from the organic fraction of municipal solid waste and food waste under the concepts of back to earth alternatives and circular economy, Waste and Biomass Valorization, 10 (2019) 465-481.

[60] F. Tambone, V. Orzi, G. D'Imporzano, F. Adani, Solid and liquid fractionation of digestate: Mass balance, chemical characterization, and agronomic and environmental value, Bioresource Technology, 243 (2017) 1251-1256.

[61] J.J. Walsh, D.L. Jones, D.R. Chadwick, A.P. Williams, Repeated application of anaerobic digestate, undigested cattle slurry and inorganic fertilizer N: Impacts on pasture yield and quality, Grass and Forage Science, 73 (2018) 758-763.

[62] S. Huttunen, K. Manninen, P. Leskinen, Combining biogas LCA reviews with stakeholder interviews to analyse life cycle impacts at a practical level, Journal of Cleaner Production, 80 (2014) 5-16.

[63] T. Zhang, X. He, Y. Deng, D.C.W. Tsang, R. Jiang, G.C. Becker, A. Kruse, Phosphorus recovered from digestate by hydrothermal processes with struvite

crystallization and its potential as a fertilizer, Science of the Total Environment, 698 (2020) 134240.

[64] E. Tampio, T. Salo, J. Rintala, Agronomic characteristics of five different urban waste digestates, Journal of Environmental Management, 169 (2016) 293-302.

[65] A. Yasar, R. Rasheed, A.B. Tabinda, A. Tahir, F. Sarwar, Life cycle assessment of a medium commercial scale biogas plant and nutritional assessment of effluent slurry, Renewable and Sustainable Energy Reviews, 67 (2017) 364-371.

[66] J.L. Campos, D. Crutchik, Ó. Franchi, J.P. Pavissich, M. Belmonte, A. Pedrouso, A. Mosquera-Corral, Á. Val del Río, Nitrogen and phosphorus recovery from anaerobically pretreated agro-food wastes: A review, Frontiers in Sustainable Food Systems, 2 (2019).

[67] F. Monlau, C. Sambusiti, N. Antoniou, A. Zabaniotou, A. Solhy, A. Barakat, Pyrochars from bioenergy residue as novel bio-adsorbents for lignocellulosic hydrolysate detoxification, Bioresource Technology, 187 (2015) 379-386.

[68] F. Monlau, C. Sambusiti, E. Ficara, A. Aboulkas, A. Barakat, H. Carrère, New opportunities for agricultural digestate valorization: current situation and perspectives, Energy & Environmental Science, 8 (2015) 2600-2621.

[69] C. Ledda, A. Schievano, S. Salati, F. Adani, Nitrogen and water recovery from animal slurries by a new integrated ultrafiltration, reverse osmosis and cold stripping process: A case study, Water Research, 47 (2013) 6157-6166.

[70] M.T. Vu, H.P. Vu, L.N. Nguyen, G.U. Semblante, M.A.H. Johir, L.D. Nghiem, A hybrid anaerobic and microalgal membrane reactor for energy and microalgal biomass production from wastewater, Environmental Technology & Innovation, 19 (2020) 100834.

[71] A. Zarebska, D. Romero Nieto, K.V. Christensen, L. Fjerbæk Søtoft, B. Norddahl, Ammonium fertilizers production from manure: A critical review, Critical Reviews in Environmental Science and Technology, 45 (2015) 1469-1521.

[72] K. Meixner, W. Fuchs, T. Valkova, K. Svardal, C. Loderer, M. Neureiter, G. Bochmann, B. Drosg, Effect of precipitating agents on centrifugation and ultrafiltration performance of thin stillage digestate, Separation and Purification Technology, 145 (2015) 154-160.

[73] Y. Chen, X. Li, W. Zizeng, L. Feng, J. Xie, Z. Lin, Z. Xu, B. Liu, X. Li, H. Zheng, Research on a new cationic polyacrylamide (CPAM) with a cationic microblock structure and its enhanced effect on sludge condition and dewatering, Environmental Science and Pollution Research, 28 (2021) 51865-51878.

[74] M.T. Vu, L.N. Nguyen, I. Ibrahim, M. Abu Hasan Johir, N. Bich Hoang, X. Zhang, L.D. Nghiem, Nutrient recovery from digested sludge centrate using alkali metals from steel-making slag, Chemical Engineering Journal, 450 (2022) 138186.

[75] Managing urban stormwater: Harvesting and reuse, Dept. of Environment and Conservation NSW, Sydney South, N.S.W, 2006.

[76] E. Desmidt, K. Ghyselbrecht, Y. Zhang, L. Pinoy, B. Van der Bruggen, W. Verstraete, K. Rabaey, B. Meesschaert, Global phosphorus scarcity and full-scale P-recovery techniques: A review, Critical Reviews in Environmental Science and Technology, 45 (2015) 336-384.

[77] A. Yesigat, A. Worku, A. Mekonnen, W. Bae, G.L. Feyisa, S. Gatew, J.-L. Han, W. Liu, A. Wang, A. Guadie, Phosphorus recovery as K-struvite from a waste stream: A review of influencing factors, advantages, disadvantages and challenges, Environmental Research, (2022) 114086.

[78] M.T. Vu, L.N. Nguyen, M.A. Hasan Johir, X. Zhang, L.D. Nghiem, M. Elimelech, Biogas sparging to control fouling and enhance resource recovery from anaerobically digested sludge centrate by forward osmosis, Journal of Membrane Science, (2021) 119176.

[79] Z. Thong, Y. Cui, Y.K. Ong, T.-S. Chung, Molecular design of nanofiltration membranes for the recovery of phosphorus from sewage sludge, ACS Sustainable Chemistry & Engineering, 4 (2016) 5570-5577.

[80] M. Xie, H.K. Shon, S.R. Gray, M. Elimelech, Membrane-based processes for wastewater nutrient recovery: Technology, challenges, and future direction, Water Research, 89 (2016) 210-221.

[81] B.M. Souza-Chaves, M.A. Alhussaini, V. Felix, L.K. Presson, W.Q. Betancourt, K.L. Hickenbottom, A. Achilli, Extending the life of water reuse reverse osmosis membranes using chlorination, Journal of Membrane Science, 642 (2022) 119897.

[82] L. Tian, P. Zhou, Z. Su, T. Liu, N. Graham, T. Bond, W. Yu, Insights into the properties of surface waters and their associated nanofiltration membrane fouling: The importance of biopolymers and high molecular weight humics, Chemical Engineering Journal, 451 (2023) 138682.

[83] Q. Jiang, J. Liu, X. Song, Y. Qiu, J. Xue, Y. Shao, Y. Feng, Energy efficient bioelectro-concentration and recovery system of nutrients from human urine by integrating forward osmosis, Resources, Conservation and Recycling, 181 (2022) 106253.

[84] A. Charfi, S. Kim, Y. Yoon, J. Cho, Optimal cleaning strategy to alleviate fouling in membrane distillation process to treat anaerobic digestate, Chemosphere, 279 (2021) 130524.

[85] E.U. Khan, Å. Nordberg, Membrane distillation process for concentration of nutrients and water recovery from digestate reject water, Separation and Purification Technology, 206 (2018) 90-98.

[86] A.J. Ward, K. Arola, E. Thompson Brewster, C.M. Mehta, D.J. Batstone, Nutrient recovery from wastewater through pilot scale electrodialysis, Water Research, 135 (2018) 57-65.

[87] M.T. Vu, A.J. Ansari, F.I. Hai, L.D. Nghiem, Performance of a seawater-driven forward osmosis process for pre-concentrating digested sludge centrate: organic enrichment and membrane fouling, Environmental Science: Water Research & Technology, 4 (2018) 1047-1056.

[88] R.W. Holloway, A.E. Childress, K.E. Dennett, T.Y. Cath, Forward osmosis for concentration of anaerobic digester centrate, Water Research, 41 (2007) 4005-4014.

[89] M. Xie, L.D. Nghiem, W.E. Price, M. Elimelech, Toward resource recovery from wastewater: Extraction of phosphorus from digested sludge using a hybrid forward osmosis–membrane distillation process, Environmental Science & Technology Letters, 1 (2014) 191-195.

[90] E. Thompson Brewster, A.J. Ward, C.M. Mehta, J. Radjenovic, D.J. Batstone, Predicting scale formation during electrodialytic nutrient recovery, Water Research, 110 (2017) 202-210.

[91] V. Carrillo, B. Fuentes, G. Gómez, G. Vidal, Characterization and recovery of phosphorus from wastewater by combined technologies, Reviews in Environmental Science and Bio/Technology, 19 (2020) 389-418.

[92] A. Hasanoğlu, J. Romero, B. Pérez, A. Plaza, Ammonia removal from wastewater streams through membrane contactors: Experimental and theoretical analysis of operation parameters and configuration, Chemical Engineering Journal, 160 (2010) 530-537.

[93] J. Nagy, J. Kaljunen, A.J. Toth, Nitrogen recovery from wastewater and human urine with hydrophobic gas separation membrane: experiments and modelling, Chemical Papers, 73 (2019) 1903-1915.

[94] W. Moerman, M. Carballa, A. Vandekerckhove, D. Derycke, W. Verstraete, Phosphate removal in agro-industry: Pilot- and full-scale operational considerations of struvite crystallization, Water Research, 43 (2009) 1887-1892.

[95] A. Gysin, D. Lycke, S. Wirtel, The Pearl® and WASSTRIP® processes (Canada), in: C. Schaum (Ed.) Phosphorus: Polluter and Resource of the Future – Removal and Recovery from Wastewater, IWA Publishing, 2018, pp. 0.

[96] S. Günther, M. Grunert, S. Müller, Overview of recent advances in phosphorus recovery for fertilizer production, Engineering in Life Sciences, 18 (2018) 434-439.

[97] S. Sengupta, T. Nawaz, J. Beaudry, Nitrogen and phosphorus recovery from wastewater, Current Pollution Reports, 1 (2015) 155-166.

[98] S. Kataki, H. West, M. Clarke, D.C. Baruah, Phosphorus recovery as struvite: Recent concerns for use of seed, alternative Mg source, nitrogen conservation and fertilizer potential, Resources, Conservation and Recycling, 107 (2016) 142-156.

[99] S.I. Lee, S.Y. Weon, C.W. Lee, B. Koopman, Removal of nitrogen and phosphate from wastewater by addition of bittern, Chemosphere, 51 (2003) 265-271.

[100] M. Quintana, E. Sánchez, M.F. Colmenarejo, J. Barrera, G. García, R. Borja, Kinetics of phosphorus removal and struvite formation by the utilization of by-product of magnesium oxide production, Chemical Engineering Journal, 111 (2005) 45-52.

[101] Y. Song, H.H. Hahn, E. Hoffmann, The effect of carbonate on the precipitation of calcium phosphate, Environmental Technology, 23 (2002) 207-215.

[102] A.T.K. Tran, Y. Zhang, D. De Corte, J.-B. Hannes, W. Ye, P. Mondal, N. Jullok, B. Meesschaert, L. Pinoy, B. Van der Bruggen, P-recovery as calcium phosphate from

wastewater using an integrated selectrodialysis/crystallization process, Journal of Cleaner Production, 77 (2014) 140-151.

[103] S. Yeoman, T. Stephenson, J.N. Lester, R. Perry, The removal of phosphorus during wastewater treatment: A review, Environmental Pollution, 49 (1988) 183-233.

[104] H. Wang, K. Xiao, J. Yang, Z. Yu, W. Yu, Q. Xu, Q. Wu, S. Liang, J. Hu, H. Hou, B. Liu, Phosphorus recovery from the liquid phase of anaerobic digestate using biochar derived from iron−rich sludge: A potential phosphorus fertilizer, Water Research, 174 (2020) 115629.

[105] F. Yang, S. Zhang, Y. Sun, D.C.W. Tsang, K. Cheng, Y.S. Ok, Assembling biochar with various layered double hydroxides for enhancement of phosphorus recovery, Journal of Hazardous Materials, 365 (2019) 665-673.

[106] M.T. Vu, L.N. Nguyen, M.A. Hasan Johir, H.H. Ngo, C. Skidmore, A. Fontana, B. Galway, H. Bustamante, L.D. Nghiem, Phosphorus removal from aqueous solution by steel making slag – Mechanisms and performance optimisation, Journal of Cleaner Production, 284 (2021) 124753.

[107] Y. Yin, G. Xu, Y. Xu, M. Guo, Y. Xiao, T. Ma, C. Liu, Adsorption of inorganic and organic phosphorus onto polypyrrole modified red mud: Evidence from batch and column experiments, Chemosphere, 286 (2022) 131862.

[108] I.W. Almanassra, V. Kochkodan, G. McKay, M.A. Atieh, T. Al-Ansari, Review of phosphate removal from water by carbonaceous sorbents, Journal of Environmental Management, 287 (2021) 112245.

[109] C. Barca, D. Meyer, M. Liira, P. Drissen, Y. Comeau, Y. Andrès, F. Chazarenc, Steel slag filters to upgrade phosphorus removal in small wastewater treatment plants: Removal mechanisms and performance, Ecological Engineering, 68 (2014) 214-222.

[110] C. Barca, C. Gérente, D. Meyer, F. Chazarenc, Y. Andrès, Phosphate removal from synthetic and real wastewater using steel slags produced in Europe, Water Research, 46 (2012) 2376-2384.

[111] J.W. Lim, L.H. Chew, T.S.Y. Choong, C. Tezara, M.H. Yazdi, Overview of steel slag application and utilization, MATEC Web Conf., 74 (2016).

[112] A. Jonidi Jafari, M. Moslemzadeh, Investigation of phosphorus removal using steel slag from aqueous solutions: a systematic review study, International Journal of Environmental Analytical Chemistry, (2020).

[113] C. Maharaj, D. White, R. Maharaj, C. Morin, Re-use of steel slag as an aggregate to asphaltic road pavement surface, Cogent Engineering, 4 (2017) 1416889.

[114] A. Hedström, Ion exchange of ammonium in zeolites: A literature review, Journal of Environmental Engineering, 127 (2001) 673-681.

[115] K. Larsdotter, Wastewater treatment with microalgae - A literature review, VATTEN, 63 (2006) 31 - 38.

[116] L. Aditya, T.M.I. Mahlia, L.N. Nguyen, H.P. Vu, L.D. Nghiem, Microalgae-bacteria consortium for wastewater treatment and biomass production, Science of the Total Environment, 838 (2022) 155871.

[117] L.N. Nguyen, L. Aditya, H.P. Vu, A.H. Johir, L. Bennar, P. Ralph, N.B. Hoang, J. Zdarta, L.D. Nghiem, Nutrient removal by algae-based wastewater treatment, Current Pollution Reports, (2022).

[118] A. Fernández;, F. Gabriel;, Gómez-Serrano;, C. Fernández-Sevilla;, J. María, Recovery of nutrients from wastewaters using microalgae, Frontiers in Sustainable Food Systems, 2 (2018).

[119] M.I. Khan, J.H. Shin, J.D. Kim, The promising future of microalgae: current status, challenges, and optimization of a sustainable and renewable industry for biofuels, feed, and other products, Microbial cell factories, 17 (2018) 36-36.

[120] S.P. Singh, P. Singh, Effect of temperature and light on the growth of algae species: A review, Renewable and Sustainable Energy Reviews, 50 (2015) 431-444.

[121] F. Marazzi, E. Ficara, R. Fornaroli, V. Mezzanotte, Factors affecting the growth of microalgae on blackwater from biosolid dewatering, Water, Air, & Soil Pollution, 228 (2017) 68.

[122] R.I. Papry, S. Miah, H. Hasegawa, Integrated environmental factor-dependent growth and arsenic biotransformation by aquatic microalgae: A review, Chemosphere, 303 (2022) 135164.

[123] A.P. Peter, A.K. Koyande, K.W. Chew, S.-H. Ho, W.-H. Chen, J.-S. Chang, R. Krishnamoorthy, F. Banat, P.L. Show, Continuous cultivation of microalgae in photobioreactors as a source of renewable energy: Current status and future challenges, Renewable and Sustainable Energy Reviews, 154 (2022) 111852.

[124] F. Sayedin, A. Kermanshahi-pour, Q.S. He, S.M. Tibbetts, C.G.E. Lalonde, S.K. Brar, Microalgae cultivation in thin stillage anaerobic digestate for nutrient recovery and bioproduct production, Algal Research, 47 (2020) 101867.

[125] K. Kill, L. Grinberga, J. Koskiaho, Ü. Mander, O. Wahlroos, D. Lauva, J. Pärn, K. Kasak, Phosphorus removal efficiency by in-stream constructed wetlands treating agricultural runoff: Influence of vegetation and design, Ecological Engineering, 180 (2022) 106664.

[126] L. Li, J. Feng, L. Zhang, H. Yin, C. Fan, Z. Wang, M. Zhao, C. Ge, H. Song, Enhanced nitrogen and phosphorus removal by natural pyrite–based constructed wetland

with intermittent aeration, Environmental Science and Pollution Research, 28 (2021) 69012-69028.

[127] H.T.T. Ung, B.T. Leu, H.T.H. Tran, L.N. Nguyen, L.D. Nghiem, N.B. Hoang, H.T. Pham, H.C. Duong, Combining flowform cascade with constructed wetland to enhance domestic wastewater treatment, Environmental Technology & Innovation, 27 (2022) 102537.

[128] Z. Ji, W. Tang, Y. Pei, Constructed wetland substrates: A review on development, function mechanisms, and application in contaminants removal, Chemosphere, 286 (2022) 131564.

[129] J. Li, B. Zheng, X. Chen, Z. Li, Q. Xia, H. Wang, Y. Yang, Y. Zhou, H. Yang, The use of constructed wetland for mitigating nitrogen and phosphorus from agricultural runoff: A review, Water, 13 (2021) 476.

[130] A.K. Haritash, S. Dutta, A. Sharma, Phosphate uptake and translocation in a tropical Canna-based constructed wetland, Ecological Processes, 6 (2017) 12.

[131] M.C. Perdana, S. Hadisusanto, I.L.S. Purnama, Implementation of a full-scale constructed wetland to treat greywater from tourism in Suluban Uluwatu Beach, Bali, Indonesia, Heliyon, 6 (2020) e05038.

[132] H. Zhao, T. Piccone, Large scale constructed wetlands for phosphorus removal, an effective nonpoint source pollution treatment technology, Ecological Engineering, 145 (2020) 105711.

[133] J. García, P. Aguirre, J. Barragán, R. Mujeriego, V. Matamoros, J.M. Bayona, Effect of key design parameters on the efficiency of horizontal subsurface flow constructed wetlands, Ecological Engineering, 25 (2005) 405-418.

[134] L. Mu, L. Zhang, K. Zhu, J. Ma, M. Ifran, A. Li, Anaerobic co-digestion of sewage sludge, food waste and yard waste: Synergistic enhancement on process stability and biogas production, Science of the Total Environment, 704 (2020) 135429.

[135] S. Xie, M.J. Higgins, H. Bustamante, B. Galway, L.D. Nghiem, Current status and perspectives on anaerobic co-digestion and associated downstream processes, Environmental Science: Water Research & Technology, 4 (2018) 1759-1770.

[136] Q. Wang, W. Zhang, Z. Yang, Q. Xu, P. Yang, D. Wang, Enhancement of anaerobic digestion sludge dewatering performance using in-situ crystallization in combination with cationic organic polymers flocculation, Water Research, 146 (2018) 19-29.

[137] H.P. Vu, L.N. Nguyen, J. Zdarta, T.T.V. Nga, L.D. Nghiem, Blue-green algae in surface water: Problems and opportunities, Current Pollution Reports, 6 (2020) 105-122.

[138] J. Chen, S. Tang, F. Yan, Z. Zhang, Efficient recovery of phosphorus in sewage sludge through hydroxylapatite enhancement formation aided by calcium-based additives, Water Research, 171 (2020) 115450.

[139] T. Prot, W. Wijdeveld, L.E. Eshun, A.I. Dugulan, K. Goubitz, L. Korving, M.C.M. Van Loosdrecht, Full-scale increased iron dosage to stimulate the formation of vivianite and its recovery from digested sewage sludge, Water Research, 182 (2020) 115911.

[140] A.J. Ansari, F.I. Hai, W.E. Price, J.E. Drewes, L.D. Nghiem, Forward osmosis as a platform for resource recovery from municipal wastewater - A critical assessment of the literature, Journal of Membrane Science, 529 (2017) 195-206.

[141] L. Zheng, W.E. Price, J. McDonald, S.J. Khan, T. Fujioka, L.D. Nghiem, New insights into the relationship between draw solution chemistry and trace organic rejection by forward osmosis, Journal of Membrane Science, 587 (2019) 117184.

[142] A. Achilli, T.Y. Cath, A.E. Childress, Selection of inorganic-based draw solutions for forward osmosis applications, Journal of Membrane Science, 364 (2010) 233-241.

[143] X. Bao, Q. Wu, W. Shi, W. Wang, Z. Zhu, Z. Zhang, R. Zhang, X. Zhang, B. Zhang, Y. Guo, F. Cui, Insights into simultaneous ammonia-selective and anti-fouling mechanism over forward osmosis membrane for resource recovery from domestic wastewater, Journal of Membrane Science, 573 (2019) 135-144.

[144] T.N.-D. Cao, S.-S. Chen, H.-M. Chang, S.S. Ray, H.Q. Le, C.C. Duong, T.X. Bui, Evaluating the performance of polystyrene sulfonate coupling with non ionic Triton-X114 surfactant as draw solution in forward osmosis and membrane distillation systems, Environmental Technology & Innovation, 19 (2020) 100993.

[145] H.-M. Chang, S.-S. Chen, Y.-T. Chen, W.-S. Chang, C.-W. Li, N.C. Nguyen, S.S. Ray, D.T.N. Cao, Recovery of iodide as triiodide from thin-film transistor liquid crystal display wastewater by forward osmosis, Journal of Hazardous Materials, 403 (2021) 123637.

[146] S. Daly, A. Allen, V. Koutsos, A.J.C. Semião, Influence of organic fouling layer characteristics and osmotic backwashing conditions on cleaning efficiency of RO membranes, Journal of Membrane Science, 616 (2020) 118604.

[147] C. Ding, M. Yi, B. Liu, C. Han, X. Yu, Y. Wang, Forward osmosis-extraction hybrid process for resource recovery from dye wastewater, Journal of Membrane Science, 612 (2020) 118376.

[148] T.Y. Cath, M. Elimelech, J.R. McCutcheon, R.L. McGinnis, A. Achilli, D. Anastasio, A.R. Brady, A.E. Childress, I.V. Farr, N.T. Hancock, J. Lampi, L.D. Nghiem, M. Xie, N.Y. Yip, Standard methodology for evaluating membrane performance in osmotically driven membrane processes, Desalination, 312 (2013) 31-38.

[149] R. Wickham, S. Xie, B. Galway, H. Bustamante, L.D. Nghiem, Anaerobic digestion of soft drink beverage waste and sewage sludge, Bioresource Technology, 262 (2018) 141-147.

[150] M.T. Vu, L.N. Nguyen, K. Li, Q. Fu, M.A.H. Johir, A. Fontana, L.D. Nghiem, Biomethane production from anaerobic co-digestion and steel-making slag: A new waste-to-resource pathway, Science of the Total Environment, (2020) 139764.

[151] Q. She, R. Wang, A.G. Fane, C.Y. Tang, Membrane fouling in osmotically driven membrane processes: A review, Journal of Membrane Science, 499 (2016) 201-233.

[152] M. Elimelech, Z. Xiaohua, A.E. Childress, H. Seungkwan, Role of membrane surface morphology in colloidal fouling of cellulose acetate and composite aromatic polyamide reverse osmosis membranes, Journal of Membrane Science, 127 (1997) 101-109.

[153] M. Keskar, C. Sabatini, C. Cheng, M.T. Swihart, Synthesis and characterization of silver nanoparticle-loaded amorphous calcium phosphate microspheres for dental applications, Nanoscale Advances, 1 (2019) 627-635.

[154] Y.-B. Hu, M. Wolthers, D.A. Wolf-Gladrow, G. Nehrke, Effect of pH and phosphate on calcium carbonate polymorphs precipitated at near-freezing temperature, Crystal Growth & Design, 15 (2015) 1596-1601.

[155] S. Barua, B.S. Zakaria, T. Chung, F.I. Hai, T. Haile, A. Al-Mamun, B.R. Dhar, Microbial electrolysis followed by chemical precipitation for effective nutrients recovery from digested sludge centrate in WWTPs, Chemical Engineering Journal, 361 (2019) 256-265.

[156] F. Zeng, Q. Zhao, W. Jin, Y. Liu, K. Wang, D.-J. Lee, Struvite precipitation from anaerobic sludge supernatant and mixed fresh/stale human urine, Chemical Engineering Journal, 344 (2018) 254-261.

[157] S. Johansson, M. Ruscalleda, B. Saerens, J. Colprim, Potassium recovery from centrate: taking advantage of autotrophic nitrogen removal for multi-nutrient recovery, Journal of Chemical Technology & Biotechnology, 94 (2019) 819-828.

[158] D. Antakyali, C. Meyer, V. Preyl, W. Maier, H. Steinmetz, Large-scale application of nutrient recovery from digested sludge as struvite, Water Practice and Technology, 8 (2013) 256-262.

[159] M.T. Vu, L.N. Nguyen, J. Zdarta, J.A.H. Mohammed, N. Pathak, L.D. Nghiem, Chapter 1 - Wastewater to R3 – resource recovery, recycling, and reuse efficiency in urban wastewater treatment plants, in: A. An, V. Tyagi, M. Kumar, Z. Cetecioglu (Eds.) Clean Energy and Resource Recovery, Elsevier, 2022, pp. 3-16.

[160] H. Wu, C. Vaneeckhaute, Nutrient recovery from wastewater: A review on the integrated physicochemical technologies of ammonia stripping, adsorption and struvite precipitation, Chemical Engineering Journal, 433 (2022) 133664.

[161] K. Yetilmezsoy, F. Ilhan, E. Kocak, H.M. Akbin, Feasibility of struvite recovery process for fertilizer industry: A study of financial and economic analysis, Journal of Cleaner Production, 152 (2017) 88-102.

[162] P.J. Van der Hoek, R. Duijff, O. Reinstra, Nitrogen recovery from wastewater: Possibilities, competition with other resources, and adaptation pathways, Sustainability, 10 (2018).

[163] J. Korenak, C. Hélix-Nielsen, H. Bukšek, I. Petrinić, Efficiency and economic feasibility of forward osmosis in textile wastewater treatment, Journal of Cleaner Production, 210 (2019) 1483-1495.

[164] A. Mahto, K. Aruchamy, R. Meena, M. Kamali, S.K. Nataraj, T.M. Aminabhavi, Forward osmosis for industrial effluents treatment – sustainability considerations, Separation and Purification Technology, 254 (2021) 117568.

[165] J. Wang, X. Liu, Forward osmosis technology for water treatment: Recent advances and future perspectives, Journal of Cleaner Production, 280 (2021) 124354.

[166] Y.-J. Wang, L. Huang, Z. Fang, X.-M. Wang, M. Gao, H.-Q. Liu, W.-W. Li, T.-Y. Huang, Electrochemically self-cleanable carbon nanotube interlayered membrane for enhanced forward osmosis in wastewater treatment, Journal of Environmental Chemical Engineering, 10 (2022) 107399.

[167] J.A. Khan, L.N. Nguyen, H.C. Duong, L.D. Nghiem, Acetic acid extraction from rumen fluid by forward osmosis, Environmental Technology & Innovation, 20 (2020) 101083.

[168] M.S. Camilleri-Rumbau, J.L. Soler-Cabezas, K.V. Christensen, B. Norddahl, J.A. Mendoza-Roca, M.C. Vincent-Vela, Application of aquaporin-based forward osmosis membranes for processing of digestate liquid fractions, Chemical Engineering Journal, 371 (2019) 583-592.

[169] W. Zhang, W. Liang, Z. Zhang, T. Hao, Aerobic granular sludge (AGS) scouring to mitigate membrane fouling: Performance, hydrodynamic mechanism and contribution quantification model, Water Research, 188 (2021) 116518.

[170] V. Matthaiou, P. Oulego, Z. Frontistis, S. Collado, D. Hela, I.K. Konstantinou, M. Diaz, D. Mantzavinos, Valorization of steel slag towards a Fenton-like catalyst for the degradation of paraben by activated persulfate, Chemical Engineering Journal, 360 (2019) 728-739.

[171] P. Ahmedzade, B. Sengoz, Evaluation of steel slag coarse aggregate in hot mix asphalt concrete, Journal of Hazardous Materials, 165 (2009) 300-305.

[172] U. Kumari, S. Biswas, B.C. Meikap, Defluoridation characteristics of a novel adsorbent developed from ferroalloy electric arc furnace slag: Batch, column study and treatment of industrial wastewater, Environmental Technology & Innovation, 18 (2020) 100782.

[173] H.T. Van, L.H. Nguyen, T.K. Hoang, T.T. Nguyen, T.N.H. Tran, T.B.H. Nguyen, X.H. Vu, M.T. Pham, T.P. Tran, T.T. Pham, H.D. Nguyen, H.-P. Chao, C.-C. Lin, X.C. Nguyen, Heterogeneous Fenton oxidation of paracetamol in aqueous solution using iron slag as a catalyst: Degradation mechanisms and kinetics, Environmental Technology & Innovation, 18 (2020) 100670.

[174] N. Marti, A. Bouzas, A. Seco, J. Ferrer, Struvite precipitation assessment in anaerobic digestion processes, Chemical Engineering Journal, 141 (2008) 67-74.

[175] H. Liu, G. Hu, I.A. Basar, J. Li, N. Lyczko, A. Nzihou, C. Eskicioglu, Phosphorus recovery from municipal sludge-derived ash and hydrochar through wet-chemical technology: A review towards sustainable waste management, Chemical Engineering Journal, 417 (2021) 129300.

[176] Y. Lei, B. Song, R.D. van der Weijden, M. Saakes, C.J.N. Buisman, Electrochemical induced calcium phosphate precipitation: Importance of local pH, Environmental Science & Technology, 51 (2017) 11156-11164.

[177] H.-H. Chang, C.-L. Yeh, Y.-L. Wang, G.-W. Liu, H.-P. Lin, C.-P. Lin, Crystal growth in dentinal tubules with bio-calcium carbonate-silica sourced from equisetum grass, Journal of the Formosan Medical Association, 119 (2020) 1835-1841.

[178] D.K. Mueller, N.E. Spahr, Water-quality, streamflow, and ancillary data for nutrients in streams and rivers across the nation, 1992-2001, in: Data Series, 2005.

[179] A. Bouzas, N. Martí, S. Grau, R. Barat, D. Mangin, L. Pastor, Implementation of a global P-recovery system in urban wastewater treatment plants, Journal of Cleaner Production, 227 (2019) 130-140.

[180] V. Jegatheesan, J.L. Liow, L. Shu, S.H. Kim, C. Visvanathan, The need for global coordination in sustainable development, Journal of Cleaner Production, 17 (2009) 637-643.

[181] G. Wen, L. Huang, X. Zhang, Z. Hu, Uptake of nutrients and heavy metals in struvite recovered from a mixed wastewater of human urine and municipal sewage by two vegetables in calcareous soil, Environmental Technology & Innovation, 15 (2019) 100384.

[182] L.N. Nguyen, M.V. Truong, A.Q. Nguyen, M.A.H. Johir, A.S. Commault, P.J. Ralph, G.U. Semblante, L.D. Nghiem, A sequential membrane bioreactor followed by a membrane microalgal reactor for nutrient removal and algal biomass production, Environmental Science: Water Research & Technology, 6 (2020) 189-196.

[183] Q. Zhao, M. Yu, X. Zhang, H. Lu, B.K. Biswal, G.-H. Chen, D. Wu, Intracellularly stored polysulfur maintains homeostasis of pH and provides bioenergy for phosphorus metabolism in the sulfur-associated enhanced biological phosphorus removal (SEBPR) process, Chemosphere, 235 (2019) 211-219.

[184] A. Muhammad, A. Soares, B. Jefferson, The impact of background wastewater constituents on the selectivity and capacity of a hybrid ion exchange resin for phosphorus removal from wastewater, Chemosphere, 224 (2019) 494-501.

[185] M. Zarrabi, M.M. Soori, M.N. Sepehr, A. Amrane, S. Borji, H.R. Ghaffari, Removal of phosphorus by ion-exchange resins: Equilibrium, kinetic and thermodynamic studies, Environmental Engineering and Management Journal, 13 (2014) 891-903.

[186] S. Kumari, S. Jose, S. Jagadevan, Optimization of phosphate recovery as struvite from synthetic distillery wastewater using a chemical equilibrium model, Environmental Science and Pollution Research, 26 (2019) 30452-30462.

[187] S.P. Wei, F. van Rossum, G.J. van de Pol, M.-K.H. Winkler, Recovery of phosphorus and nitrogen from human urine by struvite precipitation, air stripping and acid scrubbing: A pilot study, Chemosphere, 212 (2018) 1030-1037.

[188] S. Yadav, H. Saleem, I. Ibrar, O. Naji, A.A. Hawari, A.A. Alanezi, S.J. Zaidi, A. Altaee, J. Zhou, Recent developments in forward osmosis membranes using carbon-based nanomaterials, Desalination, 482 (2020) 114375.

[189] J. Altmann, D. Rehfeld, K. Träder, A. Sperlich, M. Jekel, Combination of granular activated carbon adsorption and deep-bed filtration as a single advanced wastewater treatment step for organic micropollutant and phosphorus removal, Water Research, 92 (2016) 131-139.

[190] K.Y. Koh, S. Zhang, J. Paul Chen, Hydrothermally synthesized lanthanum carbonate nanorod for adsorption of phosphorus: Material synthesis and optimization, and demonstration of excellent performance, Chemical Engineering Journal, 380 (2020) 122153.

[191] K. Zhou, B. Wu, L. Su, X. Gao, X. Chai, X. Dai, Development of nano-CaO2-coated clinoptilolite for enhanced phosphorus adsorption and simultaneous removal of COD and nitrogen from sewage, Chemical Engineering Journal, 328 (2017) 35-43.

[192] A. Othman, E. Dumitrescu, D. Andreescu, S. Andreescu, Nanoporous sorbents for the removal and recovery of phosphorus from eutrophic waters: Sustainability challenges and solutions, ACS Sustainable Chemistry and Engineering, 6 (2018) 12542-12561.

[193] S. Manocha, F. Ponchon, Management of lime in steel, Metals, 8 (2018).

[194] C. Thomas, J. Rosales, J.A. Polanco, F. Agrela, 7 - Steel slags, in: J. de Brito, F. Agrela (Eds.) New Trends in Eco-efficient and Recycled Concrete, Woodhead Publishing, 2019, pp. 169-190.

[195] D.K. Panesar, 3 - Supplementary cementing materials, in: S. Mindess (Ed.) Developments in the Formulation and Reinforcement of Concrete (Second Edition), Woodhead Publishing, 2019, pp. 55-85.

[196] Y. Jiang, T.-C. Ling, C. Shi, S.-Y. Pan, Characteristics of steel slags and their use in cement and concrete—A review, Resources, Conservation and Recycling, 136 (2018) 187-197.

[197] I. Blanco, P. Molle, L.E. Sáenz de Miera, G. Ansola, Basic oxygen furnace steel slag aggregates for phosphorus treatment: Evaluation of its potential use as a substrate in constructed wetlands, Water Research, 89 (2016) 355-365.

[198] F. Liu, M.Z. Chen, F.Z. Li, Q.L. Li, S.P. Wu, Y. Sang, Effect of ground steel slag powder on cement properties, Materials Research Innovations, 19 (2015) S1-150-S151-153.

[199] J. Li, B. Wu, T. Zhou, X. Chai, Preferential removal of phosphorus using modified steel slag and cement combination for its implications in engineering applications, Environmental Technology & Innovation, 10 (2018) 264-274.

[200] D. Claveau-Mallet, É. Boutet, Y. Comeau, Steel slag filter design criteria for phosphorus removal from wastewater in decentralized applications, Water Research, 143 (2018) 28-37.

[201] H. Yamada, M. Kayama, K. Saito, M. Hara, A fundamental research on phosphate removal by using slag, Water Research, 20 (1986) 547-557.

[202] T.T.Q. Nguyen, P. Loganathan, T.V. Nguyen, S. Vigneswaran, Removing arsenic from water with an original and modified natural manganese oxide ore: batch kinetic and equilibrium adsorption studies, Environmental Science and Pollution Research, 27 (2020) 5490-5502.

[203] F.A. Razmi, N. Ngadi, S. Wong, I.M. Inuwa, L.A. Opotu, Kinetics, thermodynamics, isotherm and regeneration analysis of chitosan modified pandan adsorbent, Journal of Cleaner Production, 231 (2019) 98-109.

[204] C. Li, D. Chen, J. Ding, Z. Shi, A novel hetero-exopolysaccharide for the adsorption of methylene blue from aqueous solutions: Isotherm, kinetic, and mechanism studies, Journal of Cleaner Production, 265 (2020) 121800.

[205] S. Zu Nurain Ahmad, H. R, W. Afnizan Wan Mohamed, N. Othman, N. Shaylinda Mohd Zin, Chemical composition, pH value, and points of zero charge of high calcium and high iron electric arc furnace slag, International Journal of Engineering & Technology, 7 (2018) 1-4.

[206] Y. Deng, A. Wheatley, Mechanisms of phosphorus removal by recycled crushed concrete, International Journal of Environmental Research and Public Health, 15 (2018) 357.

[207] M. Bizi, Activated carbon and the principal mineral constituents of a natural soil in the presence of carbamazepine, Water, 11 (2019).

[208] Y.S. Ho, G. McKay, Pseudo-second order model for sorption processes, Process Biochemistry, 34 (1999) 451-465.

[209] T.A. Saleh, M.N. Siddiqui, A.A. Al-Arfaj, Kinetic and intraparticle diffusion studies of carbon nanotubes-titania for desulfurization of fuels, Petroleum Science and Technology, 34 (2016) 1468-1474.

[210] S.K. Zheng, J.J. Chen, X.M. Jiang, X.F. Li, A comprehensive assessment on commercially available standard anion resins for tertiary treatment of municipal wastewater, Chemical Engineering Journal, 169 (2011) 194-199.

[211] M. Li, J. Liu, Y. Xu, G. Qian, Phosphate adsorption on metal oxides and metal hydroxides: A comparative review, Environmental Reviews, 24 (2016) 319-332.

[212] K. Aleksandar, J.C. Wim, T. Eila, U. Risto, Potential and limitations of phosphate retention media in water protection: A process-based review of laboratory and field-scale tests, Agricultural and Food Science, 21 (2012).

[213] E. Alibakhshi, E. Ghasemi, M. Mahdavian, B. Ramezanzadeh, Corrosion inhibitor release from Zn-Al-[PO43-]-[CO32-] layered double hydroxide nanoparticles, Progress in Color, Colorants and Coatings, 9 (2016) 233-248.

[214] A. Arboleda, M. Franco, J. Caicedo, L. Tirado, C. Goyes, Synthesis and chemical and structural characterization of hydroxyapatite obtained from eggshell and tricalcium phosphate, Ingeniería y competitividad, 18 (2016) 71-78.

[215] I.S. Neira, Y.V. Kolen'ko, O.I. Lebedev, G. Van Tendeloo, H.S. Gupta, F. Guitián, M. Yoshimura, An effective morphology control of hydroxyapatite crystals via hydrothermal synthesis, Crystal Growth & Design, 9 (2009) 466-474.

[216] J.L. Soler-Cabezas, J.A. Mendoza-Roca, M.C. Vincent-Vela, M.J. Luján-Facundo, L. Pastor-Alcañiz, Simultaneous concentration of nutrients from anaerobically digested sludge centrate and pre-treatment of industrial effluents by forward osmosis, Separation and Purification Technology, 193 (2018) 289-296.

[217] D.J. Conley, H.W. Paerl, R.W. Howarth, D.F. Boesch, S.P. Seitzinger, K.E. Havens, C. Lancelot, G.E. Likens, Controlling eutrophication: Nitrogen and phosphorus, Science, 323 (2009) 1014-1015.

[218] W.K. Dodds, V.H. Smith, Nitrogen, phosphorus, and eutrophication in streams, Inland Waters, 6 (2016) 155-164.

[219] P.H. Nielsen, S.J. McIlroy, M. Albertsen, M. Nierychlo, Re-evaluating the microbiology of the enhanced biological phosphorus removal process, Current Opinion in Biotechnology, 57 (2019) 111-118.

[220] C. Zhang, A. Guisasola, J.A. Baeza, A review on the integration of mainstream P-recovery strategies with enhanced biological phosphorus removal, Water Research, 212 (2022) 118102.

[221] K.Y. Koh, Z. Chen, S. Zhang, J.P. Chen, Cost-effective phosphorus removal from aqueous solution by a chitosan/lanthanum hydrogel bead: Material development, characterization of uptake process and investigation of mechanisms, Chemosphere, 286 (2022) 131458.

[222] W. Wu, Z. Zhao, M. Li, W. Zheng, S. You, Q. Wei, Y. Liu, Electrified nanohybrid filter for enhanced phosphorus removal from water, Chemosphere, 303 (2022) 135226.

[223] F. Wu, Q. Yu, F. Gauvin, H.J.H. Brouwers, C. Liu, Phosphorus removal from aqueous solutions by adsorptive concrete aggregates, Journal of Cleaner Production, 278 (2021) 123933.

[224] W.-J. Xia, L.-X. Guo, L.-Q. Yu, Q. Zhang, J.-R. Xiong, X.-Y. Zhu, X.-C. Wang, B.-C. Huang, R.-C. Jin, Phosphorus removal from diluted wastewaters using a La/C nanocomposite-doped membrane with adsorption-filtration dual functions, Chemical Engineering Journal, 405 (2021) 126924.

[225] Z. Yang, T. Zhu, M. Xiong, A. Sun, Y. Xu, Y. Wu, W. Shu, Z. Xu, Tuning adsorption capacity of metal–organic frameworks with Al3+ for phosphorus removal: Kinetics, isotherm and regeneration, Inorganic Chemistry Communications, 132 (2021) 108804.

[226] H. Ma, X. Gao, Y. Chen, J. Zhu, T. Liu, Fe(II) enhances simultaneous phosphorus removal and denitrification in heterotrophic denitrification by chemical precipitation and stimulating denitrifiers activity, Environmental Pollution, 287 (2021) 117668.

[227] Y. Wang, P. Kuntke, M. Saakes, R.D. van der Weijden, C.J.N. Buisman, Y. Lei, Electrochemically mediated precipitation of phosphate minerals for phosphorus removal and recovery: Progress and perspective, Water Research, 209 (2022) 117891.

[228] X. Li, S. Shen, Y. Xu, T. Guo, H. Dai, X. Lu, Application of membrane separation processes in phosphorus recovery: A review, Science of the Total Environment, 767 (2021) 144346.

[229] M.-J. Liu, P. Li, Q.-W. Meng, Q. Ge, Membranes constructed by metal–ligand complexation for efficient phosphorus removal and fouling resistance in forward osmosis, Advanced Composites and Hybrid Materials, 5 (2022) 159-172.

[230] Y. Jia, S. Sun, S. Wang, X. Yan, J. Qian, B. Pan, Phosphorus in water: A review on the speciation analysis and species specific removal strategies, Critical Reviews in Environmental Science and Technology, (2022) 1-22.

[231] A. Jonidi Jafari, M. Moslemzadeh, Investigation of phosphorus removal using steel slag from aqueous solutions: a systematic review study, International Journal of Environmental Analytical Chemistry, 102 (2022) 821-833.

[232] K.-Y. Show, D.-J. Lee, J.-H. Tay, Anaerobic digestion of sewage sludge, in: Biological Sludge Minimization and Biomaterials/Bioenergy Recovery Technologies, 2012, pp. 319-347.

[233] J.C. Mendez, T. Hiemstra, Carbonate adsorption to ferrihydrite: Competitive interaction with phosphate for use in soil systems, ACS Earth and Space Chemistry, 3 (2019) 129-141.

[234] Y.-Q. Liu, S. Cinquepalmi, Exploration of mechanisms for calcium phosphate precipitation and accumulation in nitrifying granules by investigating the size effects of granules, Water Research, 206 (2021) 117753.

[235] L.N. Nguyen, J. Kumar, M.T. Vu, J.A.H. Mohammed, N. Pathak, A.S. Commault, D. Sutherland, J. Zdarta, V.K. Tyagi, L.D. Nghiem, Biomethane production from anaerobic co-digestion at wastewater treatment plants: A critical review on development

and innovations in biogas upgrading techniques, Science of the Total Environment, 765 (2021) 142753.

[236] M. Ye, J. Luo, S. Zhang, H. Yang, Y.-Y. Li, J. Liu, In-situ ammonia stripping with alkaline fermentation of waste activated sludge to improve short-chain fatty acids production and carbon source availability, Bioresource Technology, 301 (2020) 122782.

[237] T. Wirthensohn, F. Waeger, L. Jelinek, W. Fuchs, Ammonium removal from anaerobic digester effluent by ion exchange, Water Science & Technology, 60 (2009) 201-210.

[238] C. Shin, A. Szczuka, R. Jiang, W.A. Mitch, C.S. Criddle, Optimization of reverse osmosis operational conditions to maximize ammonia removal from the effluent of an anaerobic membrane bioreactor, Environmental Science: Water Research & Technology, 7 (2021) 739-747.

[239] Y.V. Nancharaiah, S. Venkata Mohan, P.N.L. Lens, Recent advances in nutrient removal and recovery in biological and bioelectrochemical systems, Bioresource Technology, 215 (2016) 173-185.

[240] N. Cong Nguyen, H. Cong Duong, S.-S. Chen, H. Thi Nguyen, H. Hao Ngo, W. Guo, H. Quang Le, C. Cong Duong, L. Thuy Trang, A. Hoang Le, X. Thanh Bui, P. Dan Nguyen, Water and nutrient recovery by a novel moving sponge – Anaerobic osmotic membrane bioreactor – Membrane distillation (AnOMBR-MD) closed-loop system, Bioresource Technology, 312 (2020) 123573.

[241] S.F. Ahmed, M. Mofijur, T.A. Parisa, N. Islam, F. Kusumo, A. Inayat, V.G. Le, I.A. Badruddin, T.M.Y. Khan, H.C. Ong, Progress and challenges of contaminate removal from wastewater using microalgae biomass, Chemosphere, 286 (2022) 131656.

[242] M.C. Deprá, R.R. Dias, I.A. Severo, C.R. de Menezes, L.Q. Zepka, E. Jacob-Lopes, Carbon dioxide capture and use in photobioreactors: The role of the carbon dioxide loads in the carbon footprint, Bioresource Technology, 314 (2020) 123745.

[243] D. Nagarajan, D.-J. Lee, J.-S. Chang, Integration of anaerobic digestion and microalgal cultivation for digestate bioremediation and biogas upgrading, Bioresource Technology, 290 (2019) 121804.

[244] C.G. Khoo, Y.K. Dasan, M.K. Lam, K.T. Lee, Algae biorefinery: Review on a broad spectrum of downstream processes and products, Bioresource Technology, 292 (2019) 121964.

[245] P.H.N. Vo, H.H. Ngo, W.S. Guo, S.W. Chang, D.D. Nguyen, P.D. Nguyen, X.T. Bui, X.B. Zhang, J.B. Guo, Can algae-based technologies be an affordable green process for biofuel production and wastewater remediation?, Bioresource Technology, 256 (2018) 491-501.

[246] W. Zhou, Y. Li, Y. Gao, H. Zhao, Nutrients removal and recovery from saline wastewater by Spirulina platensis, Bioresource Technology, 245 (2017) 10-17.

[247] F. Gao, C. Li, Z.-H. Yang, G.-M. Zeng, L.-J. Feng, J.-z. Liu, M. Liu, H.-w. Cai, Continuous microalgae cultivation in aquaculture wastewater by a membrane photobioreactor for biomass production and nutrients removal, Ecological Engineering, 92 (2016) 55-61.

[248] L.N. Nguyen, M.V. Truong, A.Q. Nguyen, M.A.H. Johir, A.S. Commault, P.J. Ralph, G.U. Semblante, L.D. Nghiem, A sequential membrane bioreactor followed by a membrane microalgal reactor for nutrient removal and algal biomass production, Environmental Science: Water Research & Technology, (2020).

[249] H.P. Vu, L.N. Nguyen, B. Emmerton, Q. Wang, P.J. Ralph, L.D. Nghiem, Factors governing microalgae harvesting efficiency by flocculation using cationic polymers, Bioresource Technology, 340 (2021) 125669.

[250] R. Boonchai, G. Seo, Microalgae membrane photobioreactor for further removal of nitrogen and phosphorus from secondary sewage effluent, Korean Journal of Chemical Engineering, 32 (2015) 2047-2052.

[251] G.H. Gim, J. Ryu, M.J. Kim, P.I. Kim, S.W. Kim, Effects of carbon source and light intensity on the growth and total lipid production of three microalgae under different culture conditions, Journal of Industrial Microbiology and Biotechnology, 43 (2016) 605-616.

[252] M. Sakarika, M. Kornaros, Effect of pH on growth and lipid accumulation kinetics of the microalga Chlorella vulgaris grown heterotrophically under sulfur limitation, Bioresource Technology, 219 (2016) 694-701.

[253] Y. Collos, P.J. Harrison, Acclimation and toxicity of high ammonium concentrations to unicellular algae, Marine Pollution Bulletin, 80 (2014) 8-23.

[254] H. Zheng, X. Wu, G. Zou, T. Zhou, Y. Liu, R. Ruan, Cultivation of Chlorella vulgaris in manure-free piggery wastewater with high-strength ammonium for nutrients removal and biomass production: Effect of ammonium concentration, carbon/nitrogen ratio and pH, Bioresource Technology, 273 (2019) 203-211.

[255] Y. Su, Revisiting carbon, nitrogen, and phosphorus metabolisms in microalgae for wastewater treatment, Science of the Total Environment, 762 (2021) 144590.

[256] A. Converti, A.A. Casazza, E.Y. Ortiz, P. Perego, M. Del Borghi, Effect of temperature and nitrogen concentration on the growth and lipid content of Nannochloropsis oculata and Chlorella vulgaris for biodiesel production, Chemical Engineering and Processing: Process Intensification, 48 (2009) 1146-1151.